Reconstructing the inflaton potential

Candidatus Scientiarum thesis by
Tor Helge Huse
Institute for Theoretical Astrophysics
University of Oslo
Norway

May 2005

Preface

Looking up into a starry night, mesmerized by the thousands of sparkling bright and faint lights, knowing that the beauty above is only a very, very small fraction of the Universe, knowing that the beauty stretches out endlessly in all directions, it is almost impossible not to be filled with thoughts of how, why and what.
For as long as I can remember, I've been fascinated by the sky above and the questions it brings. There are several ways to try and find answers to these fundamental questions. You have philosophers and theologians, and there are astrophysicists. I believe the best way to get true knowledge about the Universe is to study it, using physical laws as our basis. And although there certainly are questions which can not be answered by physics alone, I've chosen astrophysics as my way to find answers.
The work on this thesis has been carried out at the Institute for theoretical astrophysics at the University of Oslo.
I've been very lucky to have a proficient and caring supervisor in associated professor Øystein Elgarøy. He has provided invaluable help, guidance and constructive criticism on my work. So big thanks to you, Øystein.
Furthermore I would like to thank Hans Kristian Eriksen for practical help and stimulating discussions. I will also send a special thank you to Antony Lewis for very helpful discussions (concerning parameter estimation and the use of `COSMOMC`). William H. Kinney also deserves a thanks for helpful discussions.
Finally I would like to thank Lis and Kanutte for proof-reading this thesis, and thank you, Kanutte, for making me smile every day.

Abstract

During inflation, the potential of the inflaton scalar field ϕ, drives the exponential expansion of the Universe. The nature of the inflaton potential is presently unknown, but one hopes to learn more from observations of the cosmic microwave background (CMB). Models of topical interest of the inflaton potential can be divided into four classes, based on observable parameters. In this thesis we explore the possibility of reconstructing the inflaton potential from observational data using a MonteCarlo reconstruction method. A pipeline to estimate cosmological parameter constraints using a MonteCarlo MarkovChain (MCMC) is also investigated. The object is to exclude whole classes of inflaton potentials.

We find that the MonteCarlo reconstruction method is well suited to produce vast numbers of candidates for the inflaton potential, but present constraints on the cosmological parameters of interest are too weak for the MonteCarlo reconstruction to be a useful method. Furthermore we discover weaknesses with `COSMOMC`, the MCMC method commonly used to constrain cosmological parameters. Currently, `COSMOMC` fails when using B-mode polarisation data, and the time and computing power needed to analyse noise-free CMB data is far beyond what is needed for current observational data.

If the difficulties with the MCMC method are resolved, there is an exciting possibility of using the MCMC method in conjunction with the MonteCarlo reconstruction method to reconstruct the true inflaton potential from future high precision CMB observations.

Introduction

We live in a universe which, most likely, is the result of a Big Bang some 13.7 billion years ago. Most cosmologists today believe the Universe is filled with energy, but not the ordinary energy of matter. Observations indicate that baryonic matter only contributes about 4 % of the total amount of energy. A weird form of gravitationally only interacting matter, the so-called cold dark matter (CDM), contributes roughly 26 % of the total energy, while the remaining 70 % is a completely different form of energy, called vacuum energy or Dark Energy. We really do not know what the Dark Energy is. However, both CDM and Dark Energy seem to be required in order to match our models with observations.

Our Universe is spatially flat, homogeneous and isotropic, and these properties make the Big Bang model inadequate. Therefore a so-called inflationary epoch in the very early universe is propsed to solve the problems associated with the Big Bang model. The inflationary epoch lasts only for a tiny fraction of a second, but in that short time, it changes our Universe radically. The size of the Universe expands exponentially during inflation, resulting in a smooth and flat universe, and "all" problems with the Big Bang model are solved. As one understands, the concept of inflation is useful, and it is therefore essential to get knowledge of what drives inflation. A type of model which is able to explain the "force" behind inflation is a scalar field ϕ, with a corresponding potential $V(\phi)$. The scalar field ϕ is called the inflaton, and $V(\phi)$ is the inflaton potential. In most models, the so-called slow-roll models, it is assumed that the potential dominates the field during inflation. Therefore it is important to have knowledge of the shape of the potential. We wish to explore the possibility of reconstructing the inflaton potential from observational data. Currently, there is no real understanding of what the inflaton is, physically. By reconstructing, we therefore mean finding the shape of the potential as a function of ϕ during inflation. We do not intend to find anything more fundamental about the inflaton and its potential.

We first employed to reconstruct the inflaton potential, is not as fruitful as we had hoped. Therefore we proceeded to examine the chances of, from future observational data, excluding whole classes of possible inflaton potential models. We simulate observational data and employ a method to constrain the different model parameters. There are many different models for the inflaton potential, but most of them fall into one of four different classes. Luckily, these four classes belong to seperate observational parameter spaces. If we are able to constrain the parameters from the data well enough,

we should be able to exclude one or more classes of models. If this is feasible from cosmological data, it would prove very useful in future attempts to reconstruct the potential $V(\phi)$, and thus our ability to say something about the underlying physics.

Contents

Chapter 1

Cosmology

In this chapter we present an outline of modern cosmological theory. An interested reader may find a more comprehensive and thorough description in a standard cosmology textbook [1, 2].

1.1 History

As long as humans have wandered this planet we have been filled with amazement about everything we see. For many, the heavens above have been the most fascinating and it has always raised fundamental questions. Cosmology is the science which tries to explain the Universe we observe. This section is a very short and far from complete history of cosmology.

From the ancient Greeks to the people of the fifteenth century, "everybody" assumed and believed that the Earth was the center of everything in the Universe. There were no other "Suns" or planets, and the idea of galaxies was not even thought of at the time. This firm belief in the geocentric worldview was challenged by Copernicus in the early 1500s. He worked out a model where the Earth, and the other planets discovered at that time, all rotated around the Sun in perfect circles. This heliocentric model did, however, not succeed in explaining the motions of the planets any better than the geocentric model, and as it made the Sun, and not the Earth, the centre of the Universe, it was not easily accepted.

On November 11, 1572, a bright star suddenly appeared in the constellation of Cassiopeia. Initially being brighter than Venus, the star faded from view after 18 months. This supernova explosion was not easy to explain in the sixteenth century, a time when most scholars believed the heavens to be permanent and unalterable. Thus the new star could not be a star at all, but must instead be some sort of bright object quite near the Earth, possibly in

the atmosphere. Tycho Brahe, a Danish astronomer, suggested measuring the parallax of the new star to determine its distance. He failed to measure any parallax, hence showing that the star had to be much further away than anyone could imagine.

In the seventeenth century, Johannes Kepler, an assistant of Brahe, constructed a heliocentric model in which the planets move in elliptical orbits as opposed to perfect circles. This model fitted Brahe's observational data perfectly. Later Galileo Galilei, using a telescope, observed the phases of Venus and the four large moons of Jupiter, thus finding strong evidence for the heliocentric model and equally strong evidence against a geocentric model. For this he was arrested by the Roman Catholic Church.

In the mid-seventeenth century, Isaac Newton introduced his laws of motion and the science of physics was changed forever. It became possible to calculate the motions of objects using a mathematical framework.

We now take a rather big leap forward in time to 1845. Telescopes have by this time improved and the Milky Way can now be observed. For the first time the telescopes were powerful enough to observe, and see structures in other galaxies, although it was not realized at the time that they were in fact other galaxies. The astronomical community was divided in the discussion of these "island universes". Not until 1923 did Edwin Hubble settle the mattter when he measured the distance to the Andromeda "nebula", and found it to be much larger than the size of the Milky Way.

In 1916 Albert Einstein published his theory of General Relativity, changing once again our understanding of time and space completely.

Hubble discovered in the mid 1920s that not only were there other galaxies, but they were receding from us; the Universe is expanding. Yet later the theory of a Big Bang (see the next section) was born, and in the 1960s the cosmic microwave background, the remnant of this cataclysmic event, was discovered.

During the late 1990s, supernovae data [3, 4, 5, 6] have suggested that not only is the Universe expanding, the expansion is also accelerating.

To sum up: We have come from being the centre of the Universe to realizing that we are not much more than a blip in a cosmos vastly greater than we are able to imagine. Cosmology is the science we use when we try to make sense of all this.

1.2 Hot Big Bang

The standard model for the evolution of the Universe is often denoted the hot Big Bang (HBB). In this section we briefly describe this theory, and

more detailed information can be found in e.g. [7, 8, 9, 10]. The Friedmann equations describe the evolution of this homogeneous and isotropic universe model. The main components in this universe are matter and radiation fluids, and the kinematic properties (e.g. the Hubble parameter) are equivalent to those we observe in the real Universe. It is assumed that when going backwards in time the temperature increases. However, the theory does not describe what happened during the first 10^{-43} seconds of the Universe. Prior to this all known physics breaks down. The period from 10^{-43} seconds to 10^{-35} seconds after the Big Bang is called the Planck epoch. In this era the temperature T drops from approximately $T = 10^{32}\,\mathrm{K}$ to $T = 10^{27}\,\mathrm{K}$. At $t = 10^{-43}$ seconds after the Big Bang, the force of gravity separates from the three other forces (strong and weak forces and the electromagnetic force), and at $t = 10^{-36}$ seconds the strong force separates from the electronuclear force. Next follows the Grand Unification epoch (GUE) which covers the time from $t = 10^{-35}$ to $t = 10^{-12}$ seconds after the Big Bang. During GUE the temperature drops from $T = 10^{27}\,\mathrm{K}$ to $T = 10^{15}\,\mathrm{K}$. Inflation is also thought to take place during GUE. After the GUE the so-called Electroweak epoch covers the time from 10^{-12} to 10^{-6} seconds after the Big Bang. In this epoch the weak force is separated from the electromagnetic force, and the four fundamental forces we have in the Universe today are all separated. The temperature decreases further from $T = 10^{15}\,\mathrm{K}$ to $T = 10^{13}\,\mathrm{K}$.

A brief outline of the evolution of the HBB starting from $t = 10^{-6}$ seconds after the start of the Universe follows next.

In very early times (note that the inflationary epoch (chapter 2) is not included in the standard HBB picture described here, as that is thought to take place right after the Planck epoch) it is thought that the Universe consisted of a very hot and dense gas containing several particle species. These particle species must not be confused with the particles we see in the Universe today, although among these particle species we also find radiation, i.e. photons, which are also found in the present Universe. The radiation in the primordial gas is observed as the cosmic microwave background today. This is also the reason why the model is termed hot; the radiation component in the present universe is of a hot cosmological origin. As this hot, dense primordial cosmic soup expands it cools and the cooling introduces phase transitions. Many of these transitions separate the different cosmological epochs in the HBB model, but not all cosmological epochs are separated by phase transitions.

The first epoch is the radiation dominated era. In this epoch the total energy density is dominated by ultra relativistic particles such as photons and high energy bosons and fermions. The momentum distribution is that of a blackbody since the photons and particles are in a thermal equilibrium.

It can be shown that the temperature T varies with expansion as $T \propto \frac{1}{a}$ during this epoch. At $T \geq 1$ MeV the neutrinos (assumed massless) are no longer at thermal equilibrium with the rest of the cosmic soup. The neutrinos, being massless, will keep the momentum distribution form with an effective temperature $T_\nu \propto \frac{1}{a}$. A short time after this (approximately 1 second after the Big Bang) all electrons and positrons become non-relativistic and annihilate, except for one electron for each proton. This ensures electrical neutrality in the Universe. When the temperature finally drops low enough, atomic nuclei (deuterium) are produced and are stable enough to collide with other deuterium nuclei and produce heavier elements (75 % hydrogen, 25 % helium and trace amounts of lithium, deuterium, berillium and boron). Elements heavier than boron are not produced due to the high temperatures required (deuterium, which is needed in the first place, is only produced at lower temperatures). This period, which lasts from approximately 1 second to 3 minutes after the big bang is called the epoch of Nucleosynthesis.

After a few hundred thousand years, the Universe has cooled to about 3000 kelvin and the atomic nuclei (hydrogen) can capture electrons and form stable atoms in an event known as recombination. This event is important as the previously free electrons can no longer scatter the photons (through Thompson scattering) and the Universe becomes transparent to light. It is these photons we observe today as the cosmic microwave background with a temperature of 2.726 K due to the expansion of the Universe (cosmic redshift). The CMB is often said to originate from the surface of last scattering, or the last scattering surface (lss), as it is last time the photons have been scattered. After this the Universe becomes matter dominated and all objects such as galaxies, clusters, quasars, stars and planets are eventually formed through gravitational collapse.

1.3 Classical cosmology

By "classical cosmology" we mean cosmological models within the framework of Einstein's theory of general relativity (GR) [11]. The GR framework enables us to describe an evolving universe and we will look at some of the basic ideas of GR and also a few "classic" models founded on the GR-framework. The purpose is to familiarize the reader with perhaps the most important theoretical basis in current cosmology. GR allows us to develop widely different models of the Universe depending on the kinds of energies and energy densities we allow in the models. A very important part of any GR based model is the chosen metric. In cosmology the Robertson-Walker metric (RW-metric) is used, which is the unique metric for a homogenous and isotropic

universe. The RW-line-element is given by [11]:

$$ds^2 = c^2dt^2 - a^2(t)\left[\frac{dr^2}{1-kr^2} + r^2d\theta^2 + r^2\sin^2\theta d\phi^2\right] \tag{1.1}$$

and depends on the curvature k of our 3-dimensional universe and the scale factor $a(t)$. The curvature is normally scaled to -1, 0 or +1 for negative curvature, no-curvature (flat) and positive curvature respectively. The scale factor a is generally time-dependent and is found using the metric and the Einstein equations. With the time-dependence of the scale factor we can describe a universe with changing comoving volume, i.e. expansion or contraction of the universe. It is clear that the scale factor is an important quantity if we are to learn something about the evolution of the universe, since its birth and final fate can be seen from the scale factor.

1.3.1 The Einstein equations

Using general relativity, we relate the geometry of space-time, i.e. the metric, to the matter content of the Universe through the following set of equations [11]:

$$E^{\mu\nu} = \frac{8\pi G}{c^4}T^{\mu\nu} \tag{1.2}$$

$$E^{\mu\nu} = R^{\mu\nu} - \frac{1}{2}g^{\mu\nu}R \tag{1.3}$$

where the indices μ and ν represent the space-time coordinates t and $\underline{x}$. One normally denotes the space-time coordinates with $0, 1, 2, 3$, where 0 is the time coordinate. In expressions like equation (1.2) and (1.3) one sum over repeated indices, so that the above equations in reality are a set of equations, i.e. $E^{00} = \frac{8\pi G}{c^4}T^{00}$, $E^{01} = \frac{8\pi G}{c^4}T^{01}$, and so on.

In the above equations, $E^{\mu\nu}$ is the Einstein tensor describing the geometry, $T^{\mu\nu}$ the energy-momentum tensor, $R^{\mu\nu}$ is the Ricci tensor and R the Ricci scalar. The metric $g_{\mu\nu}$ is related to the RW-line-element (1.1) through

$$ds^2 = g_{\mu\nu}dx^\mu dx^\nu$$

and is an important quantity when describing the geometry of space-time [11]. The first equations (1.2), called the Einstein equations, tell us that the geometry of space-time is governed by the mass-energy distribution in the universe. In other words this means that mass tells space-time how to curve and space-time tells mass how to move. If we assume that the universe

consists of perfect fluids, i.e. no viscosity, then the energy-momentum tensor $T^{\mu\nu}$ is given by [1,page 7]:

$$T^{\mu\nu} = (p + \rho c^2)U^\mu U^\nu - pg^{\mu\nu} \tag{1.4}$$

where p is the pressure and ρ the energy density associated with the fluid. U^μ is the 4-speed $U^\mu \equiv \frac{dx^\mu}{ds}$. Given $E^{\mu\nu}$ and $T^{\mu\nu}$ we can solve the Einstein equations. Using the RW-metric we find the Friedmann equations:

$$\ddot{a} = -\frac{4\pi G}{3}\left(\rho + 3\frac{p}{c^2}\right)a \tag{1.5}$$

$$a\ddot{a} + 2\dot{a}^2 + 2kc^2 = 4\pi G\left(\rho - \frac{p}{c^2}\right)a^2 \tag{1.6}$$

$$\dot{a}^2 + kc^2 = \frac{8\pi G}{3}\rho a^2 \tag{1.7}$$

One can derive equation (1.7) from equations (1.5) and (1.6), so that the last two are the only non-trivial equations. If we further assume that the universe expands adiabatically we find:

$$d(\rho c^2 a^3) = -pda^3 \tag{1.8}$$

only one of the Friedmann equations is needed to derive the remaining two equations. Adiabatic expansion is equivalent to energy-momentum conservation, $T^{ij}_{;j} = 0$, which is thought to be a reasonable assumption. Adiabatic expansion is also a consequence of homogeneity and isotropy; there can be no heat flow between volume elements in a homogeneous and isotropic fluid. From equations (1.8) and (1.7) one can derive equation (1.5) by first finding the derivative of (1.7) with respect to cosmic time and then apply the assumption of adiabatic expansion. We have defined the Einstein tensor without a cosmological constant Λ and instead taken a more modern, and mathematically equivalent view and given vacuum an energy density ρ_Λ and a pressure p_Λ. When we apply this view, we consider the cosmological constant not to be a geometrical effect of space-time, but say that empty space is not completely void when it comes to energy and pressure. The cosmological constant is treated as a cosmic fluid in the same way as dust and radiation, and therefore has similar fluid properties. Perhaps one of the most important properties of a fluid in this context, is its equation of state, which tells us how the pressure relates to the energy density:

$$p = w(t)\rho c^2 \tag{1.9}$$

Here we have written the parameter w as a function of time, but it is often more convenient to write it $w = w(z)$, where z is the redshift. It is also

common in cosmology to use units where $c = 1$. For a universe model containing only dust, we have $w = 0$ since dust has no pressure. For radiation, the equation of state is $p = \frac{1}{3}\rho$, and the cosmological constant fluid has $w = -1$. We see that these three models have time-independent equations of state. It is not known whether w for dark energy is time-dependent or not. However, with recent high-quality data it has become possible to search for the time-dependence of the effective equation of state, that is the total contribution from all the cosmic fluids. If this time-dependence is found, it can possibly help us come closer to explaining the nature of the dark energy.

With the equation of state we can find the time-dependence or the evolution of e.g. the energy density with respect to the scale factor a. Differentiating equation (1.8) with respect to time and substituting for equation (1.9) we get:

$$\begin{aligned} \dot{\rho}a^3 + 3\rho a^2\dot{a} &= -3pa^2\dot{a} \\ \frac{\dot{\rho}}{\rho} &= -3(1+w)\frac{\dot{a}}{a} \\ \rho &= \rho_0\left(\frac{a_0}{a}\right)^{3(1+w)} \end{aligned} \tag{1.10}$$

assuming w is time-independent. Equation (1.10) is obviously a very important equation when we wish to describe how the energy or matter density in the universe evolves.

1.3.2 Density parameters

A universe with curvature $k = 0$, which means a spatially flat one, is said to have critical density. If there is no Λ or dark energy, this universe defines the boundary between a model which expands forever and one that eventually collapses. We can derive an expression for the critical density from the Friedmann equations [1,page 13]:

$$\begin{aligned} \dot{a}^2 + kc^2 &= \frac{8\pi G}{3}\rho a^2, k = 0 \\ \Rightarrow \rho_c(t) &= \frac{3}{8\pi G}\left(\frac{\dot{a}}{a}\right)^2 \\ \Rightarrow \rho_c(t) &= \frac{3}{8\pi G}H^2(t) \end{aligned} \tag{1.11}$$

The critical density is a function of time and changes with the value of the Hubble parameter. The present value is: $\rho_{c,0} = \rho(t_0) = \frac{3H_0^2}{8\pi G} = 1.88 \cdot 10^{-29}h^2\ \mathrm{gcm}^{-3}$ and with $h \simeq 0.7$ this corresponds to about 0.01 hydrogen

atoms for every cm^3. It is convenient to define a set of density parameters, and from the Friedmann equation (1.7) we get:

$$\dot{a}^2 + kc^2 = \frac{8\pi G}{3}\rho a^2 + \frac{8\pi G}{3}\frac{\Lambda c^2}{8\pi G}a^2 \tag{1.12}$$

and further define the cosmological constant's energy density $\rho_\Lambda c^2 = \frac{\Lambda c^2}{8\pi G}$. For the present epoch $t = t_0$:

$$\begin{aligned} \dot{a_0}^2 + kc^2 &= \frac{8\pi G}{3}\rho_0 a_0^2 + \frac{1}{3}\Lambda c^2 a_0^2 \\ \Rightarrow 1 + \frac{kc^2}{a_0^2 H_0^2} &= \frac{\rho_0}{\rho_c} + \frac{\rho_{\Lambda 0}}{\rho_c} \\ \Rightarrow 1 &= \Omega_0 + \Omega_{\Lambda 0} + \Omega_{k0} \end{aligned} \tag{1.13}$$

where we have defined the density parameters $\Omega_0 = \frac{\rho_0}{\rho_c}$, $\Omega_{\Lambda 0} = \frac{\rho_{\Lambda 0}}{\rho_c}$ and $\Omega_{k0} = -\frac{kc^2}{a_0^2 H_0^2}$. One should also note that the matter density parameter Ω_0 contains both the baryon and CDM matter, so that $\Omega_0 = \Omega_{b\,0} + \Omega_{dm\,0}$. The value of the scale factor today is often set to equal to unity, $a_0 = 1$. The relation (1.13) is useful as it is independent of the geometry of the universe and valid for all the models we will consider.

1.3.3 Cosmological horizons

When we observe the night sky we see light in all directions and one could easily think that what we see is the whole Universe. However, because light travels at a finite speed and the Universe expands, what we see is not necessarily the whole picture. The evolution of the scale factor determines what we are able to see, and in a general model what we see is restricted by a horizon.

The concept of a horizon arises in many parts of astrophysics, and in the following a more mathematical description of some of the horizons encountered in cosmology will be presented [1,pages 45–48]. Consider an observer at the origin of a coordinate system O at time t. We want to find the set of points capable of sending light signals that can be received by the observer. This is equivalent to finding the points casually connected with the origin at time t. Any light signal received at the origin O by time t must have been emitted by a source at some time $t' \in [0, t]$. The set of points we seek must hence be inside a sphere centred upon O with the proper radius

$$\mathcal{R}_H(t) = a(t)\int_0^t \frac{c\,dt'}{a(t')} \tag{1.14}$$

where $c\,\mathrm{d}t'$ is the generic distance travelled by a light ray between t' and $t'+\mathrm{d}t'$. When multiplied with $\frac{a(t)}{a(t')}$ and integrated, we find the proper distance travelled. The integral (1.14) can possibly diverge if the lower limit is zero, because $a(t) \to 0$ for small values of t. If this is the case, the observer in O can have received light signals from the whole Universe. The other possibility comes about when the integral gives a finite value. Then the observer can only have received light signals from within a sphere with centre O and radius $\mathcal{R}_H$. The surface of this sphere is called the particle horizon at time t, and it is important to note that the observer cannot, at any previous time, have received light signals, or any other signals, from sources situated at proper distances greater than $\mathcal{R}_H(t)$. The particle horizon divides the set of all points into two groups, those within the horizon which can, in principle, have been observed by O, and those which cannot have been observed and therefore must be outside the horizon. Another horizon often encountered, and arguably the most important one, is the Hubble distance, frequently just called the horizon. The radius of the Hubble sphere, called the Hubble distance, is defined to be the distance from O to an object moving with the cosmological expansion at the speed of light with respect to O:

$$\mathcal{R}_c \equiv c\frac{a}{\dot{a}} = \frac{c}{H} \tag{1.15}$$

The Hubble distance gives an estimate of the distance light can travel while the Universe expands appreciably. This means that for most purposes we can ignore expansion of the Universe in a region much smaller than the Hubble distance during a time interval much less than the Hubble time ($t_H = \frac{1}{H}$).

We also mention the so-called event horizon. This horizon is not used much in cosmology, perhaps mostly because it does not exist in Friedmann models with $-\frac{1}{3} < w < 1$. However it does exist in a de Sitter model. The event horizon is defined as:

$$R_E = a(t)\int_t^{t_{max}} \frac{c\,dt'}{a(t')} \tag{1.16}$$

and we see that it is equal to the particle horizon except that the limits of the integral have changed. The upper limit t_{max} is dependent on the cosmological model discussed. For a closed model, which ends with a Big Crunch $t_{\mathbf{max}} = t_f$, where t_f is the time of the Big Crunch. In an open or flat model we have $t_{\mathbf{max}} = \infty$.

1.4 Classic models

Now we will take a brief look at some "classic" models in cosmology. These models are special cases of the equation of state $p = w\rho$, with the assumption of a flat universe; $\Omega_{tot} = 1$, $\Omega_{tot} = \Omega_m + \Omega_{rad} + \Omega_\Lambda$. From equation (1.7) we obtain:

$$\begin{aligned}\left(\frac{\dot{a}}{a}\right)^2 &= H^2(t) \\ &= H_0^2 \left(\frac{a_0}{a}\right)^2 \left[\Omega_{tot0} \left(\frac{a_0}{a}\right)^{1+3w} + (1 - \Omega_{tot0})\right]\end{aligned}$$

By setting $\Omega_{tot0} = 1$ and integrating the equation above we find:

$$a(t) = a_0 \left(\frac{t}{t_0}\right)^{\frac{2}{3(1+w)}} \tag{1.17}$$

with $t_0 = \frac{2}{3(1+w)H_0}$ being the time from the Big-Bang singularity to the present.

1.4.1 Dust

For $w = 0$ we have $a(t) = a_0 \left(\frac{t}{t_0}\right)^{\frac{2}{3}}$ and $t_0 = \frac{2}{3H_0}$. This corresponds to a universe consisting of a pressureless gas, more commonly known as dust. This particular dust-model is known as the Einstein de Sitter model (EdS-model/universe) [1,pages 36–37]. It's an elegant model, but is easily ruled out by observations. We have $t_0 = \frac{2}{3h} \cdot 9.778\,\text{Gyr}$ and the currently favoured value $h \simeq 0.7$ leads to $t_0 \simeq 9.31\,\text{Gyr}$. As some of the oldest stars have estimated ages far beyond this (approximately 13 billion years) this forces us to conclude that the EdS-model is incorrect. From equation (1.10) we find that for dust the energy $U = \rho a^3$ is constant, which means that the mass in a comoving volume is constant during expansion. It is interesting to compare the evolution of the horizon for different cosmological models. Using equation (1.14) and the expression for the scale factor $a(t)$ above we find:

$$\begin{aligned}\mathcal{R}_H(t) &= \int_0^t \frac{c\,dt'}{a(t')} \\ &= ct^{\frac{2}{3}} \int_0^t t^{-\frac{2}{3}} dt' \\ &= 3ct\end{aligned} \tag{1.18}$$

where we have used the common definition $a_0 = 1$. For a comparison with other classic cosmological models see figure (1.1).

1.4.2 Radiation

Radiative models have an equation of state

$$p(t) = \frac{1}{3}\rho(t)$$

By radiation we mean a gas of photons or ultra-relativistic particles. In this model we find ρa^4 =constant (see equation (1.10) with $w = \frac{1}{3}$). The energy U in a comoving volume is proportional to $\frac{1}{a}$ during expansion, meaning the radiation energy decreases during the expansion. One way of explaining this is to say that the number of photons within a comoving volume is constant, but they lose energy with time because of cosmological redshift. An alternative explanation from the first law of thermodynamics is:

$$\begin{aligned} dU + pdV &= 0 \\ \Rightarrow \quad dU &= -pdV \end{aligned}$$

Which means that energy is being drained from a radiation-filled comoving volume due to a thermodynamical work being done at the surface of the comoving volume transporting energy to the outside. From (1.17) we find that the scale factor for a radiation model varies as

$$a(t) = \left(\frac{t}{t_0}\right)^{\frac{1}{2}}$$

with $a_0 = 1$. Together with (1.14) this yields:

$$\begin{aligned} \mathcal{R}_H(t) &= \int_0^t \frac{c\,dt'}{a(t')} \\ &= ct^{\frac{1}{2}} \int_0^t t^{-\frac{1}{2}} dt' \\ &= 2ct \end{aligned} \tag{1.19}$$

See figure (1.1) for the radiation model plotted together with a dust model and a cosmological constant model.

1.4.3 Cosmological constant

Introduced by Einstein in 1917 to give a static universe, the cosmological constant Λ is now considered by many to give a possible solution to the fact that the Universe seems to be accelerating [3, 4, 5, 6]. A flat, empty universe with only a cosmological constant will give a Hubble parameter constant in

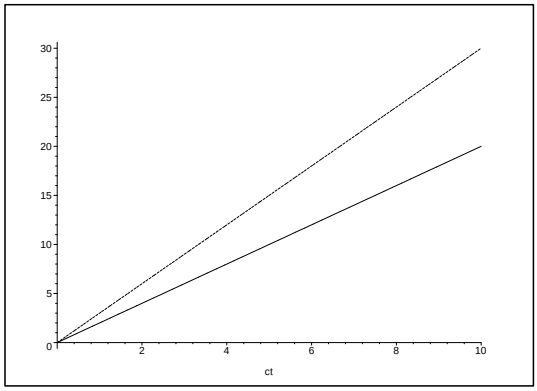

Figure 1.1: The evolution of the particle horizon for different cosmological models plotted as dunction of ct. The dust model is the upper model, and we see that the horizon size grows quicker for this model than for the radiation model.

time, $H(t) = H_0$. This is called the de Sitter universe. A Lorentz Invariant Vacuum Energy (LIVE) [11] has an energy-momentum tensor proportional to the metric tensor:

$$T_{\mu\nu} = \rho g_{\mu\nu}$$

Assuming that vacuum can be described as a perfect fluid we find

$$\begin{aligned} T_{\mu\nu} &= (\rho + p)u_\mu u_\nu - p g_{\mu\nu} \\ \Rightarrow \quad p &= -\rho \end{aligned}$$

Further we assume that energy densities are positive also for vacuum, yielding $p < 0$. Vacuum is in a stretched condition, and one can show that pressure ($p > 0$) or stretch ($p < 0$) have a gravitational influence. Stretch actually contributes to a repulsive gravitational effect. The cosmological constant is considered to represent LIVE's energy-momentum tensor.

From equation (1.10) we find that the energy density of vacuum is constant during expansion, $\rho(t) = \rho_0$. This means the energy of vacuum increases inside a comoving volume during expansion.

Evolution of the de Sitter universe

Let us solve the Friedman equation (1.12) for a spatially flat ($k = 0$) universe containing nothing but the cosmological constant ($\rho = 0$). We find

$$\left(\frac{\dot{a}}{a}\right)^2 = \frac{\Lambda}{3} \tag{1.20}$$

which implies that Λ is positive. A general solution of (1.20) has the form:

$$a = A \exp\left[\left(\frac{1}{3}\Lambda\right)^{\frac{1}{2}} t\right] \tag{1.21}$$

It is here interesting to note that the Hubble "constant" $H = \frac{\dot{a}}{a} = \left(\frac{\Lambda}{3}\right)^{\frac{1}{2}}$ is actually constant in time in the de Sitter universe. That also implies that the Hubble radius is constant in this model. Any test particles will move away from each other due to the repulsive gravitational effect of the cosmological constant. In the de Sitter universe there is no Big Bang at $t = 0$, and as can be seen from the expression for the scale factor above, the scale factor will not be 0 at $t = 0$, but instead approach 0 only when $t \to -\infty$. This means there is no particle horizon in the de Sitter model. To see this e solve equation (1.14) with the lower limit set equal to $-\infty$:

$$\begin{aligned} \mathcal{R}_H(t) &= \int_{-\infty}^{t} \frac{c\,dt'}{a(t')} \\ &= ce^{Ht} \int_{-\infty}^{t} e^{-Ht'} dt' \\ &= \frac{c}{H}\left[e^{Ht} - e^{\infty}\right] \end{aligned} \tag{1.22}$$

which obviously diverges.

1.4.4 Real life - The ΛCDM model

The model which fits today's ever growing set of observations best, is the so-called ΛCDM model [12]. This model is radically different from a dust or radiation dominated model. The primary contents of the Universe in this model is vacuum energy ($\Omega_{\Lambda 0} \sim 70\,\%$) and the exotic CDM ($\Omega_{0CDM} \sim 26\,\%$).

CDM is matter because it interacts gravitationally with ordinary matter (baryons etc.). It is dark in the sense that we cannot see it in any other way than through its gravitational influence on the visible matter in our cosmos, and it is cold due to its dust-like behaviour, i.e. it has no, or negligible, random motion (temperature).

Assuming the total energy density Ω_{tot} is unity and $\Omega_{tot} = \Omega_{\Lambda 0} + \Omega_0$ we have $\Omega_{b0} = 0.04$, where $\Omega_0 = \Omega_{0CDM} + \Omega_{b0}$ and Ω_{b0} is the total baryon energy density in the Universe. It looks like only 4 % of the energy in our universe is known to us.

Recent supernovae data suggest that the expansion of the Universe is accelerating. This is, at least in the ΛCDM model, due to the repulsive

nature of vacuum energy. We have seen that ρ_Λ will not decrease as ρ_{rad}, nor stay constant as ρ_m, with an expanding universe. Rather it increases within a comoving volume during expansion, and Λ will therefore become increasingly dominant in the Universe as the scale factor grows.

Chapter 2

Inflation

2.1 Why inflation?

Historically the idea of inflation was introduced to make the main cosmological event, the Big Bang, seem more plausible [13, 14]. As already mentioned the Universe is very close to being perfectly spatially flat, homogenous and isotropic, which makes the equations describing the Universe simpler. In the following it will be explained that these properties introduce a need to fine-tune the initial conditions if the hot Big Bang is the correct description of the Universe. Such a degree of fine-tuning is generally considered a bad thing in any physical model. It is therefore better to seek models which explain the observed properties without fine-tuning of initial parameters. Hence the idea of inflation is introduced in the hot Big Bang model. Let us now take a closer look at some of the problems that arise when inflation is not considered:

1. **The flatness problem, or, why is the Universe so old?**
   One problem arises when one tries to explain the observed spatially flatness in the Universe. The problem is connected to the fact that the Universe is as old as it is. For the Universe to get so old the density parameter Ω must be extremely fine-tuned during the early stages of Big Bang. Let us see exactly how much fine-tuning is needed. From equation (1.13) we can write equation (1.7) as:

   $$\Omega - 1 = \frac{k}{a^2 H^2} \tag{2.1}$$

   where $\Omega = \Omega_{m\,0} + \Omega_{\Lambda\,0}$. It is easy to see that if the Universe at some time is flat, i.e. $k = 0$ or equivalently $\Omega = 1$, then the Universe will stay flat forever. On the other hand, if the Universe is not flat, the density parameter Ω will evolve as time rolls by. For a nearly flat

matter dominated universe we have

$$|1 - \Omega| \propto t^{\frac{2}{3}}$$

and for radiation domination we have

$$|1 - \Omega| \propto t$$

Today we know Ω to be close to unity and this means that earlier Ω had to be even closer to 1. At the time of nucleosynthesis, approximately 1 second after the Big Bang we must have

$$|\Omega(t_{\text{nuc}}) - 1| \leq 10^{-16}$$

if the Universe is to evolve to what it is today [15, 2]. For still earlier times $|1 - \Omega|$ must be even smaller. Any further deviaton from unity would either cause the expansion to reverse and the Universe to recollapse ($\Omega > 1$), or the expansion would never stop and the Universe would very quickly become a very cold and empty place ($\Omega < 1$). The traditional Big Bang theory has no explanation for this fine-tuning and it must be part of the initial conditions.

2. **Trouble at the Horizon**
   The cosmic microwave background is observed to be very uniform. Its temperature is 2.73 K to a precision of 10^{-5} on the entire sky. This is a problem because there is no reason why two points on the sky should have the same temperature unless they have been in causal contact with each other. But when the CMB photons were released approximately 300000 years after the Big Bang the comoving distance causal processes could occur over was $\approx 180\Omega_0^{-\frac{1}{2}}h^{-1}$ Mpc. After this decoupling radiation has traveled a comoving distance of approximately $5820h^{-1}$ Mpc. This implies that radiation coming from regions separated by more than the horizon scale at last scattering, which is about 0.8 angular degrees, cannot have interacted before decoupling [2,page 37]. So why do they have the same temperature? The HBB is not able to explain this and it must be part of the initial conditions.

3. **Homogeneity and isotropy**
   The Universe is not perfectly homogeneous and isotropic. On small scales, this deviation from perfect homogeneity and isotropy is easily seen as stars and galaxies. The Universe does however get very close to being homogeneous and isotropic on large enough scales. When we observe the CMB we see anisotropies and interpret these as irregularities

at the last scattering surface. Furthermore we believe these irregularities to be the seeds of the large-scale structures in the present universe. The observed size of the anisotropies today indicate that their physical scale at the time of last scattering is much larger than the horizon scale at that time. This relates to the horizon problem above. How could physical structures larger than the horizon scale be formed? There is no causal physical process that can work over such great distances. To explain the large-scale structures within the HBB model they must be part of the initial conditions.

There are also other phenomena the hot Big Bang model cannot satisfactorily explain, like the magnetic monopole problem and other unwanted relics (gravitino, topological defects, etc.), but the three discussed above are more than enough to raise questions about the Hot Big Bang model and to make us seek a better understanding of the early universe.

2.2 Inflation in brief

In this section we give a brief introduction to the concept of inflation following [2]. The idea of inflation is not a stand-alone theory to replace the Big Bang model. It is rather something extra, an "add-on", that solves many of the problems associated with the HBB - model, but also poses some new ones. Inflation is an epoch in the very early universe where the expansion is accelerating:

$$\text{Inflation} \Longleftrightarrow \ddot{a} > 0 \tag{2.2}$$

Another way to say this is:

$$\frac{d}{dt}\frac{c}{aH(t)} = \frac{d}{dt}\frac{c}{a\frac{\dot{a}}{a}} = c\frac{d}{dt}\frac{1}{\dot{a}} = -\frac{c}{\dot{a}^2}\ddot{a} < 0 \,\text{for}\, \ddot{a} > 0 \tag{2.3}$$

i.e. inflation $\Leftrightarrow \frac{d}{dt}\frac{c}{aH(t)} < 0$ which can give us a more physical meaning to inflationary idea. $\frac{c}{H(t)}$, called the Hubble length, is the distance light travels during a typical expansion time, and $\frac{c}{aH(t)}$ is the comoving Hubble length. And as seen, the comoving Hubble length decreases with time during inflation, i.e. seen in coordinates fixed with expansion the observable Universe becomes smaller during inflation. The problems discussed in the previous section can all be solved if inflation occurs. The solution to the flatness problem is the easiest to see: $\frac{d}{dt}\frac{1}{a(t)H(t)} < 0$ and from $|\Omega(t) - 1| \propto \frac{K}{|a(t)H(t)|^2}$ we see that Ω is driven towards 1 since $\frac{1}{aH}$ will be driven towards 0 during inflation. An example of this is the de Sitter model where $a \propto e^{\mu t}$, $H \propto \frac{e^{\mu t}}{e^{\mu t}} = \text{const.}$

$\Rightarrow aH \propto e^{\mu t} \Rightarrow \Omega - 1 \propto e^{-\mu t} \rightarrow 0$. The solution to the horizon problem is as follows. A region with proper size ℓ can only be casually connected when the Hubble radius is $R_H = \ell$. In a Friedmann-model, we have $R_H \propto t$ in the early universe, while the proper size of a region with given comoving coordinate size grows as t^β with $\beta < 1$. The radius of the Hubble-sphere decides the causal properties of a given epoch, and during inflation this is a more useful quantity to consider than the particle horizon. The Hubble sphere radius is known as the Hubble-length. The proper size of the Hubble length is $R_c = \frac{c}{H} = \frac{ca}{\dot{a}}$ and the comoving length is $r_c = R_c \frac{a_0}{a} = \frac{ca_0}{\dot{a}}$. This implies that a comoving scale enters inside the Hubble length at a time $t_H(\ell_0) \neq 0$ because r_c increases with time. The main point here is that during inflation the comoving Hubble radius decreases dramatically, thus allowing our entire observable region (the "Universe") to lie within a region that was well inside the Hubble radius at the start of inflation. The Universe expands so much during inflation that our observable universe can originate from a very small region casually connected prior to inflation.

From (1.5) we see that inflation is equivalent with

$$\rho + 3p < 0 \tag{2.4}$$

If we assume general relativity to be valid, inflation can be seen as a question of pressure and energy density. The pressure must be less than $-\frac{1}{3}\rho$, or when we write the equation of state $p = w\rho$ we have $w < -\frac{1}{3}$. Which means a negative pressure is needed to have inflation.

2.3 Scalar fields

As seen in chapter 2.2, a negative pressure is needed to drive inflation. A way of ending inflation once it is under way is also required. The cosmological constant has negative pressure, but it is also a constant and inflation would thus never end. A fluid with the property of negative pressure and time variation could fill the requirements. A scalar field describing scalar particles, i.e. particles with spin 0, can have these properties. An example of a 0-spin particle is the long-sought-after Higgs boson. In modern particle physics, scalar fields and their associated particles are important when it comes to symmetry breaking between the fundamental forces. The scalar field introduced in cosmology to drive inflation, is called the inflaton [2,page 41]. An unusual feature of scalar fields which make them useful when describing inflation, is that the potential energy associated with the field may redshift extremely slowly as the Universe expands, corresponding to an effective equation of state with a negative pressure [2,page 41]. If we were to do

this properly we would use the field's Lagrangian, and we make use of that when we talk more about generation of perturbations, but for now we only state that pressure and energy density of the inflaton field $\phi(t)$ is:

$$\rho_\phi = \frac{1}{2}\dot{\phi}^2 + V(\phi) \tag{2.5}$$

$$p_\phi = \frac{1}{2}\dot{\phi}^2 - V(\phi) \tag{2.6}$$

$V(\phi)$ is the potential of the field and perhaps the most important quantity to specify, as it is the potential that gives inflation. One hopes to find a shape of $V(\phi)$ from particle physics since different $V(\phi)$ correspond to different inflationary models. The energy density ρ_ϕ and pressure p_ϕ cannot be related through an equation of state because any given ρ_ϕ can correspond to different values of the pressure if the energy is distributed differently between the potential and kinetic terms:

$$\frac{p_\phi}{\rho_\phi} = \frac{\frac{1}{2}\dot{\phi}^2 - V(\phi)}{\frac{1}{2}\dot{\phi}^2 + V(\phi)} \neq \text{const.} \tag{2.7}$$

However, if $\dot{\phi}^2 \ll V(\phi)$ the scalar field will mimic a cosmological constant with $p_\phi \simeq -\rho_\phi$. The dynamics of the scalar field universe can be found if we in the Friedmann equations and continuity equations use equations (2.5) and (2.6). Assuming $k = 0$ we find:

$$H^2 = \frac{1}{3M_{Pl}^2}\left[V(\phi) + \frac{1}{2}\dot{\phi}^2\right] \tag{2.8}$$

$$\left(\frac{\ddot{a}}{a}\right) = \frac{8\pi}{3m_{\rm Pl}^2}\left[V(\phi) - \dot{\phi}^2\right] \tag{2.9}$$

$$\ddot{\phi} + 3H\dot{\phi} = -\frac{dV}{d\phi} \tag{2.10}$$

$$\Updownarrow$$

$$\frac{d}{dt}(\rho_\phi a^3) = -p_\phi \frac{d}{dt}a^3 \tag{2.11}$$

where $M_{Pl}^2 = \frac{1}{8\pi G}$ is the reduced Planck mass. It is also easy to see that the condition for inflation; $\rho + 3p < 0$ is satisfied for $V > \dot{\phi}^2$. This does not have to be the case initially, provided the potential is suitably flat and the scalar field is not at the minimum. Any curvature term in the Friedmann equation will become less important as soon as inflation starts. Even if it is not negligible from the start of inflation, the early stages of inflation will make it so, therefore $k = 0$ is a reasonable assumption.

We write the Hubble parameter $H = \left(\frac{\dot{a}}{a}\right)$ as a function of the scalar field ϕ, that is $H = H(\phi)$. This can be done if ϕ is monotonic in cosmic time. This gives another set of equations of motion:

$$\dot{\phi} = -\frac{m_{\rm Pl}^2}{4\pi} H'(\phi) \tag{2.12}$$

$$[H'(\phi)]^2 - \frac{12\pi}{m_{\rm Pl}^2} H^2(\phi) = -\frac{32\pi^2}{m_{\rm Pl}^4} V(\phi) \tag{2.13}$$

Equation (2.13) is often called the *Hamilton-Jacobi* equation [16]. The Hamilton-Jacobi formalism is introduced because it allows an easier derivation of many inflation results. It also has applications to the general inhomogeneous situatuion [2], as it is a geometric quantity, and $V(\phi)$ is not. This means inflation is more naturally described using the Hamilton-Jacobi formalism [2]. We define the slow-roll (SR) parameter $\epsilon(\phi)$ as

$$\epsilon(\phi) \equiv \frac{m_{\rm Pl}^2}{4\pi} \left(\frac{H'(\phi)}{H(\phi)}\right)^2 \tag{2.14}$$

and furthermore define

$$\sqrt{\epsilon} = +\frac{m_{\rm Pl}}{2\sqrt{\pi}} \left(\frac{H'}{H}\right) \tag{2.15}$$

Later we will define other SR-parameters. Using $\epsilon(\phi)$ allows us to rewrite the Hamilton-Jacobi equation as:

$$H^2(\phi)[1 - \frac{1}{3}\epsilon(\phi)] = \left(\frac{8\pi}{3m_{\rm Pl}^2}\right) V(\phi) \tag{2.16}$$

Using ϵ we can also rewrite (2.9) as:

$$\left(\frac{\ddot{a}}{a}\right) = H^2(\phi)\,[1 - \epsilon(\phi)] \tag{2.17}$$

As explained in chapter 2, inflation is defined as a period when $\frac{\ddot{a}}{a} > 0$. From equation (2.17) above we see that inflation will take place for $\epsilon < 1$.

2.4 Slow-roll

The following section is based mostly on [2,pages 42–56] and references therein. The common technique when studying inflation is to assume the

slow-roll (SR) approximation. This assumption simplifies the dynamic equations of inflation:

$$H^2 \simeq \frac{V(\phi)}{3M_{Pl}^2} \tag{2.18}$$

$$3H\dot{\phi} \simeq -V'(\phi) \tag{2.19}$$

where the prime denotes derivative with respect to the field ϕ. The slow-roll approximation means that we assume the field to be dominated by its potential ($V(\phi) \gg \frac{1}{2}\dot{\phi}^2$) and this to be sufficiently flat and generally well behaved. The condition $\ddot{\phi} \ll 3|H\dot{\phi}|$ ensures that $\ddot{\phi}$ is small, meaning $\dot{\phi}$ grows slowly and we can have inflation for some time. The SR-approximation is consistent if V' and $V'' << V$. For the approximation to hold we need the following conditions to be fulfilled:

$$\epsilon(\phi) \ll 1 \tag{2.20}$$

$$|\eta(\phi)| \ll 1 \tag{2.21}$$

ϵ and η are called the slow-roll parameters and are sometimes defined as

$$\epsilon_V(\phi) = \frac{M_{Pl}^2}{2}\left(\frac{V'}{V}\right)^2 \tag{2.22}$$

$$\eta_V(\phi) = M_{Pl}^2\frac{V''}{V} \tag{2.23}$$

and in this section we will use the above definiton. However, another often used definition is the following

$$\epsilon \equiv \frac{m_{\rm Pl}^2}{4\pi}\left(\frac{H'(\phi)}{H(\phi)}\right)^2 \tag{2.24}$$

$$\eta \equiv \frac{m_{\rm Pl}^2}{4\pi}\left(\frac{H''(\phi)}{H(\phi)}\right) \tag{2.25}$$

$$\sigma \equiv \frac{m_{\rm Pl}}{4\pi}\left[\frac{1}{2}\left(\frac{H''}{H}\right) - \left(\frac{H'}{H}\right)^2\right] \tag{2.26}$$

$$^{\ell}\lambda_{\rm H} \equiv \left(\frac{m_{\rm Pl}^2}{4\pi}\right)^{\ell}\frac{(H')^{\ell-1}}{H^{\ell}}\frac{d^{(\ell+1)}H}{d\phi^{(\ell+1)}} \tag{2.27}$$

which is an infinite hierarchy. For most of the thesis we will use this definition of the slow-roll parameters.

It is easily seen by substitution that equations (2.20) and (2.21) are necessary for the SR-approximation to hold. However they are not sufficient.

This is because they do not put any restrictions on the kinetic term $\dot{\phi}^2$, only on the shape of the potential $V(\phi)$. The problem with this is that the full scalar wave equation is second-order, and so the value of $\dot{\phi}$ can be chosen freely, it can even violate the SR-approximation. What saves the model is what might seem like an assumption; $3H\dot{\phi} \simeq -V'(\phi)$. This "assumption" can be proven (see section 2.4.3), and the solution, the attractor behaviour of the equations of motion, is in fact vital for the slow-roll approximation to succeed. If the SR conditions are fulfilled we will have inflation. Consider the condition for inflation (equation 2.2) rewritten as:

$$\begin{aligned} \frac{\ddot{a}}{a} &= \dot{H} + H^2 > 0 \\ \Rightarrow \quad -\tfrac{\dot{H}}{H^2} &< 1 \end{aligned}$$

Furthermore equations (2.18) and (2.19) yields

$$-\frac{\dot{H}}{H^2} \simeq \frac{M_{Pl}^2}{2}\left(\frac{V'}{V}\right)^2 = \epsilon_V \tag{2.28}$$

This means that if the slow-roll approximation is valid, i.e. $\epsilon \ll 1$, then inflation will occur. We will stress the point that inflation will occur with slow-roll, but it is not a necessary condition for inflation to take place. It is quite possible to have inflation and violate the slow-roll condition, but the amount of inflation is then usually very small.

2.4.1 Amount of inflation

During the inflationary epoch, the scale factor grows exponentially and the Universe expands vastly. The ratio between the value of the scale factor at the end of inflation and at the beginning of inflation, or some other initial time, is used as a measurement of how much the Universe expands during inflation. This ratio is usually very large and one therefore takes the logarithm of this ratio and ends up with the number of e-foldings N during inflation:

$$N(t) \equiv \ln \frac{a(t_{\text{end}})}{a(t_i)} \tag{2.29}$$

N is a measure of the amount of inflation after t_i. As seen earlier inflation can solve both the horizon and flatness problems and for that about 60 e-foldings

of inflation is needed. We see that:

$$\begin{aligned} N &\equiv \ln \frac{a_{t_{\rm end}}}{a_{t_{\rm i}}} \\ &= \int_{t_{\rm i}}^{t_{\rm end}} H(t)dt \\ &\simeq -\int_{t_{\rm i}}^{t_{\rm end}} \frac{1}{M_{Pl}^2}\frac{V(\phi)}{V'(\phi)}\frac{\dot{\phi}\,dt}{d\phi} \\ &= \frac{1}{M_{Pl}^2}\int_{\phi_{\rm end}}^{\phi_{\rm i}} \frac{V}{V'}d\phi \end{aligned} \tag{2.30}$$

Assuming $\epsilon(\phi_{\rm end}) = 1$ it is possible to find the energy scale of the scalar field during inflation. Consider the potential $V(\phi) = \lambda\phi^4$. From equation (2.22) we find $\epsilon_V(\phi)$ as:

$$\epsilon_V(\phi) = \frac{M_{Pl}^2}{2}\left(\frac{4\lambda^3}{\lambda^4}\right)^2 = \frac{8M_{Pl}^2}{\phi^2} \tag{2.31}$$

And from the assumption $\epsilon(\phi_{\rm end}) = 1$ we get:

$$\phi_{\rm end}^2 = 8M_{Pl}^2 \tag{2.32}$$

Inserting this into equation (2.30) yields:

$$\begin{aligned} N &= \frac{1}{M_{Pl}^2}\int_{\phi_{\rm end}}^{\phi} \frac{\lambda\phi^4}{4\lambda\phi^3}d\phi \\ &= \frac{1}{4M_{Pl}^2}\int_{\phi_{\rm end}=8M_{Pl}^2}^{\phi} \phi d\phi \\ &= \frac{\phi^2}{8M_{Pl}^2} - 1 \end{aligned}$$

If we then furthermore assume that inflation lasts for $N = 60$ e-foldings we can find an estimate for the energy scale when inflation starts ($\phi_{\rm start}$):

$$N = 60 \rightarrow \phi_{\rm start} \simeq 2\sqrt{120}\,M_{Pl} \simeq 20M_{Pl}$$

2.4.2 Examples of $V(\phi)$

There are many models for the inflaton potential. Some are influenced by particle physics like the Higgs-like potential:

$$V(\phi) = \lambda(\phi^2 - M^2)^2 \tag{2.33}$$

while another example of an inflaton potential is the self-interacting potential:

$$V(\phi) = \lambda\phi^4 \tag{2.34}$$

Power-law inflation corresponds to a potential of the type:

$$V(\phi) = V_0 \exp\left(-\sqrt{\frac{2}{p}}\frac{\phi}{M_{Pl}}\right) \tag{2.35}$$

We will take a brief look at one of the simplest models for the inflaton potential. Consider a massive, free scalar field which has potential:

$$V(\phi) = \frac{1}{2}m^2\phi^2 \tag{2.36}$$

where m is the mass of the scalar field. The slow-roll equations (2.18, 2.19) then yield:

$$H^2(t) = \simeq \frac{m^2\phi^2}{6M_{Pl}^2} \tag{2.37}$$

$$3H\dot{\phi} + m^2\phi = 0 \tag{2.38}$$

Furthermore we have for the SR-parameters:

$$\epsilon_V = \frac{M_{Pl}^2}{2}\left(\frac{m^2\phi}{\frac{1}{2}m^2\phi^2}\right)^2 = \frac{2M_{Pl}^2}{\phi^2} \tag{2.39}$$

$$\eta_V = M_{Pl}^2\frac{m^2}{\frac{1}{2}m^2\phi^2} = \epsilon_V \tag{2.40}$$

Using $\epsilon < 1$ as the condition to end inflation, we see that inflation takes place as long as $\phi^2 > 2M_{Pl}^2$.

The inflationary epoch will end when the field reaches an energy scale below the energy scale needed to sustain inflation. However, it is possible to have an oscillating behaviour from the field after the end of inflation and the Universe will in that case undergo a period of so-called reheating due to oscillations, decay of inflaton particles and thermalization of the decay products (see section 2.4.4). The energy density contained in the inflaton will be transferred back to conventional matter and also radiation during reheating as ϕ interacts with other fields. This oscillating behaviour can be seen from our model $V(\phi) = \frac{1}{2}m^2\phi^2$. At the opposite side of the slow-roll approximation we have

$$\ddot{\phi} \simeq -\frac{dV}{d\phi} \tag{2.41}$$

which gives

$$\begin{aligned} \ddot{\phi} + m^2\phi &= 0 \\ \Rightarrow \phi &= e^{\pm \imath m\, t} \end{aligned} \tag{2.42}$$

Since the mass m of the potential is assumed to be very small, the solution above will yield rapid oscillations of ϕ.

2.4.3 Inflationary Attractor

We hope inflation can give insight into the generation of perturbations and the overall evolution of the Universe. If inflation is to give us that insight it must be predictive, i.e. for any given point on the potential, the evolution of the scalar field has to be independent of the initial conditions. If this is not the case, any result, such as the the amplitude of density perturbations, would depend on the initial conditions, which in turn are unknowable. Unfortunately the scalar wave equation (2.10) is a second-order equation, and so, in principle, $\dot{\phi}$ can take any value anywhere on the potential, thus contradicting the requirement of a unique solution at each point of the potential. The only way inflation can be predictive is if the solutions display an attractor behaviour, i.e. all differences due to different initial conditions vanish rapidly with time. We will show that the inflationary equations actually do have an attractor behaviour [16, 17]. When we introduced the SR-approximation we also reduced the order of the inflationary equations by one. Thus an initial value of $\dot{\phi}$ is not a free parameter, but is instead determined by the slow-roll equations. If the slow-roll solution shall represent the whole single-parameter family of solutions it replaces, it must also display an attractor behaviour. The Hamilton-Jacobi formalism [16] makes it easier to show the attractor behaviour. As first shown by [16] it is sufficient to assume linear homogeneous perturbations since, classically at least, inflation generates large smooth patches. Furthermore we assume that the perturbations do not change the sign of $\dot{\phi}$, but it can be shown that the result holds under more general circumstances. Having chosen ϕ to increase with time, our task is to show that all solutions rapidly approach one another as ϕ increases. We assume $H_0(\phi)$ to be a solution to

$$\left[H'(\phi)\right]^2 - \frac{3}{2M_{Pl}^2} H^2(\phi) = -\frac{1}{2M_{Pl}^4} V(\phi) \tag{2.43}$$

either inflationary or non-inflationary. By perturbing this solution using a linear homogeneous perturbation $\delta H(\phi)$, the attractor condition will be

satisfied if $\delta H(\phi)$ becomes small as ϕ increases. Substituting $H(\phi) = H_0(\phi) + \delta H(\phi)$ into equation (2.43) and linearizing, we find:

$$\left[H_0'(\phi) + \delta H'(\phi)\right]^2 - \frac{3}{2M_{Pl}^2}\left[H_0 + \delta H\right]^2 = -\frac{1}{2M_{Pl}^4}V(\phi) \quad (2.44)$$

$$\rightarrow H_0'\delta H' = \frac{3}{2M_{Pl}^2}H_0\delta H \quad (2.45)$$

which has the general solution

$$\delta H(\phi) = \delta H(\phi_i)\exp\left(\frac{3}{2M_{Pl}^2}\int_{\phi_i}^{\phi}\frac{H_0(\phi)}{H_0'(\phi)}d\phi\right) \quad (2.46)$$

where $\delta H(\phi_i)$ is the value at some initial point ϕ_i. Since H_0' and $d\phi$ have opposite signs, the integrand within the exponential term is negative definite, and therefore all linear perturbations vanishes. Neither the assumption of linearity nor the assumption that $\dot{\phi}$ does not change sign is very restrictive. The latter can only matter if the perturbation takes the field over the top of the maximum in the potential. Otherwise it will simply roll up, reverse its direction, and pass back down through the same point. At that point it can be regarded as a perturbation on the original solution with the same sign of $\dot{\phi}$. When it comes to non-linear perturbations the solutions are more complicated, but due to the full equation only being first order it is easy to see that solutions are compelled to approach one another regardless of whether the perturbation is linear or not. One should note that the slow-roll solution is not precisely the attractor solution that all solutions to the full equations approach. The slow-roll solution is however, generally, a good approximation to the attractor solution whenever the SR-conditions are fullfilled.

2.4.4 Reheating

As inflation ends there is a transition process before the standard hot Big Bang evolution takes over. This transition process is known as reheating. Normally there are three stages to the reheating process:

1. non-inflationary scalar field dynamics

2. decay of inflaton particles, and

3. thermalization of the decay products

Scalar field oscillations

As we have described earlier (section 2.4.2), the scalar field oscillates about the minimum of the inflaton potential once inflation has ended. The oscillations are coherent, i.e. they have the same phase at all points in the large homogeneous regions created by inflation. If the only particle decay channels are into fermions there will be no rapid particle decays. The oscillating phase could then last a considerable time due to the particle decay time being much larger than the Hubble time. This phase could be described by considering the time-averaged behaviour of the scalar field. If the potential can be approximated as ϕ^2 near its minimum, the equation of motion is that of a harmonic oscillator, and the average energy $\overline{\rho_\phi} =< \dot{\phi}^2 >$ obeys the equation:

$$\dot{\overline{\rho_\phi}} + 3H\overline{\rho_\phi} = 0 \tag{2.47}$$

Remembering equation (1.10) we see that equation (2.47) is the equation for the density of non-relativistic matter and we have shown (section 1.4.1) that the energy density falls as a^{-3} for this type. This means that during the coherent oscillation phase, the decay of the amplitude of the oscillations represents a fall in the scalar field potential energy density.

Coherent inflaton decays

When the Hubble time reaches the decay time there will be decays of inflaton particles. If only fermionic decay routes are available one can introduce a phenomenological decay term $\Gamma_\phi\dot{\phi}$ into $\ddot{\phi} + 3H\dot{\phi} = -V'(\phi)$ provided it is used only on a slow-decay case and that the equation only refers to the time-averaged scalar field. This yields:

$$\dot{\overline{\rho_\phi}} + (3H + \Gamma_\phi)\overline{\rho}_\phi = 0 \tag{2.48}$$

Equation (2.48) now describes the "envelope" of the oscillations. If we instead of only having fermionic decay routes also allow the inflaton to decay into bosonic particles, we get a much more interesting situation. The bosonic decay path allows a decay by parametric resonance [18] which in many models can be broad [19, 20]. This permits an extremely rapid decay of inflaton particles, so fast that the oscillating phase ends nearly as soon as it has begun. The decays can be into a second bosonic field, or into quanta of the inflaton field itself, and the process has been termed preheating to distinguish it from the later stage of particle decay and thermalization. Parametric resonance generally generates huge occupation numbers and this helps explaining why preheating does not occur if only fermionic decay routes are allowed. The Pauli exclusion principle will prevent further decays as soon as the energy

states are filled. The occupation numbers being so huge also leaves the created bosons a long way from thermal equilibrium.

Decay and thermalization

Once parametric resonance has created the high occupation number states or, for some reason, it is ineffective, the remainder of reheating can proceed according to the standard slow-decay picture [21, 22]. The bosonic particles should decay, interact and finally reach thermal equilibrium. The details of this process will heavily depend on the field theory adopted, and the chosen field theory will in the end determine the temperature at which the Universe can be said to have reached thermal equilibrium and re-enter the standard hot Big Bang behaviour.

2.5 Quantum Generation of Pertubations

This section will discuss the quantum mechanical fluctuations that the inflaton and gravitational field undergo during inflation. These fluctuations have a possible great impact on the large-scale structure of the Universe in our epoch. Both the inflaton and metric fluctuations produce perturbations in a similar fashion, and we will therefore begin with a qualitative description of the effects of the former, followed by a calculation of both spectra and their present expected amplitudes [23], [2,pages 164–203, 333–347], [1,pages 263–287], [24].

2.5.1 Density perturbations - a qualitative discussion

As mentioned earlier, inflation provides a natural mechanism to produce density perturbations and thus generates the observed large-scale structures in the Universe today.

The inflaton field ϕ is not a classical field, but is subject to quantum fluctuations. These fluctuations cause inflation to not end at the exact same time at different points in space. Consequently the evolution of the scale factor a is unique to each point in space. In more mathematical terms one can say that a constant density perturbation $\delta\phi$ does not correspond to a constant time hypersurface.

It is thought that in addition to producing the scalar density perturbations the quantum fluctuations also give rise to gravitational waves (i.e. tensor fluctuations) and the anisotropies in the temperature distribution of the CMB.

A "normal" inflationary scenario predicts a density perturbation spectrum which is Gaussian and scale dependent. In these "normal" scenarios the inflaton field is only weakly coupled to other fields, and the models we work with in our simulations are "normal" in that sense. It is however possible to construct non-Gaussian inflationary models, i.e. inflation does not imply Gaussianity.

The fluctuations were originally thought to be of a scale-invariant (Harrison - Zel'dovich [25, 26]) form, but it was quickly realized thath this could only be an approximation as the scalar field must evolve to end inflation. This evolution leads to a scale dependence in the spectrum.

Following is a brief description of the perturbation generation mechanism. Inflation is able to generate density perturbations on large scales because the comoving Hubble radius $\frac{1}{aH}$ is decreasing during inflation. In a spatially flat, isotropic and homogeneous universe the Hubble radius H^{-1} represents the scale which no causal physical process can operate beyond.

To a first approximation everything is dragged along during expansion and thus we are chiefly interested in comoving scales when discussing large-scale structures. A given perturbation's scale compared to the Hubble radius decides the scales behaviour. Without inflation ($\ddot{a} < 0$), the comoving Hubble radius $\frac{1}{aH}$ is always increasing and any scale is therefore initially much larger than this. Thus no causal process can alter the scale's evolution. As the scale finally enters within the Hubble radius it will stay inside it forever. In a standard scenario (still no inflation), looking at the CMB anisotropies, we see large-scale perturbations at a time when they were much larger than the Hubble radius. Accordingly, no mechanism could have produced the perturbations.

With inflation any given perturbation could have a much more complicated history than outlined above. Early on during inflation, a scale can be within the Hubble radius and causal physics can modify the scale. This helps solve the horizon problem and generates homogeneity, but also sets up small perturbations. Prior to the end of inflation the scale will cross outside the Hubble radius and causal physics can no longer manipulate it. Hence the generated perturbations become "frozen in". It should be noted that long after inflation has ended, the perturbations will re-enter the Hubble radius (see figure 2.1) since the comoving Hubble radius is now increasing.

Perturbations are obviously generated on a wide range of scales, but the easiest to observe today are those that are of a size comparable to the present Hubble radius and down to a few orders of magnitude smaller.

The main point of this qualitative discussion is that inflation can generate perturbations on scales larger than the present horizon without violating

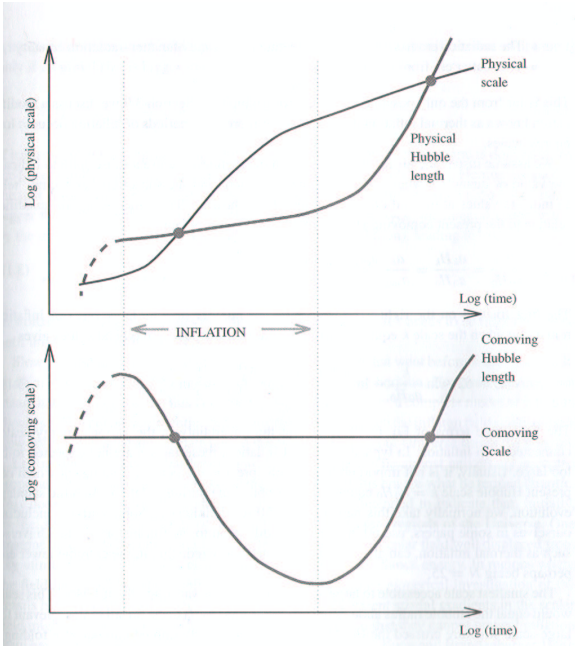

Figure 2.1: The evolution of the comoving scale k relative to the horizon scale (Hubble radius). Figure from [2]

causality.

Vacuum fluctuations and Gaussian perturbations

Classical physics predicts that the inflaton field ϕ becomes homogeneous and isotropic on scales well inside the horizon during inflation. However, this is not entirely true. Due to the quantum nature of the Universe there will be a vacuum fluctuation $\delta\phi$ in the inflaton field [2,page 59]. We will look at these fluctuations and their probability distributions. First we Fourier expand $\delta\phi$ in a comoving box with sides of comoving length L (physical length aL):

$$\delta\phi(\underline{x},t) = \sum_{\underline{k}} \delta\phi_{\underline{k}}(t) e^{i\underline{k}\cdot\underline{x}}$$

where $\underline{x}$ is related to the physical position $\underline{r}$ through $\underline{r} = a(t)\underline{x}$, and the physical wavenumber is $\frac{k}{a}$. The possible values of $\underline{k}$ form a cubic lattice with spacing

$$\Delta k = \frac{2\pi}{L}$$

Expanding inside a box imposes an artificial periodicity, but if we have a large enough box, i.e. much larger than any scale we are interested in, this

periodicity will not matter.

The inverse wavenumber $\frac{a}{k}$ defines a distance scale carried along with the expansion, which is specified conveniently by its present value $\frac{1}{k}$. If $\frac{aH}{k}$ is less than unity, a scale is said to be inside the horizon, and outside if it is bigger. The scales we are interested in leave the horizon at some epoch during inflation and re-enter it long after inflation ends. For each Fourier component $\delta\phi_{\underline{k}}(t)$ there is a vacuum fluctuation, which evolves independently of the others. A few e-foldings (Hubble times) after horizon exit, the vacuum fluctuation can be regarded as a classical quantity, with an almost constant value, which we denote $\delta\phi_{\underline{k}}(t_*)$ [2,page 60]. Many e-folds after horizon exit $\delta\phi_{\underline{k}}(t)$ may have had time to change significantly, but we are interested only in its value at the time t_*, taken to be a few e-folds after horizon exit. This is because the curvature perturbation will have become frozen-in to a constant value by then. The perturbation $\delta\phi(\underline{x},t)$ also leads to a perturbation $\delta\rho(\underline{x},t)$ in the energy density, and hence the metric of space-time. After inflation, as the inflaton field decays into conventional matter (section 2.4.4), there will be inherited perturbations $\delta\rho_i(\underline{x},t)$ in the densities of each individiual particle species. In addition there are more (and also more complicated) perturbations, but they are all determined by $\delta\phi_{\underline{k}}(t_*)$. A generic perturbation $g(\underline{x},t)$ can be Fourier expanded

$$g(\underline{x},t) = \sum_{\underline{k}} g_{\underline{k}}(t) e^{i\underline{k}\cdot\underline{x}}$$

and as long as the perturbations are small, the time dependence for a given $\underline{k}$ is given by a set of linear differential equations with no coupling between different modes $\underline{k}$ [2,page 60]. For a given $\underline{k}$-mode of any quantity, the solution of these equations is determined by $\delta\phi_{\underline{k}}(t_*)$ and the equations, being linear, yields a solution of form

$$g_{\underline{k}}(t) = T_g(t,k)\delta\phi_{\underline{k}}(t_*)$$

The transfer function $T_g(t,k)$ is fixed by the cosmological model under consideration. Physical processes, such as radiation, collisions between relativistic particles and hot and cold dark matter, influence the growth of the density perturbations, and the transfer function describes the change of the shape of the original power spectrum due to these processes [1,page 328]. Note that T_g is independent of the direction of $\underline{k}$ because the evolution equations are rotational invariant. The Fourier coefficients $\delta\phi_{\underline{k}}$, being in the quantum state, do not at any instant have well-defined values [2,page 60]. We can however expand the vacuum state in terms of states where they have well-defined values, and the probability of finding a given set of values is the

modulus squared of the relevant coefficients in the expansion. Although we apply quantum physics to describe the density perturbations, there are a few things that should be noted. In ordinary applications of quantum physics the phrase "probability of finding" can be replaced by "probability that a measurement yields", but this appears unreasonable for the Universe. Surely the density perturbation exists whether we observe it or not. Therefore one instead asserts that our Universe corresponds to a typical member of the ensemble of possible Universes obtained when we expand the vacuum state into states with a definite inflaton-field perturbation. This allows us to make definite predictions, which can be compared with observations. As is normal in ordinary quantum mechanics, we do not ponder about how a particular member (our Universe) of the ensemble has been chosen.

From quantum field theory we have that the real and imaginary parts of each component $\delta\phi_{\underline{k}}$ have the dynamics of a harmonic oscillator. In the vacuum state each real and imaginary part has a Gaussian probability distribution, with no correlation between them except for the reality condition[1] [2]. From the model of inflation one can calculate the variances (=mean squares) of the probability distributions. They are independent of the direction of $\underline{k}$, and for a given $\underline{k}$ they are the same for the real and imaginary parts. Equivalently, for a given $\underline{k}$, the phase of $\delta\phi_{\underline{k}}$ is drawn randomly from a uniform distribution. The Fourier components $g_{\underline{k}} = T_g(t,k)\delta\phi_{\underline{k}}$ of a generic distribution inherit these properties, and they define what is called a *Gaussian perturbation* [2]. It is the Fourier coefficients having independent probability distributions which makes the perturbations what mathematicians call Gaussian. In addition, the fact that the variances are independent of the direction $\underline{k}$ and are equal for the real and imaginary parts, gives the perturbations the additional property that its stochastic properties are invariant under translations and rotations. As cosmologists we take this additional property for granted, and take the term Gaussian to include it.

2.5.2 Quantitative analysis

We will now perform a more thorough quantitative analysis of the perturbation generation. It is imperative to have accurate predictions for the spectra arising from the various inflation models if we are to make full use of very

[1] In fact, nothing depends on the shapes of the probability distributions of the Fourier coefficients; what matters is their independence. The reason being that in the limit of large box size, we will sum over an infinite number of values of $\underline{k}$, within an infinitesimal cell of $\underline{k}$-space. Then, according to the central limit theorem, the probability distribution of the sum will be Gaussian for any (reasonable) probability distributions of the individual terms. Thus we lose no generality in writing the probability distributions as Gaussian.

accurate observations expected to be made in the future. The process of calculating the C_ℓ's include many subtle physical effects, but researchers are determined to calculate the spectra to within 1 percent. Since the slow-roll (SR) parameters typically are at least a few percent that means the spectra must be determined to at least one order beyond SR. In our calculations we use/apply linear perturbation theory which is considerably more accurate than the slow-roll approximation due to the anisotropies being so small. It is possible, but not necessary, to go beyond the linear approximation.

In order to avoid any possible confusion we will specify what we mean by first-order, second-order and higher-order expressions. An expression containing only terms like $\sigma\epsilon\delta$ where σ, ϵ and δ are SR-parameters, and only to the first power in any SR-parameter, is said to be of first or lowest order. An expression with terms $\sigma^2\epsilon\delta$ or $\sigma\epsilon^2\delta$ is said to be of the next-lowest order, shortened to next-order.

Perturbations and the perturbation spectrum

In the following section we will derive an expression for the scalar perturbation spectrum form the scalar perturbations. It is also possible to do the same for the gravitational wave perturbations, we will however not show the derivation here. Instead we quote the corresponding expression for the tensor perturbation spectrum and refer the eager reader to [23] or [24], as this section is based on these articles. When we are considering perturbations we divide the total space-time into a background and a perturbation part. The background is described by the RW-metric (equation 1.1) while the perturbation part is a measurement of how much the real universe deviates from this ideal background. The most general form of the line-element describing both the background and perturbations is given by [1,page 9]:

$$ds^2 = a^2(\tau)\left[(1+2A)d\tau^2 - 2\partial_i B dx^i d\tau - (1-2\Psi)\delta_{ij} + 2\partial_i\partial_j E dx^i dx^j\right] \tag{2.49}$$

Here $\tau \equiv \int \frac{dt}{a(t)}$ is conformal time and A, B, Ψ and E are quantities describing the nature of scalar perturbations. All are functions of both space and time.

Let $\delta\phi$ denote the fluctuation of the inflaton field. One can then measure the scalar perturbations through the intrinsic curvature perturbation, $\mathcal{R}$, of the comoving hypersurface:

$$\mathcal{R} = -\Psi - \frac{H}{\dot{\phi}}\delta\phi \tag{2.50}$$

where H and $\dot{\phi}$ are calculated from the background field equations. We now

introduce the gauge-invariant potential [24]:

$$u \equiv a\left[\delta\phi + \frac{\dot{\phi}}{H}\Psi\right] \tag{2.51}$$

and define a new variable

$$z \equiv \frac{a\dot{\phi}}{H} \tag{2.52}$$

One now readily see that

$$u = -z\mathcal{R} \tag{2.53}$$

If we perform a Taylor expansion of the Lagrangian about a fixed value of the scalar field, apply the background field equations and integrate by parts, we obtain the following Lagrangian:

$$\mathcal{L} = \frac{1}{2}\left[(\partial_\tau u)^2 - \delta^{ij}\partial_i u \partial_j u + \frac{z_{\tau\tau}}{z}u^2\right] \tag{2.54}$$

where a subscribt τ represents partial differentiation with respect to conformal time τ. From this we find the momentum canonical to u:

$$\pi(\tau, \underline{x}) = \frac{\partial\mathcal{L}}{\partial(u_\tau)} = u_\tau(\tau, \underline{x}) \tag{2.55}$$

So far the treatment of the perturbations and potential u have been classical. To quantize the theory we start by promoting u and π to operators, $\hat{u}$ and $\hat{\pi}$ respectively. These operators satisfy the commutation relations

$$\left[\hat{u}(\tau, \underline{x}), \hat{u}(\tau, \underline{y})\right] = \left[\hat{\pi}(\tau, \underline{x}), \hat{\pi}(\tau, \underline{y})\right] = 0 \tag{2.56}$$

$$\left[\hat{u}(\tau, \underline{x}), \hat{\pi}(\tau, \underline{y})\right] = i\delta^{(3)}(\underline{x} - \underline{y}) \tag{2.57}$$

on the hypersurface defined by τ =constant. To proceed we perform a plane wave expansion of the operator $\hat{u}$ and find

$$\hat{u}(\tau, \underline{x}) = \int \frac{d^3\underline{k}}{(2\pi)^{\frac{3}{2}}}\left[u_k(\tau)\hat{a}_{\underline{k}}e^{i\underline{k}\cdot\underline{x}} + u_k^*(\tau)\hat{a}_{\underline{k}}^\dagger e^{-i\underline{k}\cdot\underline{x}}\right] \tag{2.58}$$

The annihilation and creation operators $a_{\underline{k}}$ and $a_{\underline{k}}^*$ obey the commutation relation for bosons:

$$[\hat{a}_{\underline{k}}, \hat{a}_{\underline{l}}] = \left[\hat{a}_{\underline{k}}^\dagger, \hat{a}_{\underline{l}}^\dagger\right] = 0 \tag{2.59}$$

$$\left[\hat{a}_{\underline{k}}, \hat{a}_{\underline{l}}^\dagger\right] = \delta^{(3)}\left(\underline{k} - \underline{l}\right) \tag{2.60}$$

The Einstein action S describes the evolution of the perturbations and is given as

$$S = \int d^4x\mathcal{L} = \frac{1}{2}\int d\tau d^3\underline{x}\left[(\partial_\tau u)^2 - \delta^{ij}\partial_i u\partial_j u + \frac{z_{\tau\tau}}{z}u^2\right] \tag{2.61}$$

Taking the derivative of S with respect to u to be zero ($\frac{\partial S}{\partial u} = 0$) yields the field equations for the coefficients u_k:

$$\frac{d^2u_k}{d\tau^2} + \left(k^2 - \frac{1}{z}\frac{d^2z}{d\tau^2}\right)u_k = 0 \tag{2.62}$$

At short distances the modes $u_k(\tau)$ should reproduce ordinary flat space-time quantum field theory [27], thus we have that modes in the limit $\frac{k}{aH} \to \infty$ have form of plane waves

$$u_k(\tau) \overset{\frac{k}{aH}\to\infty}{\longrightarrow} \frac{1}{\sqrt{2k}}e^{-k\tau} \tag{2.63}$$

In the case of long-wavelength, i.e. one can neglect k, one sees that the growing mode solution of (equation 2.62) is

$$u_k \propto z \tag{2.64}$$

And in this there is no dependence on the scale factor a, except implicitly through the definition of z (equation 2.52). We claimed the perturbations could be measured by the curvature perturbation $\mathcal{R}$, therefore we need to obtain a useful expression for this. Fourier expanding $\mathcal{R}$ results in

$$\mathcal{R} = \int \frac{d^3\underline{k}}{(2\pi)^{\frac{3}{2}}}\mathcal{R}_{\underline{k}}(\tau)e^{i\underline{k}\cdot\underline{x}} \tag{2.65}$$

We now define the power spectrum $\mathcal{P}_\mathcal{R}(k)$in terms of the vacuum expectation value of $\mathcal{R}$:

$$< \mathcal{R}_{\underline{k}}\mathcal{R}^*_{\underline{l}} >= \frac{2\pi^2}{k^3}\mathcal{P}_\mathcal{R}\delta^{(3)}(\underline{k} - \underline{l}) \tag{2.66}$$

Combining equations (2.53), (2.60) and (2.65) give us an expression for the left hand side of equation (2.66)

$$< \mathcal{R}_{\underline{k}}\mathcal{R}^*_{\underline{l}} >= \frac{1}{z^2} \mid u_k \mid^2 \delta^{(3)}(\underline{k} - \underline{l}) \tag{2.67}$$

and from equation (2.66) and equation (2.67) we see that the power spectrum can be expressed as

$$\mathcal{P}^{\frac{1}{2}}_\mathcal{R}(k) = \sqrt{\frac{k^3}{2\pi^2}} \mid \frac{u_k}{z} \mid \tag{2.68}$$

2.5.3 Power-law

Power-law inflation is inflationary models with scale factor $a \propto t^p$, where $p > 1$. It can be shown that this corresponds to an inflation potential of the form [2,page 49]:

$$V(\phi) = V_0 \exp(-\sqrt{\frac{2}{p}}\frac{\phi}{M_{Pl}}) \tag{2.69}$$

where $M_{Pl} \equiv \frac{\sqrt{8\pi}}{m_{Pl}}$. As we have seen, single-field inflation models generate Gaussian spectra of purely adiabatic density perturbations (scalar perturbations) and gravitational waves (tensor perturbations). For power-law models we are able to find the exact solution for the power spectra $\mathcal{P}_{\mathcal{R}}(k)$ and $\mathcal{P}_g(k)$. We have previously shown that the scalar perturbations are given as:

$$\mathcal{P}_{\mathcal{R}}^{\frac{1}{2}}(k) = \sqrt{\frac{k^3}{2\pi^2}} \mid \frac{u_{\underline{\mathbf{k}}}}{z} \mid \tag{2.70}$$

and to find this we must first solve for $u_{\underline{\mathbf{k}}}$ from equation (2.62):

$$\frac{d^2 u_{\underline{\mathbf{k}}}}{d\tau^2} + (k^2 - \frac{1}{z}\frac{d^2 z}{d\tau^2})u_{\underline{\mathbf{k}}} \tag{2.71}$$

As $\frac{aH}{k} \to 0$ we have

$$u_k \to \frac{1}{\sqrt{2k}} \exp(-\imath k\tau) \tag{2.72}$$

It can be shown that $\frac{1}{z}\frac{d^2 z}{d\tau^2}$ can be rewritten as [2]:

$$\frac{1}{z}\frac{d^2 z}{d\tau^2} = 2a^2 H^2 \left[1 + \epsilon - \frac{3}{2}\eta + \epsilon^2 - 2\epsilon\eta + \frac{1}{2}\eta^2 + \frac{1}{2}\xi^2\right] \tag{2.73}$$

or as [23]:

$$\frac{1}{z}\frac{d^2 z}{d\tau^2} = 2a^2 H^2 \left[1 + \frac{3}{2}\delta_1 + \epsilon_1 + \frac{1}{2}\delta_1^2 + \frac{1}{2}\epsilon_1\delta_1 + \frac{1}{2H}\dot{\epsilon_1} + \frac{1}{2H}\dot{\delta_1}\right] \tag{2.74}$$

where we have used the following definitions:

$$\epsilon \equiv \frac{m_{Pl}^2}{4\pi}\left(\frac{H'}{H}\right)^2 \tag{2.75}$$

$$\eta \equiv \frac{m_{Pl}^2}{4\pi}\frac{H''}{H} \tag{2.76}$$

$$\xi \equiv \frac{m_{Pl}^2}{4\pi}\left(\frac{H'H'''}{H^2}\right)^2 \tag{2.77}$$

$$\epsilon_1 \equiv \frac{-\dot{H}}{H^2} \tag{2.78}$$

$$\delta_1 \equiv \frac{\ddot{\phi}}{H\dot{\phi}} \tag{2.79}$$

Both equation (2.73) and (2.74) are exact results. From $a \propto t^p$ we have:

$$H = \frac{\dot{a}}{a} = \frac{p}{t} \tag{2.80}$$

Let us write the Hubble-parameter as a function of the inflaton field:

$$H(\phi) = H_0 \exp(\sqrt{\frac{4\pi}{p}}\frac{\phi - \phi_0}{m_{Pl}}) \tag{2.81}$$

and this yields $\epsilon = \eta = \xi = \frac{1}{p} =$ constant when the scalar field is translated so that $\phi = \phi_0$ at the time when the scale k we are interested in obeys $k = aH$. This allows us to write equation (2.74) as:

$$\frac{1}{z}\frac{d^2z}{d\tau^2} = 2a^2H^2\left[1 - \frac{1}{2}\epsilon\right] \tag{2.82}$$

A expression for the conformal time τ is obtained using integration by parts:

$$\tau \equiv \int \frac{dt}{a(t)} \quad = \int \tfrac{da}{a^2H} = \quad -\frac{1}{aH} + \int \frac{\epsilon da}{a^2H} \tag{2.83}$$

and since ϵ is constant for power-law inflation this implies

$$\tau = -\frac{1}{aH}\frac{1}{1-\epsilon} \tag{2.84}$$

From equations (2.71), (2.74) and (2.84) we find a new equation for the perturbations:

$$\left[\frac{d^2}{d\tau^2} + k^2 - \frac{\nu^2 - \frac{1}{4}}{\tau^2}\right] u_k = 0 \tag{2.85}$$

where we have defined $\nu \equiv \frac{3}{2} + \frac{\epsilon}{1-\epsilon}$. The solution to equation (2.85) with the correct short-scale behaviour (see equation 2.72) is:

$$u_k = \frac{1}{2}\sqrt{\pi}\exp(i(\nu+\frac{1}{2})\frac{\pi}{2})(-\tau)^{\frac{1}{2}}H_\nu^{(1)}(-k\tau) \tag{2.86}$$

where $H_\nu^{(1)}$ is the Hankel function of the first kind, with order ν. Since we seek the asymptotic form of the solution, that is the behaviour of the solution long after horizon exit, we let $\frac{k}{aH} \to 0$ and find:

$$u_k \to \exp(\imath(\nu+\frac{1}{2})2^{\nu-\frac{3}{2}}\frac{\Gamma(\nu)}{\Gamma(\frac{3}{2})}\frac{1}{\sqrt{2k}}(-k\tau)^{-\nu+\frac{1}{2}} \tag{2.87}$$

here Γ is the usual gamma function, $\Gamma\frac{3}{2} = \frac{1}{2}\sqrt{\pi}$. From equations (2.87) and (2.70) we get:

$$\mathcal{P}_{\mathcal{R}}^{\frac{1}{2}}(k) = \left[2^{\frac{1}{p-1}}\frac{\Gamma\nu}{\Gamma\frac{3}{2}}\left(1-\frac{1}{p}\right)^{\frac{p}{p-1}}\right]\sqrt{\frac{p}{2}}\frac{H_1}{2\pi}\left(\frac{k_1}{k}\right)^{\frac{1}{p-1}} \tag{2.88}$$

where $H_1 = H\mid_{aH=k_1}$.

We can obtain a similar expression for the equation of motion for tensor perturbations as for the equation of motion for the scalar perturbations (2.62) [23]:

$$\frac{d^2v_k}{d\tau^2} + \left(k^2 - \frac{1}{q}\frac{d^2q}{d\tau^2}\right)v_k = 0 \tag{2.89}$$

and following the same lines as we did for scalar perturbations we obtain [23]:

$$\mathcal{P}_g^{\frac{1}{2}}(k) = 2^{\mu-\frac{3}{2}}\frac{\Gamma(\mu)}{\Gamma(\frac{3}{2})}(1-\epsilon)^{\mu-\frac{1}{2}}\left.\frac{H}{2\pi}\right|_{aH=k} \tag{2.90}$$

For power law inflation the tensor perturbations can furthermore be expressed as [23, 28]

$$\mathcal{P}_g^{\frac{1}{2}}(k) = \sqrt{\frac{2}{p}}\mathcal{P}_{\mathcal{R}}^{\frac{1}{2}}(k) \tag{2.91}$$

It might look like the expressions for scalar and tensor perturbations (2.88 and 2.91 respectively) give the value of the perturbation as it crosses the Hubble radius, but in reality it gives the asymptotic value as $\frac{k}{aH} \to 0$, rewritten in terms of the values which the quantities had at Hubble radius crossing, $\frac{k}{aH} = 1$ [24].

2.5.4 General potentials - a slow-roll approach

In this section we will derive a second-order slow-roll expression for the scalar perturbation spectrum for a general potential [23]. The exact solution found in the power-law case is used as the basis for an expansion. Instead of having constant and equal slow-roll parameters we allow them to be different and to vary with time. However, the slow-roll parameters are assumed to be small, and terms that are quadratic in ϵ, η and $\frac{\dddot{\phi}}{H\ddot{\phi}} = \frac{d\ln\ddot{\phi}}{d\ln a}$. We will follow the original work of [23] in this derivation. Therefore we use the definitions (2.78) and (2.79) for the slow-roll parameters. Furthermore this definition of the slow-roll parameters allow us to write equation (2.74) as:

$$\frac{1}{z}\frac{d^z}{d\tau^2} = 2a^2H^2\left[1 + \frac{3}{2}\delta_1 + \epsilon_1 + \frac{1}{2}\delta_1^2 + \frac{1}{2}\epsilon_1\delta_1 + \frac{1}{2}\frac{\dot{\epsilon_1}}{H} + \frac{1}{2}\frac{\dot{\delta_1}}{H}\right] \tag{2.92}$$

The conformal time τ is defined as in equation (2.83). It is then straightforward to show that equation (2.92) can be written as

$$\frac{1}{z}\frac{d^2z}{d\tau^2} = \frac{1}{\tau^2}(\nu^2 - \frac{1}{4}) \tag{2.93}$$

where

$$\nu = \frac{1 + \delta_1 + \epsilon_1}{1 - \epsilon_1} + \frac{1}{2} \tag{2.94}$$

From

$$\begin{aligned}\frac{\dot{\epsilon_1}}{H} &= 2\epsilon_1(\epsilon_1 + \delta_1)\\ \frac{\dot{\delta_1}}{H} &= \delta_1(\frac{\dddot{\phi}}{H\ddot{\phi}} - \delta_1 + \epsilon_1)\end{aligned}$$

we find that ϵ_1 and δ_1 are approximately constant for small ϵ_1, δ_1 and $\dddot{\phi}$. It is therefore possible to use the results we obtained in sections (2.5.2) and (2.5.3). Expanding equation (2.94) for small ϵ_1 yields

$$\nu \simeq \frac{3}{2} + 2\epsilon_1 + \delta_1$$

and from equations (2.66), (2.67), (2.68) and (2.87) we find, to lowest order in ϵ_1 and δ_1 [23]:

$$\mathcal{P}_{\mathcal{R}}^{\frac{1}{2}}(k) \simeq [1 + (2 - \ln 2 - b)(2\epsilon_1 + \delta_1) - \epsilon_1] \times \frac{H^2}{2\pi|\dot{\phi}|}\,|_{aH=k} \tag{2.95}$$

where b is the Euler-Mascheroni constant, meaning $2 - \ln 2 - b \simeq 0.7296$.

2.6 Spectral indices, observables and the consistency relation

Previously we have seen that during inflation, the scalar field slowly rolls down its self-interacting potential. Henceforth the Hubble parameter varies as a function of cosmic time, thus also with respect to the scale at Hubble radius crossing. Equation (2.68) for the power spectrum depend on the Hubble parameter, which makes them scale-dependent. This scale dependence is commonly expressed in terms of spectral indices n_s (scalar spectral index) and n_T (tensor spectral index), and we define them as [24]:

$$n_s(k) - 1 \equiv \frac{d\ln \mathcal{P}_\mathcal{R}(k)}{d\ln k} \tag{2.96}$$

$$n_T(k) \equiv \frac{d\ln \mathcal{P}_g(k)}{d\ln k} \tag{2.97}$$

When considering power-law inflation one often defines n_s through the equation

$$\mathcal{P}_\mathcal{R}(k) \propto k^{n_s - 1} \tag{2.98}$$

and we see that the two definitions (2.96, 2.98) coincide in this case [24]. For a more general potential we could use

$$\mathcal{P}_\mathcal{R}(k) = \mathcal{P}_\mathcal{R}(k_0)\left(\frac{k}{k_0}\right)^{\tilde{n_s}(k)-1} \tag{2.99}$$

but this definition requires a specific choice of k_0 and we see that the two definitions (2.96, 2.99) do not coincide [24]. It should also be noted that for power-law inflation the spectral indices are constant, whereas for a more general form of inflation they are generally not, i.e. there is a change in the scale dependence with wavenumber k. This is called a running of the spectral index and is normally denoted α_s and α_T for the scalar spectral index n_s and tensor spectral index n_T respectively. Furthermore they are defined as:

$$\alpha_s \equiv \frac{dn_s}{d\ln k} = \frac{d^2\ln \mathcal{P}_\mathcal{R}(k)}{d\ln k^2} \tag{2.100}$$

$$\alpha_T \equiv \frac{dn_T}{d\ln k} = \frac{d^2\ln \mathcal{P}_g(k)}{d\ln k^2} \tag{2.101}$$

It is often convenient to express the spectral indicies using the slow-roll parameters. From the lowest order expressions for the perturbation spectra (see e.g. [24, 23]), we can easily obtain the following, often used expressions

[24]:

$$n_s(k) = 1 + 2\eta - 4\epsilon \quad (2.102)$$
$$n_T(k) = -2\epsilon \quad (2.103)$$

We are able, in principle, to extract knowledge of both the spectral indices and the running of the indices from observations of the CMB. One can, given precise enough data, extend this and find a possible running of the running and so on. It is also possible to find the ratio of tensor to scalar perturbations. There are several expressions for this parameter, here we define it as

$$r \equiv \frac{C_\ell^{\text{tensor}}}{C_\ell^{\text{scalar}}} \simeq 12.4\epsilon = -6.2 n_T \quad (2.104)$$

where we assume that the Universe is perfectly matter-dominated and that only the Sachs-Wolfe effect applies (section 4.1.2) [2]. We also assume that we look at an ℓ value corresponding to scales that are sufficiently small for the curvature of the last scattering surface to be negligible and yet large enough to be well above the Hubble radius at decoupling [24]. The expression (2.104) is often called the consistency relation. Assuming single-field slow-roll inflation this equation holds regardless of the scalar-field potential and is known as the consistency equation [2,page 193].

Another definition of the tensor/scalar ratio is

$$r' \equiv \frac{\mathcal{P}_g}{\mathcal{P}_\mathcal{R}} = \epsilon \quad (2.105)$$

which is exact in the case of power-law inflation, and valid to lowest order in slow-roll [29]. Yet another, frequently encountered, definition of the tensor/scalar ratio is:

$$r'' \equiv \frac{C_2^{\text{tensor}}}{C_2^{\text{scalar}}} \quad (2.106)$$

The relation between equation (2.105) and equation (2.106) depends on the background cosmology [30]. In particular the densities of matter (Ω_m) and cosmological constant (Ω_Λ) are important. For a model with $\Omega_m \simeq 0.3$ and $\Omega_\Lambda \simeq 0.7$ the relation is approximately [30]

$$r'' \simeq 10\epsilon$$

Unfortunately there are still other choices of normalization used in the literature. In this thesis the definition (2.104) is used, unless stated otherwise.

If tensor modes are detected in future observations we are able to test the inflationary models via the consistency relation. Other theories of structure formation do not have such a relation between the scalar and tensor perturbations, e.g. if one generalize to multifield inflation, the consistency relation is replaced by an inequality [2,page 201]. The consistency relation reflects the perturbations' common physical origin; both the density perturbation and gravitational wave spectra are generated during the same inflationary period from the inflaton potential $V(\phi)$ [2,page 194].

Chapter 3

Inflationary models

There are many models for the inflationary epoch and it is customary to divide the inflation scenario into three general types of models; small-field, large-field and hybrid [30]. There is also a fourth type which exists on a boundary between small- and large-field models called linear. Small-field, large-field and linear models are so-called single-field models with one field acting, whereas a hybrid model consists of two or more fields interacting to give inflation [31, 32, 33]. These are generally harder to describe and have more parameters than the single-field models. In our work we will concentrate mostly on single-field models, but we will also present the hybrid class and mention this throughout, especially when discussing the results obtained. The different classes will be discussed in greater detail in the following sections.

The single-field potential is characterized by two independent mass scales, a "height" Λ^4, corresponding to the vacuum energy density during inflation, and a "width" μ, corresponding to the change in the field value, $\Delta\Phi$, during inflation:

$$V(\Phi) = \Lambda^4 f\left(\frac{\Phi}{\mu}\right) \tag{3.1}$$

The function f separates the different models from each other [30]. One can fix the Λ parameter by normalization to the amplitude of the large-scale CMB anisotropies, and therefore μ is the only free parameter. After normalization, the parameter space for distingushing between the different model types is, to lowest order in slow-roll, the $r - n_s$ plane. If we go to next-order in slow roll, the running of n_s, $\frac{dn}{d\ln k}$, must also be introduced. We have seen that the tensor/scalar ratio can be written as

$$r \equiv \frac{C_2^{Tensor}}{C_2^{Scalar}} \simeq 10\epsilon \tag{3.2}$$

and that when using the slow-roll parameters, the scalar spectral index can be expressed as

$$n_s = 1 - 4\epsilon + 2\eta \tag{3.3}$$

The second derivative of the potential, and therefore the relationship between ϵ and η (equations 2.24 and 2.25 respectively), distinguishes the different classes of models from each other [30].

3.1 Small-field $\eta < -\epsilon$

The small-field class of inflationary models is characterized by $V''(\phi) < 0$ early on during inflation, but could at some later point become convex ($V''(\phi) > 0$). Another constraint is $\eta < -\epsilon$. Small-field models have a generic potential of the type $V(\phi) = \Lambda^4 \left[1 - \left(\frac{\phi}{\mu}\right)^p\right]$. This can be seen as a lowest-order Taylor expansion of an arbitrary potential about the origin. These potentials could come from spontaneous symmetry-breaking such as the original models of "new" inflation [34, 35], or so-called natural inflation [36]. Since ϵ is typically close to zero in small-field models, so is the tensor spectral index (equation 2.97) and the tensor/scalar ratio (equation 3.2). Because of this, any test of the consistency relation (2.104) for inflation will be hard to perform with such models. For $p = 2$, that is $V(\phi) = \Lambda^4 \left[1 - \left(\frac{\phi}{\mu}\right)^2\right]$ we find:

$$r = 5(1 - n_s) \exp\left[-1 - N(1 - n_s)\right] \tag{3.4}$$

where N is the number of e-folds of inflation. With $p > 2$ we have the result:

$$n_s \simeq 1 - \frac{2}{N}\left(\frac{p-1}{p-2}\right) \tag{3.5}$$

The scalar spectral index is in this case independent of r. If we furthermore assume that the change in the field ($\delta\phi$) during inflation is less than the Planck scale, i.e. $\mu < m_{Pl}$, we find an upper bound on r:

$$r < 5\frac{p}{N(p-2)}\left(\frac{8\pi}{Np(p-2)}\right)^{\frac{p}{p-2}} \tag{3.6}$$

For any normal inflationary scenario ($N \simeq 60$) the tensor/scalar ratio r will be very small.

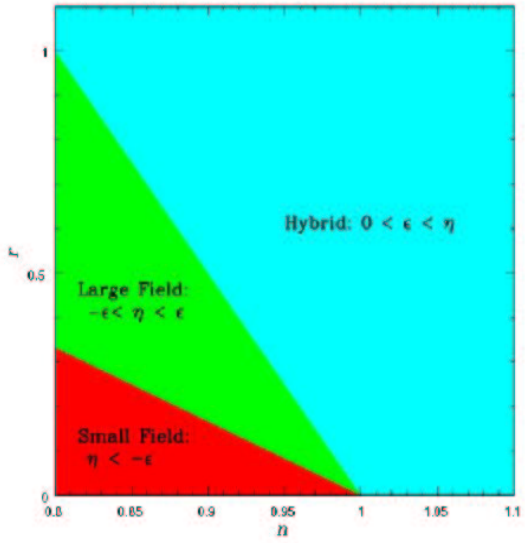

Figure 3.1: The r - n_s plane. The different types of potentials, small field, large field and hybrid, occupy different regions of the observable parameter space. Figure taken from [30]

3.2 Large-field $-\epsilon < \eta \leq \epsilon$

The models belonging to the large-field class are often so-called "chaotic" inflation scenarios [37].

When cosmological scales leave the horizon, the inflaton field is displaced from the minimum of the potential by an order of $10\,M_{Pl}$. The potential moves the field towards the minimum.

A typical example of large-field inflaton potential could be a polynomial potential

$$V(\phi) = \Lambda^4 \left(\frac{\phi}{\mu}\right)^p$$

or a exponential potential

$$V(\phi) = \Lambda^4 \exp(\frac{\phi}{\mu})$$

Large-field models have $V''(\phi) > 0$ and $-\epsilon < \eta \leq \epsilon$. As for the small-field models, we can find observational parameters for these models as well. Power-law inflation yields slow-roll parameters $\epsilon = \frac{1}{p}$ and $\eta = \frac{1}{p} = \epsilon$, both constants. Inflation takes place if $p > 1$. Due to the fact that ϵ is constant, inflation

would never end in this simple model, unless one makes some modifications. Furthermore we find the spectral indices $n_s = 1 - \frac{2}{p}$ and $n_t = -\frac{2}{p}$. The tensor/scalar ratio is given:

$$r = \frac{12.4}{p} = 6.2(1 - n_s) \tag{3.7}$$

where we use the definiton (2.104). Using the alternative definition (2.106) would give

$$r = 5(1 - n_s) \tag{3.8}$$

This is not a generic result, but only applicable to power-law models. In the power-law case we notice that observable gravitational waves are possible, unless n_s is very close to unity ($r \geq 0.1$ for $n_s \leq 0.985$).

For polynomial potentials $V(\phi) \propto \phi^p$ we find [30]

$$r = 5\left(\frac{p}{p+2}\right)(1 - n_s) \tag{3.9}$$

with the tensor/scalar ratio defined as in (3.2).

3.3 Hybrid

In hybrid inflationary models there are two fields interacting [31, 32, 33]. In addition to the ordinary slowly rolling inflaton field ϕ, we have another field ψ, which contributes to most of the energy density. The ψ-field is stabilized by ϕ in a false vacuum state, but when ϕ reaches a critical value ϕ_c, on its way towards a minimum, ψ is destabilized, and will roll towards its true vacuum state, thus ending inflation [30] (see figure 3.2).

The hybrid scenario is characterized by $V''(\phi) > 0$ and $0 < \epsilon < \eta$. A general form for the potential is $V(\phi) = \Lambda^4\left[1 + \left(\frac{\phi}{\mu}\right)^p\right]$, but as already mentioned ϕ is coupled to ψ and a total potential $V_{tot}(\phi, \psi)$ would be different. A hybrid inflation model could have a quadratic potential of the type:

$$V = \frac{1}{2}m^2\phi^2 + \frac{1}{4}\lambda\left(\psi^2 - M^2\right)^2 + \frac{1}{2}\lambda'\psi^2\phi^2 \tag{3.10}$$

where m and M are the masses assosciated with ϕ and ψ respectivly [2,page 216]. λ and λ' are coupling constants. Since the value of ϕ at the end of inflation is not determined by the inflaton field alone, we have one additional free parameter characterizing the model. This extra degree of freedom causes hybrid models to fill a large region in the $r - n_s$-plane. However, there is no

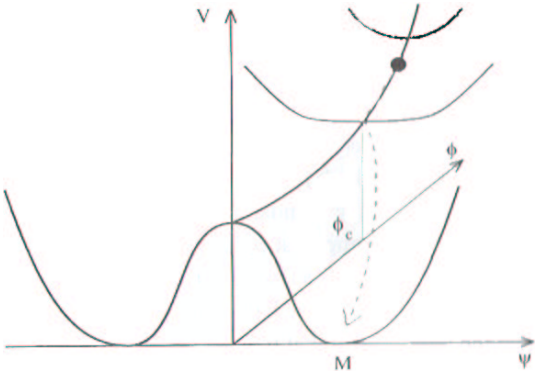

Figure 3.2: The hybrid inflation potential. The field rolls down down the $\Psi = 0$ channel, until it encounters the instability point, after which the $\Psi = 0$ solution becomes unstable and the fields roll to their true minimum at $\phi = 0$, $\Psi = \pm M$. Figure from [2]

overlap (see figure 3.1) between hybrid models and other models in this plane. If we are able to narrow down the errors on n_s and r in our observations, this could be a potentially powerful test of what class of models caused the observations. Hybrid models generally have a so-called blue spectral index, i.e. $n_s > 1$, if $\eta > 2\epsilon$, but in principle they can also have $n_s < 1$ [30]. Furthermore, hybrid models will generate isocurvature perturbations in addition to the normal adiabatic perturbations generated by single-field models. A pure isocurvature perturbation can be generated if the energy densities of the two fields add up to zero. If this happens, the primeval curvature perturbation $\mathcal{R}_{\underline{k}}$ vanishes [2,page 158]. Instead of energy fluctuations, there is a fluctuation in the entropy [1,page 328]. Since inflation ends with a phase transition in hybrid models, there is a possibility of forming topological defects, which could also prove to be a test in whether or not the model in question can be valid from observations [30].

3.4 Linear- and other models

With linear models we are referring to models that have potentials proportional to the inflaton field ϕ, i.e. $V(\phi) \propto \phi$. These have $V''(\phi) = 0$, $\eta = -\epsilon$ and are models on the bordeline between large-field models and small-field models [30]. The spectral index n_s is related to the tensor/scalar ratio (3.2) as [30]:

$$r = \frac{3}{5}(1 - n_s) \tag{3.11}$$

The categories of models we have mentioned in the last chapter certainly do not encompass all inflation models. Several single-field models do not fit this arrangement, such as logarithmic potentials $V(\phi) \propto \ln \phi$ or potentials with non-positive powers of the scalar field, $V(\phi) \propto \phi^{-p}$. These two examples require a second field to end inflation, and as such should be called hybrid models, but they reside in the small-field region of the r-n plane. The categories are complete in the sense that they cover the entire r-n_s plane (figure 3.1).

Chapter 4

The cosmic microwave background

4.1 Observations of the CMB

The cosmic microwave background (CMB) was first discovered in 1965. Two radio engineers, Penzias and Wilson [38], working with a communicating satellite project, discovered a uniform background "hiss" at microwave frequencies. They were unable to attribute this noise to any known sources. Unknown to Penzias and Wilson, Alpher and Herman [39, 40] predicted in the mid 1940's such a thermal radiation background. The cosmic microwave background is the relic of the primordial fireball phase, commonly known as the Big Bang. The CMB is the most perfect black body radiation spectrum observed in nature. Its temperature is known to be 2.725 ± 0.002K [41] over the entire sky. This near-perfect black body is seen as strong evidence for the Big Bang model.

In the following sections we describe some of the observations of the CMB, and present some important theories concerning the application of CMB observations.

4.1.1 Observing the CMB

The first observations of the CMB was made using ground- and balloon-based experiments. These first experiments were neither sensitive enough, nor able to overcome atmospheric absorbtion, to measure the CMB with great precision. But with the launch of the COBE (Cosmic Background Explorer) satellite [42] in 1989, the CMB could be measured to high precision. The COBE data showed that the microwave background is incredibly even across the whole sky, but more importantly, the data showed some small anisotropies

in the radiation. These anisotropies are very small, one part in 10^5, but they are interpreted as the seeds to the Universe we see today. For the first time, one had showed that the Big Bang theory could also result in large-scale structures. If there had not been any anisotropies in the CMB, it would have been very difficult to explain how gravitational bound objects like clusters and galaxies could have formed from the Big Bang.

During the late 1990s, several new ground- and balloon-based experiments explored the microwave background, confirming the COBE results [43, 44, 45, 46, 47]. Such experiments are clearly obstructed by being performed below the atmosphere. The observing conditions are not stable, at least not compared to space, and the earth's movement makes it hard to make observations at large scales. The ground- and balloon-based experiments must make up for the drawbacks they suffer from, compared to space-based observations, by either observing for a much longer time, by adding more detectors, or concentrating the observations on a small region of the sky. The two last options are obviously the easiest to implement, as there are few places on earth offering stable observing conditions for very long periods of time, but there is also a financial side when adding many detectors. Due to the limitations faced on ground, a new, next-generation, space-based experiment was needed. In 2001, NASA [48] launched the WMAP (Wilkinson Microwave Anisotropy Probe) satellite [49], and in 2003, the first year data [50] were made public (one is still waiting for the second-year data). The WMAP observations confirmed the anisotropies found earlier, and they were measured to a much higher sensitivity and angular resolution than COBE. The WMAP satellite has provided the first detailed full-sky map of the cosmic microwave background, and the official first year WMAP data strongly supports the so-called concordance model [51]. One could get the impression that everything about the CMB was now known. This is certainly not true, but it will become much more true in 2007, when ESA [52] launches the third-generation CMB satellite, the Planck satellite [52].

The Planck project, named after Max Planck, originally started out as two mission proposals called COBRAS (Cosmic Background Radiation Anisotropy Satellite) and SAMBA (Satellite for Measurement of Background Anisotropies), and as can be seen from the names, these two proposals had very similar objectives. Therefore COBRAS and SAMBA was merged into one mission. Beginning back in 1994, these two mission proposals were first studied by ESA and later ended up as Planck, and part of ESA's Horizon 2000 scientific program. After take-off, the Planck satellite will eventually arrive at a the 'L2' point between the Earth and the Sun. At this point in space the combined gravity from the Earth and the Sun is so that the satellite will follow Earth's rotation around the Sun. Also it will be reasonably far

away from the Sun, Earth and the Moon to avoid any undesirable emission. Using a 1.5 m primary mirror the satellite will focus received radiation onto two detectors, the Low Frequency Instrument (LFI) and the High Frequency Instrument (HFI). As their names indicate these two instruments will operate at different frequencies, but they will also perform the measurements in different ways. When measuring the CMB anisotropies, what we actually do, is to look at the temperature difference between two points on the sky. Due to the anisotropies in the CMB radiation being so small, the detectors onboard Planck will both have to be highly sensitive, and be cooled to such low temperatures that their own heat emission won't interfere with the radiation they are supposed to measure. The two instruments will work using different techniques. LFI will receive data at low frequencies, meaning between 30 GHz and 100 GHz. It is unfeasible to cover all frequencies and therefore the 22 radio receivers making up the LFI will be grouped and tuned to four frequency channels. To overcome the heat emission the LFI receivers will be cooled and operated at $-253°$ C. Other than the extreme temperature and fine-tuning, the LFI instrument works pretty much like your ordinary transistor radio.

The HFI is using another method to collect data. Designed to operate between 100 GHz and 857 GHz an array of 52 bolometric detectors will convert the received radiation to heat, and an electrical thermometer will measure the amount of heat. One easily sees that with this setup heat emission from the instrument itself will be even harder to avoid. It is therefore constructed to work at a temperature of $-272.9°$ C, just one tenth of a degree above absolute zero [53].

The Planck satellite will have a long integration time when measuring the CMB, which ensures a high sensitivity. The integration time will be approximately 30 times that of Boomerang, and 1000 times that of Archeops [54, 44, 55]. One hope, and expect, that Planck will have the capacity to map the full sky polarisation of the CMB well enough to put meaningful constraints on both EE and BB polarisation spectra [54].

Ground- and balloon-based experiments are not necessarily competing with the satellite projects. The fact is that the different methods complete each other. Being on earth, means that certain measurements are more difficult to perform than others, especially large-scale and full-sky surveys are hard to do from earth. Therefore the ground- and balloon based experiments often concentrate on very small regions of the sky and make high precision observations of these. On the other hand, satellites have easy access to the whole sky, and give us a fairly detailed overview of the full picture (see figure 4.1). Thus one get accurate observations of both large- and small-scale anisotropies.

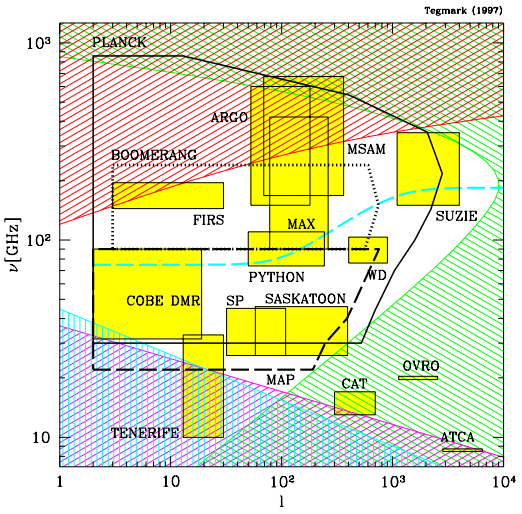

Figure 4.1: The scales and frequencies observed by the different CMB experiments. Figure obtained from [56].

4.1.2 Extracting information from the CMB

The observed temperature anisotropies are frequently expressed as

$$\frac{\delta T}{T}(\theta,\phi) = \frac{T(\theta,\phi) - T_0}{T_0} \tag{4.1}$$

which give the temperature fluctuations as fractions of the mean temperature T_0, and of angular position on the sky. It is important to realize that since the CMB originates from the early stages of the Big Bang, it will also carry the imprint of physical processes, both during, and after its production. The observed anisotropies, or level of isotropy in the CMB radiation, are important in several respects:

- The high degree of isotropy so far uncovered is strong evidence for large-scale isotropy of the Universe
- It excludes any model in which the radiation has a galactic origin or is produced by a random distribution of sources, i.e. steady-state models.
- Observations can provide information about the origin, nature and evolution of density fluctuations which are thought to give rise to galaxies and large-scale structures in the Universe

There are several sources of anisotropy; primary, secondary and "tertiary" sources [57, 58, 1]. By primary sources, we refer to physical processes occuring prior to, and at decoupling. Secondary sources are sources that influence

the CMB photons on their way between the last scattering surface and us. "Tertiary" sources are sources which are more localized and in the foreground, such as radio- or IR-point sources, processes in the galactic plane or the solar system and instrument noise. We do not discuss any "tertiary" sources in the following treatment.

We now proceed by describing some of the primary and secondary sources of anisotropy:

1. The dipole anisotropy: Due to the motion of an observer through a reference frame, in which the CMB is "at rest", i.e. the frame where the CMB appears isotropic, there exists a dipole anisotropy (a variation on a scale of 180°):

$$T(\vartheta) = T_0 \left(1 + \frac{\delta T_D}{T_0} \cos\vartheta\right) \tag{4.2}$$

   The dipole is the result of our galaxy's movement towards the constellation of Hydra-Centarus, and the measured speed ($v \approx 600\text{km/s}$) can be used to determine Ω_0.

2. If there are inhomogeneities in the distribution of matter on the surface of last scattering (see section 1.2), these can produce anisotropies by the redshift or blueshift of photons from regions of different gravitational potential. This is called the Sachs-Wolfe effect [59].

3. If the material on the last scattering surface (LSS) is moving, the Doppler effect will cause temperature fluctuations.

4. Radiation-matter coupling at the LSS may imply that dense regions are by themselves hotter than underdense regions.

5. If the material between us and the LSS is inhomogeneously distributed then inverse Compton scattering of CMB photons by free electrons in a hot intergalactic plasma may induce anisotropy. This effect is known as the Sunyaev-Zel'dovich effect [60, 61] and can be used to determine H_0.

6. The integrated Sachs-Wolfe effect (ISW) [59] is due to gravitational potential wells evolving in time along the line of sight. This introduces a redshift or blueshift to photons travelling through these wells. E.g. the well could become deeper while the photon is in it and consequently the photon will be more redshifted as it climbs out of the well than blueshifted as it entered the well, resulting in a net redshift.

7. In the case of a time-varying gravitational potential, photons travelling through this will experience a similar effect to the ISW effect usually called the Rees-Sciama effect [62]. The CMB photons travel through local gravitational sources such as galaxies and galaxy clusters on their way to us. These non-linear perturbations cause the gravitational potential to vary with time. The Rees-Sciama effect is manifested on smaller scales than the ISW.

When we observe the CMB, we see the inside of an imaginary sphere, and therefore we expand the temperature fluctuations in spherical harmonics (analogous to a Fourier expansion of a plane function). The spherical harmonics are defined as

$$Y_{\ell m}(\theta,\phi) = \sqrt{\frac{2\ell+(\ell+m)!}{4\pi(\ell+m)!}}\mathcal{P}_\ell^m(\cos\theta)e^{im\phi} \tag{4.3}$$

where $\mathcal{P}_\ell^m$ are the associated Legendre functions, and ℓ and m are integers such that $\ell > 0$ and $|m| \leq \ell$. Furthermore the spherical harmonics have the following symmetry property:

$$Y_{\ell,-m} = (-1)^m Y_{\ell m}^* \tag{4.4}$$

where $*$ denotes complex conjugation. The functions $Y_{\ell m}(\theta,\phi)$ form a complete orthonormal set on the unit sphere, and this orthonormality means that

$$\int Y_{\ell m}^*(\theta,\phi)Y_{\ell' m'}^*(\theta,\phi)d\Omega = \delta_{\ell\ell'}\delta_{mm'} \tag{4.5}$$

where $d\Omega = \sin\theta d\theta d\phi$.
We now define the multipoles $a_{\ell m}$ of the cosmic microwave background anisotropy as

$$\frac{\delta T(\underline{e})}{T} = \sum_{\ell m} a_{\ell m} Y_{\ell m}(\underline{e}) \tag{4.6}$$

where $\underline{e}$ is the unit vector in the direction we are observing. The monopole a_{00} is unobservable, and the dipole $a_{1,\pm 1}$ is the dipole anisotropy discussed earlier in this section. The rest of the multipoles, i.e. the $a_{\ell m}$'s with $\ell \geq 2$, represents the intrinsic anisotropy of the CMB.

When we later analyze the CMB, we work with the power spectrum, represented by a dataset of values C_ℓ for each mode ℓ. Some simulated power spectra can be seen in figure (6.1). The C_ℓ's are related to the multipoles $a_{\ell m}$ through

$$< a_{\ell m}^*\, a_{\ell' m'} >= C_\ell \delta_{\ell\ell'}\delta_{mm'} \tag{4.7}$$

It can be shown [2] that the multipoles can be calculated in terms of the primeval curvature perturbation $\mathcal{R}_{\underline{k}}$ (equation (2.50)) as

$$a_{\ell m} = \frac{4\pi}{(2\pi)^{\frac{3}{2}}} \int_0^\infty T_\theta(k,\ell)\mathcal{R}_{\ell m}(k) k dk \tag{4.8}$$

The transfer function $T_\theta(k,\ell)$ is independent of m due to invariance under rotation. Furthermore, we can express the spectrum of the cosmic microwave background, C_ℓ, as

$$C_\ell = 4\pi \int_0^\infty T_\theta^2(k,\ell)\mathcal{P}_\mathcal{R}(k)\frac{dk}{k} \tag{4.9}$$

$$C_\ell^{TE} = 4\pi \int_0^\infty T_\theta T_E(k,\ell)\mathcal{P}_\mathcal{R}(k)\frac{dk}{k} \tag{4.10}$$

$$C_\ell^{EE} = 4\pi \int_0^\infty T_E^2(k,\ell)\mathcal{P}_\mathcal{R}(k)\frac{dk}{k} \tag{4.11}$$

$$C_\ell^{BB} = 4\pi \int_0^\infty T_B^2(k,\ell)\mathcal{P}_\mathcal{R}(k)\frac{dk}{k} \tag{4.12}$$

$$\tag{4.13}$$

where T_E and T_B are transfer functions.
We define the correlation function of the CMB anisotropy as

$$C(\theta_{1\,2}) \equiv \left\langle \frac{\delta T(\underline{e}_1)}{T}\frac{\delta T(\underline{e}_2)}{T} \right\rangle \tag{4.14}$$

where $\theta_{1\,2}$ is the angle between $\underline{e}_1$ and $\underline{e}_2$.

Due to polarization of the CMB radiation and the possibility of gravitational waves, there are four sets of C_ℓ's. These C_ℓ's are the temperature-temperature correlation (C_ℓ^{TT}), the polarization correlation (C_ℓ^{EE}), the cross correlation between temperature and polarization (C_ℓ^{TE}), and the tensor correlation (C_ℓ^{BB}). The latter is caused by gravitational waves and is very hard to measure.

The initial density perturbations generated in the early Universe, are the result of the opposing forces of gravity and radiation. Gravity will cause over-dense regions to collapse, while radiation pressure, as long as radiation is tightly coupled to matter, will prevent structures from forming. This struggle between gravity and radiation generates acoustic oscillations in the photon-baryon plasma [54, 58], and the acoustic oscillations in turn, causes peaks and throughs in the anisotropy spatial power spectrum [54]. On scales smaller than the horizon size the original perturbations will be modified

by some transfer function. The transfer function depends on the physical processes behind the acoustic oscillations. Because of these modifications of the original perturbations, it is possible to learn about the energy density and the Hubble constant from the observed CMB anisotropies. The energy density is connected to the relative height of the acoustic peaks, and the relative height also depends on the strength of the damping term due to expansion, i.e. it is connected to the Hubble constant. The physical size of a perturbation is transformed to a angular size when we measure it on the sky, and the transformation depends on the geometry of space. Thus, also the curvature and cosmological constant can be derived from the CMB anisotropies [54].

In the following we discuss polarisation. Polarisation can only be generated at last scattering. Furthermore, the polarisation depends on the Thomson cross section upon the polarisation states of the incoming and outgoing photons, $\sigma_T \propto |\underline{\epsilon}_i, \underline{\epsilon}_i|^2$ [54]. This means that a quadrupole in radiation density at some point at last scattering creates polarisation in a direction perpendicular to that of the maximum of the quadrupole tangentially to the surface of last scattering [54]. Since polarisation is only generated from quadrupoles, measurements of polarisation can possibly be used to separate between different sources of anisotropies (monopoles, dipoles, quadrupoles), and thus hopefully remove some of the degeneracies among cosmological parameters [54].

We now define the Stokes parameters [63]. The polarisation state of any incoming transverse electromagnetic wave is completely described in a given reference frame by the four Stokes parameters I, Q, U and V:

$$I = < |E_x|^2 > + < |E_y|^2 > \tag{4.15}$$

$$Q = < |E_x|^2 > - < |E_y|^2 > \tag{4.16}$$

$$U = < E_x E_y^\dagger > + < E_y E_x^\dagger > \tag{4.17}$$

$$V = i(< E_x E_y^\dagger > + < E_y E_x^\dagger >) \tag{4.18}$$

Here E_x and E_y are Fourier components from a Fourier series in the time variable of the electrical field of a plane-wave arriving at the observer's position from the $+z$ direction [2,page 126]. In the above expressions, one also takes the average over frequency, and E_x and E_y are time-independent amplitudes [2,page 126]. Furthermore, I represents the total intensity, while Q and U describe the linearly polarised part of the radiation. The last parameter, V, describes the circularly polarised part of the radiation, and vanishes in this case, since no V-type polarisation is expected in the CMB [54].

The measured Stokes parameters depend on the given reference frame. One can transform from one frame (X, Y), to another (X', Y') [54], through

$$\begin{pmatrix} I' \\ Q' \\ U' \\ V' \end{pmatrix} = \begin{pmatrix} 1 & 0 & 0 & 0 \\ 0 & \cos 2\psi & \sin 2\psi & 0 \\ 0 & -\sin 2\psi & \cos 2\psi & 0 \\ 0 & 0 & 0 & 1 \end{pmatrix} \begin{pmatrix} I \\ Q \\ U \\ V \end{pmatrix} \tag{4.19}$$

From this transformation matrix, we see that Q and U are defined in a frame dependent way. If, for instance, we have a reflection $y \to -y$, or $x \to -x$, we see that

$$\begin{pmatrix} Q' \\ U' \end{pmatrix} \to \begin{pmatrix} Q \\ -U \end{pmatrix} \tag{4.20}$$

which is a parity transformation. The ordinary right-handed coordinate system is changed into a left-handed one [2,page 127].

If we rotate the coordinate system (X, Y) by an angle α, the combination $Q \pm iU$ transforms as

$$Q \pm iU \to e^{\mp 2i\alpha}(Q \pm iU) \tag{4.21}$$

Thus $Q \pm iU$ can be considered to be the eigenmodes of the "rotation by α" operator on the plane, associated to eigenvalues of $e^{\mp 2i\alpha}$ [54]. The eigenmodes are spin ± 2 quantities, and we can decompose them on a sphere on the basis of spin 2 spherical harmonics ${}_{\pm 2}Y_{\ell m}$ as [54]:

$$Q(\theta, \phi) \pm iU(\theta, \phi) = \sum_{\ell m} a_{\pm 2, \ell m} {}_{\pm 2}Y_{\ell m}(\theta, \phi) \tag{4.22}$$

Then the E and B polarisation fields can be expressed as

$$E = \sum_{\ell m} a^E_{\ell m} Y_{\ell m}(\theta, \phi) \tag{4.23}$$

$$B = \sum_{\ell m} a^B_{\ell m} Y_{\ell m}(\theta, \phi) \tag{4.24}$$

where

$$a^E_{\ell m} = -\frac{a_{2,\ell m} + a_{-2,\ell m}}{2} \tag{4.25}$$

and

$$a^B_{\ell m} = i\frac{a_{2,\ell m} - a_{-2,\ell m}}{2} \tag{4.26}$$

Now the intensity and polarisation of the CMB radiation is described by I, E, B and V. Furthermore, the spatial power spectrum of the intensity and

polarisation field of the CMB is given as

$$C_\ell^{XY} =< a_{\ell m}^X a_{\ell m}^{Y\dagger} >= \begin{pmatrix} C_\ell^{TT} & C_\ell^{TE} & 0 & 0 \\ C_\ell^{TE} & C_\ell^{EE} & 0 & 0 \\ 0 & 0 & C_\ell^{BB} & 0 \\ 0 & 0 & 0 & 0 \end{pmatrix} \tag{4.27}$$

All cross terms involving B vanish for parity reasons [54, 64]. Thus the intensity and polarisation power spectrum of the CMB is fully described, for each ℓ, by four quantities; C_ℓ^{TT}, C_ℓ^{TE}, C_ℓ^{EE} and C_ℓ^{BB} [54]. It is possible to calculate all four for a given model, allowing us to compare observations with theoretical models.

The polarisation signal is much weaker than the temperature anisotropies. The amplitude of the polarisation fluctuations from scalar modes are expected to be as low as one tenth of the CMB anisotropies on small scales, and relatively much lower still on large scales. The contribution from gravitational waves can be as low as an order of magnitude smaller than the scalar mode polarisation [54].

In the way pattern of peaks and troughs in the polarisation spectra is connected to cosmological parameters, it can, given a noise free experiment, tell us approximately the same as the pattern in the temperature power spectrum. But if instrument noise is dominating the polarisation spectra, we will in the future still get most of the information from the C_ℓ^{TT} data. Measurements of the polarisation spectra are required if we are to determine other inflationary parameters other than n_s and A_s. It is not possible to get constraints on e.g. the tensor/scalar ratio, or tensor spectral index n_T, from the temperature power spectrum alone. Because B-mode polarisation is only generated by tensor fluctuations, measurements of B polarisation, that is obtaining a C_ℓ^{BB} power spectrum, is the best, possibly the only, way of putting tight constraints on the inflationary parameters involving tensor fluctuations, i.e. n_T, r and eventually $\frac{dn_T}{d\ln k}$ [54].

Chapter 5

Reconstructing the inflaton potential

5.1 Introduction

Our initial intention with this project was to find a way of "reconstructing" the inflaton potential, and in this chapter we describe our findings in that respect.

The traditional approach to the task of reconstructing the inflaton potential has been to apply a perturbative framework [24], and in the following section (5.2) we describe this framework, and mention what should be possible to do, using this method. Another way of reconstructing the inflaton potential is to apply a so-called Monte Carlo reconstruction [30] method, where we use the method to produce many models with associated observables, i.e. quantities we can observe today, such as the tensor/scalar ratio r, the scalar spectral index n_s and the "running" of n_s; $\frac{dn_s}{d\ln k}$. If we put constraints, derived from observational data, on the calculated observables, we would effectively also be able to find possible inflaton potentials allowed by current cosmological observations, as the equations leading to the observables also give the evolution of the potential during inflation. The Monte Carlo reconstruction scheme is presented in detail in section 5.3, with results obtained using this method presented in section 5.5. We conclude this chapter with some discussion (section 5.6) concerning the future application of the Monte Carlo reconstruction method.

5.2 Traditional approaches to the reconstruction problem

5.2.1 The perturbative reconstruction framework

The framework of the perturbative reconstruction of the inflaton is based on a perturbation of the inflaton potential itself [24]. The basics of the framework will be described in the following. The inflaton rolls slowly down the potential $V(\phi)$ for inflation to take place, and modes leading to observable effects first crossed the Hubble radius approximately $50 - 60\, e$-foldings prior to the end of inflation. Since this crossing takes place during a relatively short period of time ($\delta N \simeq 10$) the corresponding change in the inflaton ϕ is small due to the slow roll. This means the field value ϕ in the potential $V(\phi)$ is more or less constant (ϕ_0) during crossing. The idea is then to Taylor expand the potential about this point (ϕ_0) [65, 66, 67, 68, 69], and from a set of observables [70], be able to reconstruct the shape of the potential during this period. One must realize that any observation can only give information about the potential from this small period of time (Hubble crossing), and one is thus not able to reconstruct the full potential from observations, only part of it (see figure 5.1).

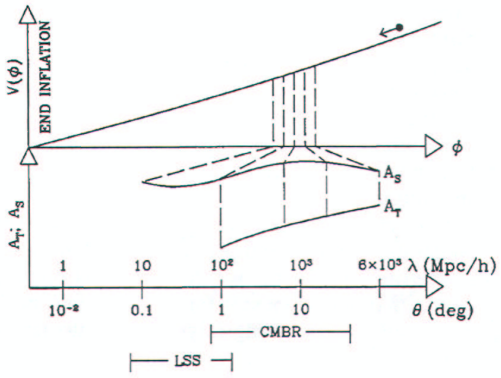

Figure 5.1: The portion of the true inflaton potential which can be accessed by observations. Figure taken from [24]

The perturbative reconstruction can be based on the slow-roll (SR) expansion (see section 2.4), and by going to higher orders in SR as the observational data improve. The dynamics (i.e. the SR-expansion) can be taken to arbitrary high order, but unfortunately the expansion of perturbations is only available to next-order [24].

Taylor expanding the potential $V(\phi)$ about the point ϕ_0 yields:

$$V(\phi) = V(\phi_0) + V'(\phi_0)\delta\phi + \frac{1}{2}V''(\phi_0)\delta\phi^2 + \dots \tag{5.1}$$

To second-order the above equation reduces the Hamilton-Jacobi equation(2.13) to

$$V(\phi) = \frac{3m_{Pl}^2}{8\pi}H^2(\phi) \tag{5.2}$$

and thus the expansion of the potential (5.1) can be expressed using the slow-roll parameters (2.18, 2.19). It then follows that the potential (5.1) can be written as:

$$V(\phi) = \frac{3m_{Pl}^2 H_0^2}{8\pi}\left[1 - (16\pi\epsilon_0)^{\frac{1}{2}}\frac{\delta\phi}{m_{Pl}} + 4\pi(\epsilon_0+\eta_0)\frac{(\delta\phi)^2}{m_{Pl}^2} + \mathcal{O}\left(\frac{(\delta\phi)^3}{m_{Pl}^3}\right)\right] \tag{5.3}$$

One must note that the subscript 0 does not refer to the present, but instead implies that quantities should be evaluated at $\phi = \phi_0$. H_0 therefore represents the expansion rate when the scale corresponding to this value of the scalar field first crossed the Hubble radius during inflation. We define the scalar and tensor power spectrum $A_s(K)$ and $A_T(k)$ as

$$A_s(k) = \frac{2}{5}\mathcal{P}_{\mathcal{R}}^{\frac{1}{2}}(k) \tag{5.4}$$

$$A_T(k) = \frac{1}{10}\mathcal{P}_g^{\frac{1}{2}}(k) \tag{5.5}$$

where $\mathcal{P}_{\mathcal{R}}^{\frac{1}{2}}(k)$ and $\mathcal{P}_g^{\frac{1}{2}}(k)$ are defined in section (2.5.3). Using the definitions of the spectra (equation 5.4 and 5.5), the slow-roll parameter definitions (equation 2.18, 2.19) and the expression for the scalar spectral index (equation 3.3) we write the coefficients in equation (5.3) as [24]:

$$V(\phi_0) = \frac{75m_{Pl}^4}{32}A_T^2(k_0) \tag{5.6}$$

$$V'(\phi_0) = -\frac{75\sqrt{\pi}}{8}m_{Pl}^3\frac{A_T^3(k_0)}{A_s(k_0)} \tag{5.7}$$

$$V''(\phi_0) = m_{Pl}^2 A_T^2(k_0)\left[9\frac{A_T^2(k_0)}{A_s^2(k_0)} - \frac{3}{2}(1 - n_{s,0})\right] \tag{5.8}$$

k_0 being the scale at which the amplitude and spectral indices are determined.

It is clear from the above equations (5.6, 5.7, 5.8) that some measurment of the gravitational-wave (tensor) amplitude must be made for the perturbative reconstruction framework to succeed. The spectra are also expanded

about k_0 in terms of $\ln \frac{k}{k_0}$:

$$\ln A_s^2(k) = \ln A_s^2(k_0) + [(n_s(k_0) - 1] \ln \frac{k}{k_0} + \frac{1}{2} \frac{dn_s}{d \ln k}|_{k_0} \ln^2 \frac{k}{k_0} + \ldots (5.9)$$

$$\ln A_T^2(k) = \ln A_T^2(k_0) + [(n_T(k_0) - 1] \ln \frac{k}{k_0} + \frac{1}{2} \frac{dn_T}{d \ln k}|_{k_0} \ln^2 \frac{k}{k_0} + . (5.10)$$

where the expansion is continued as far as observations permit, most likely to $\ln^2 \frac{k}{k_0}$ in the forseeable future. We assume that $A_s(k)$ and $A_T(k)$ can be measured over a range of scales ($\delta \ln \left(\frac{k}{k_0} \right)$), which for the scalar perturbations most likely is $-5 < \ln \left(\frac{k}{k_0} \right) < 5$, and unfortunately much shorter for the tensor perturbations. This range of scales corresponds to the range of the scalar field $\delta\phi$ accessible to observations. It is expected that $\ln \left(\frac{k}{k_0} \right)$ can be greater than unity, meaning equations (5.9) and (5.10) can only converge if the successive coefficients are smaller than 1. Since the scalar spectral index n_s seems to be close to unity [41], the SR-parameters are small (equation 2.24, 2.25), and thus the expansions (5.9, 5.10) may converge well outside the observed $\delta \ln \left(\frac{k}{k_0} \right)$. This again yields a smooth reconstruction of $V(\phi)$ about ϕ_0, and an extrapolation of $V(\phi)$ to regions beyond the observable range can be considered relatively "safe".

The expansions, and the expressions obtained from them in this section are not considered to be sufficient for the next-generation CMB experiments [24], i.e. WMAP and Planck (see chapter 4.1.1). In those cases, one must expand to higher orders in all expressions. This will not be discussed here, but an eager reader can find more information in [24].

5.2.2 Results from the perturbative reconstruction framework

The perturbative reconstruction framework depends, as we saw in the previous section, on the amplitude A_T^2 of the tensor power spectrum. No current observational datasets are sensitive enough to put meaningful constraints on this parameter, and concequently the perturbative reconstruction framework has not been utilized in any extent. To examine the potential of the method, one can use simulated datasets, and in [24] two toy models are presented. We will here briefly outline the procedure and results obtained from these toy models, and comment on the possible uses of the perturbative reconstruction framework in the future. The two toy models considered were a power-law inflation model with index $p = 21$, a choice which gives $n_s - 1 = n_T = -0.1$,

and a intermediate inflation model [71], which gives a scale-invariant spectrum of density perturbations, but still possesses significant gravitational waves [24]. The two models are of course chosen because they both have substantial gravitational waves, and hence tensor perturbations. When simulating the spectra for the two models, only multipoles up to $\ell = 200$ for the scalar perturbations and to $\ell = 40$ for the tensors, were generated. For the scalar perturbations, the error bars were consistent with cosmic variance (see Appendix 8.1), and for the tensor perturbations the error bars were chosen to reproduce the observational uncertainty in the tensor amplitude suggested by [72]. A range of $\Delta\ell = 200$ corresponds to $\Delta \ln k = 4.6$, or approximately two orders of magnitude in wavenumber k.

Ref. [24] found that for these two toy models it is still hard to get good constraints on the tensor spectral index n_T, but still the amplitude of the tensor perturbations is constrained well enough to obtain a unique reconstruction, i.e. the lowest order consistency equation (2.104) is satisfied [24]. The derived inflationary parameters are found to be consistent with the input parameters for both models, except $n_s - 1$ for the second model, and n_T for the first. The reconstructed potentials are found to be consistent with the true underlying potentials when the observational/simulated errors are taken into account [24].

The next-order reconstruction method did not improve the parameter constraints significantly compared to the lowest-order reconstruction [24]. Here we would like to note that it could be interesting to test this method using for instance simulated datasets, extending the range of wavenumber k accessible to the reconstruction process, i.e. going to higher values of ℓ. One could use scalar data up to at least $\ell = 2000$, which is expected to be measured with Planck, and tensor data possibly up to $\ell = 1000$, although the tensor contribution begin to cut of as early as $\ell \simeq 40$ [24].

It is even clearer from the use of the above toy models that the perturbative reconstruction framework is only effective as long as there is a considerable, i.e. measureable, B-mode polarisation in the real CMB. If not, it is almost impossible to get a strong handle on A_T^2 and n_T, and the perturbative reconstruction framework would fail. So far, the constraints on the tensor/scalar ratio is just $r < 0.90$ (at 95 % CL) [41], and no good constraints on n_T either. This clearly indicates that we must at least wait for Planck data before the perturbative reconstruction framework will be useful.

5.3 The Monte Carlo reconstruction formalism

One of the main objects of our project is to "reconstruct" the inflaton potential, that is the potential that drives the early period in the history of the universe through an exponential growth explained in chapter 2. It is natural to take a look at the underlying formalism used to describe such an epoch.

We use the slow-roll formalism derived in chapter 2. Remembering the infinite hiearchy of slow-roll parameters:

$$\epsilon \equiv \frac{m_{\rm Pl}^2}{4\pi}\left(\frac{H'(\phi)}{H(\phi)}\right)^2 \tag{5.11}$$

$$\eta \equiv \frac{m_{\rm Pl}^2}{4\pi}\left(\frac{H''(\phi)}{H(\phi)}\right) \tag{5.12}$$

$$\sigma \equiv \frac{m_{\rm Pl}}{4\pi}\left[\frac{1}{2}\left(\frac{H''}{H}\right) - \left(\frac{H'}{H}\right)^2\right] \tag{5.13}$$

$${}^{\ell}\lambda_{\rm H} \equiv \left(\frac{m_{\rm Pl}^2}{4\pi}\right)^{\ell} \frac{(H')^{\ell-1}}{H^{\ell}} \frac{d^{(\ell+1)}H}{d\phi^{(\ell+1)}} \tag{5.14}$$

we choose to truncate the series at $\ell = 6$. That means we assume all ${}^{\ell}\lambda_{\rm H}$ with $\ell > 6$ to be equal to 0. We see that the slow-roll parameters involve higher derivatives of H with respect to the field.

We are interested in the *evolution* of the parameters, evolution in time to be precise, and as we have seen in chapter 2, the number of e-foldings N is related to time t through the equation $N = \int_t^{t_e} H dt$, and further related to the field value ϕ during inflation (equation 2.30). Therefore N is chosen as our measure of time. From equation (2.30) it is also seen that N increases as one goes backward in time. The derivative with respect to N is related to the derivate of ϕ through (see Appendix 8.4):

$$\frac{d}{dN} = \frac{d}{d\ln a} = \frac{m_{\rm Pl}}{2\sqrt{\pi}}\sqrt{\epsilon}\frac{d}{d\phi} \tag{5.15}$$

Below we define the "flow" equations (derived in Appendix 8.4). These are equations that will give the evolution of the SR-parameters during inflation, and should therefore also tell us something about the potential through the

relation (2.16).

$$\frac{d\epsilon}{dN} = \epsilon[\sigma + 2\epsilon] \tag{5.16}$$

$$\frac{d\sigma}{dN} = 2^2\lambda_{\rm H} - 5\sigma\epsilon - 12\epsilon^2 \tag{5.17}$$

$$\frac{d\left({}^{\ell}\lambda_{\rm H}\right)}{dN} = \left[\frac{\ell-1}{2}\sigma + (\ell-2)\epsilon\right]\left({}^{\ell}\lambda_{\rm H}\right) + {}^{\ell+1}\lambda_{\rm H} \tag{5.18}$$

From equation (5.15) we have

$$\frac{d\phi}{dN} = \frac{m_{\rm Pl}}{2\sqrt{\pi}}\sqrt{\epsilon} \tag{5.19}$$

and we also find that

$$\frac{1}{H}\frac{dH}{dN} = \epsilon \tag{5.20}$$

Thus we have a set of flow equations (5.16, 5.17, 5.18, 5.19 and 5.20) which can give the inflaton potential $V(\phi)$ via the Hamilton-Jacobi equation (2.13). To obtain the inflaton potential $V(\phi)$, we must solve the flow equations for initial starting conditions. In the next section we describe the process in greater detail, but note here that the inital value of ϕ is arbitrary [73, 74], and we take it to be equal to zero. The Hubble parameter is not arbitrary, and must be normalized based on observations [75]. We apply the condition that the density fluctuatuion amplitude, as determined by a first-order slow roll expression, be of order 10^{-5} [75, 30, 23]:

$$\frac{\delta\rho}{\rho} \simeq \frac{H}{2\pi m_{\rm Pl}\sqrt{\epsilon}} = 10^{-5}$$

This is the basic theory/equations needed, so now we will go on to describe how the "flow equations" are solved and the inflaton reconstructed.

5.4 The process

The object of the process is to "reconstruct" a potential, V(ϕ). We will attempt to follow the procedure of [29, 30], were we say *"that given a path in slow-roll parameter space the form of the potential is fixed"*. The flow equations will be solved numerically from a set of initial values for the SR-parameters. Random values will be drawn for the initial conditions, uni-

formly distributed in the following intervals;

$$\begin{aligned} N_{\text{exit}} &\in [40, 70], \\ \epsilon &\in [0.0, 0.8], \\ \sigma &\in [-0.5, 0.5], \\ {}^1\lambda_{\text{H}} &\in [-0.05, 0.05], \\ {}^2\lambda_{\text{H}} &\in [-0.025, 0.025], \\ {}^3\lambda_{\text{H}} &\in [-0.01, 0.01], \\ {}^4\lambda_{\text{H}} &\in [-0.005, 0.005], \\ {}^5\lambda_{\text{H}} &\in [-0.0025, 0.0025], \\ {}^6\lambda_{\text{H}} &\in [-0.001, 0.001], \\ {}^7\lambda_{\text{H}} &= 0 \end{aligned} \tag{5.21}$$

We seek solutions that either end up with a so-called late-time fixed point ($\epsilon = {}^\ell\lambda_{\text{H}} = 0, \sigma =$ constant, note however that ${}^1\lambda_{\text{H}}$ does not have to be 0, but must be constant), or inflation ends ($\epsilon > 1$).

There is another possibility of course, the result from the integration does not give anything sensible, i.e., we integrate from a random N forward in time ($dN < 0$) until $N = 0$, and inflation neither ends nor reaches a late-time fixed point. These undesirable results will be discarded. We say that $N = 0$ when inflation ends or reaches a late-time fixed point. If inflation ends ($\epsilon > 1$), we will have to evaluate the flow equations backwards in time, that is from $N = 0$ to some $N = N_{\text{exit}}$, because scales of the order of the current horizon size exited the horizon at $N_{\text{exit}} \simeq 60$.

Now we must decide on what to do with our desirable results. We must see if they are probable in any way, that is, could they give the Universe we see today? SR-parameters are related to the observables r, $n_s - 1$ and $\frac{dn_s}{d\ln k}$ to second order in slow roll through the equations [30]:

$$r = 10\epsilon[1 - C(\sigma + 2\epsilon)] \tag{5.22}$$

$$n_s - 1 = \sigma - (5 - 3C)\epsilon^2 - \frac{1}{4}(3 - 5C)\sigma\epsilon + \frac{1}{2}(3 - C)({}^2\lambda_{\text{H}}) \tag{5.23}$$

$$\frac{dn_s}{d\ln k} = -\left(\frac{1}{1-\epsilon}\right)\frac{dn_s}{dN} \tag{5.24}$$

We find $\frac{dn_s}{d\ln k}$ to be:

$$\begin{aligned}\frac{dn_s}{d\ln k} &= -\frac{1}{1-\epsilon}\Big[(-12-\frac{31}{4}\sigma+\frac{9}{4}C\sigma)\epsilon^2-5\epsilon\sigma \\ &\quad +(2-\frac{3}{2}\epsilon+\frac{5}{2}C\epsilon+\frac{3}{4}\sigma-\frac{C}{4}\sigma)^2\lambda_{\rm H} \\ &\quad -(11+3C)\epsilon^3-(\frac{3}{4}+\frac{5}{4}C)\epsilon\sigma^2+\frac{1}{2}(3-C)^3\lambda_{\rm H}\Big]\end{aligned}$$

Where the constant C is given as $C \equiv 4(\ln 2+\gamma)-5 = 0.0814514$ and γ is Euler's constant.

It is now fairly simple to calculate the observables using our obtained SR-parameters. After calculating the observables we have to decide if it is a "desirable" result, i.e. if the observables lie within a specified "window" in parameter space. Here we take as a starting point the current best estimates for r, n_s-1 and $\frac{dn_s}{d\ln k}$ and allow for values in a range around these estimates, ending up with:

$$\begin{aligned} r &\in [0, 1.5] \\ n_s &\in [0.5, 1.5] \\ \frac{dn_s}{d\ln k} &\in [-0.05, 0.05]\end{aligned}$$

The observable parameter constraints are loose compared to e.g. WMAPdata [41]. If we end up with allowed values of observables we record those values and do the whole process as many times as needed.

To sum up the process in a few short steps it is:

1. Pick initial values for the SR-parameters.
2. Evalutate the "flow" equations forward in time until either inflation ends ($\epsilon > 1$) or inflation reaches a late-time fix point.
3. If
   - **a)** inflation ends, evaluate the "flow equations" N e-folds backward in time and calculate the observables r, n_s-1 and $\frac{dn_s}{d\ln k}$ there
   - **b)** inflation reaches a late-time fix point find the observables for that point.
4. Decide whether or not the calculated observables are in the allowed window. If they are, record the values, if not, discard them.

5. Repeat steps 1-4 as many times as wished/needed.

If we find a solution to the flow equation which gives observables in the allowed parameter space, a so-called non-trivial point, the computed potential is saved so that it is possible to examine this later. In the following section we describe the computational process in greater detail.

5.4.1 Programming

Solving the problem is relatively easy, but there are of course some obstacles to be tackled. First of all we choose to code the program in the C language. There are several methods needed to get the results we seek, and those are; a method for integrating the initial "flow" equations, a method to evolve the flow equations backwards in time, should ϵ happen to become larger than one, and thus end inflation. Furthermore we need a method for calculating the observables and determining whether they are in the specified window or not.

To do the integration we rely on a ready-to-use method from Numerical Algorithms Group (NAG) [76] called `nag_ode_ivp_rk_onestep`, which is an ordinary differential equations (ODE) solver. It takes a number of ODE's, with initial values, and evaluate the equations one time step (increasing N with dN), using a 4th order Runge-Kutta method. The integration method(`integrator`) calls the NAG-method as long as needed and the NAG-method does not return an error message. If we get an error the program must deal with it, in most cases that is to just discard the current calculation and begin over with new initial values. If ϵ gets larger than one the integration method calls another function(`backint`), which is basically the same routine, the main difference is that it integrates forwards in N, and does of course not choose random initial values as the `integrator` method does, except for the number of e-foldings N_{exit} it should integrate backwards. The other initial values are taken to be the final values of the `integrator` method. When done, `backint` calls `observables`, which do the almost obvious, calculate the observables from the final SR-parameters. The `integrator` also calls this method if, instead of $\epsilon > 1$, it reaches a late-time fixed point. After calculating the observable parameters, the `observables` function checks if the parameters are in the allowed window by making a call to the `inWindow` function. If that is the case, it adds the results to a file using a file writer subroutine and the computed potential is written to a seperate file together with the corresponding values of ϕ and N. The main function performs this whole procedure as many times as specified, i.e. until we get enough results to get good statistics.

5.5 Results

We solve the flow equations numerically for 1000000 iterations. For this first run we do not compute the potentials for each iteration, as the objective is to find how the sets of observables (n_s, r and $\frac{dn_s}{d\ln k}$) are distributed in parameter space. The 10^6 iterations result in 943721 iterations where a late-time fixed point is reached, but the observables are outside the parameter window. Approximately 16320 late-time fixed points give observables within the allowed parameter space. Furthermore there are 33775 iterations where $\epsilon > 1$, and of these 5428 give allowed observables. The remaining 6184 points are points where $|^{\ell}\lambda_H| > 100$, i.e. one or more of the higher order slow-roll parameters gets very large, and this is an unwanted behaviour as we are using approximate expressions, and the slow-roll parameters should therefore be small. These solutions are discarded.

Plotting the various parameter pairs ((n_s, r), $(n_s, \frac{dn_s}{d\ln k})$ and $(r, \frac{dn_s}{d\ln k})$) we obtain an overview of the distribution in parameter space. In figure (5.2) we see that in the $n_s - r$ plane there are allowed models in virtually the whole plane, but most lie close to $r = 0$, and values of n_s in the entire allowed range, with perhaps some predominance in the interval $n_s \in [1.1, 1.5]$. In figure (5.3) we look at r and the running of the spectral index, $\frac{dn_s}{d\ln k}$, and see that most of the models end up within a small "box" with sides $r \in [0.0, 0.1]$ and $\frac{dn_s}{d\ln k} \in [0.01, -0.03]$. It is interesting to note that so many of the models have a negative running. From figure (5.4), where we plot n_s together with $\frac{dn_s}{d\ln k}$, we see that many models have both negative running and a blue spectrum ($n_s > 1$). But still most models have no running, no significant tensor/scalar ratio, and no preferrable scalar spectral index.

After establising an overview of the parameter distribution in observable space, we change focus, and reconstruct the inflaton potential. We tighten the parameter constraints furhter, and now allow parameters in the ranges

$$\begin{aligned} n_s &\in [0.8, 1.1] \\ r &\in [0, 0.7] \\ \frac{dn_s}{d\ln k} &\in [-0.05, 0.05] \end{aligned}$$

which is in better agreement with current observational constraints [41]. With these constraints, we reconstruct 100 potentials and plot these. In figure (5.5) we have plotted the potentials with $\frac{\phi}{m_{\rm Pl}}$ along the x-axis and $\ln\left(\frac{V(\phi)}{m_{\rm Pl}^4}\right)$ along the y-axis. We observe that there are quite a lot of possible potentials allowed. We scale the potentials to have the same height at $\phi = 0$ (figure 5.6) and both same height at $\phi = 0$ and $\frac{\phi_{\rm max}}{m_{\rm Pl}} = 1$ in figure (5.7).

From these plots we observe that most of the reconstructed potentials have qualitatively the same shape.

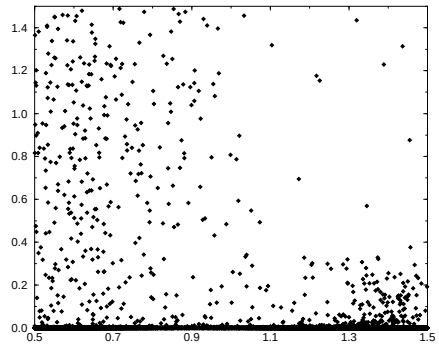

Figure 5.2: Models in the allowed parameter window. $n_s - 1$ along the x-axis and r along the y-axis

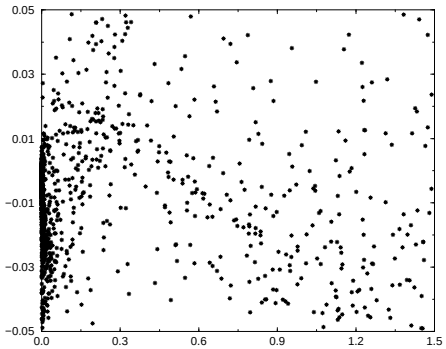

Figure 5.3: Models in the allow parameter window. r along the x-axis and $\frac{dn_s}{d\ln k}$ along the y-axis

5.6 Discussion

We have shown that the Monte Carlo reconstruction method proposed by [75] is capable of reconstructing inflaton potentials which fit current observations. It is an fairly effective method in that it takes a relatively short amount of time to produce a large number of reconstructed inflaton potentials. To

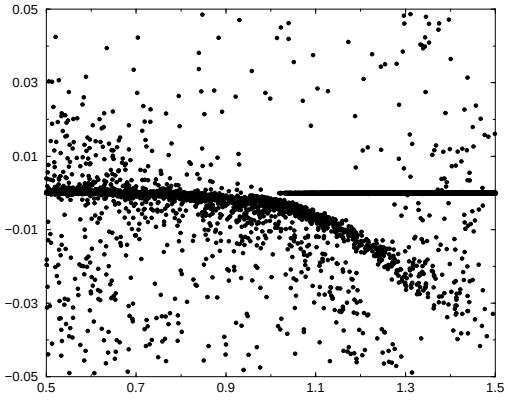

Figure 5.4: Models within the allowed parameter window. n_s along the x-axis and $\frac{dn_s}{d\ln k}$ along the y-axis

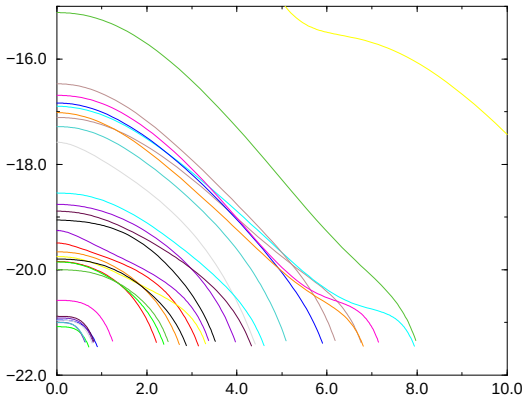

Figure 5.5: Reconstructed potentials in the parameter window $0 < r < 0.7$, $0.8 < n_s < 1.1$ and $-0.05 < \frac{dn_s}{d\ln k} < 0.05$. The x-axis is ϕ/m_{Pl} and the y-axis is $\log\left(\frac{V(\phi)}{m_{Pl}^4}\right)$

generate 1000 potentials, satisfying observational constraints, would take no more than an hour on a standard desktop computer. However, it does suffer from some possible drawbacks. One is that in itself, the method is inefficient. As we stated in the previous section, approximately 95 % of every attempted reconstruction iteration does not lead to a interesting result (other than being

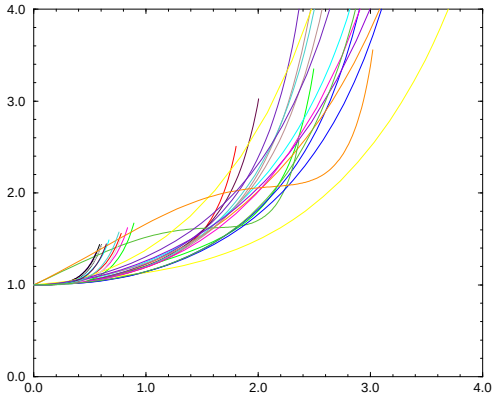

Figure 5.6: The reconstructed potentials, scaled to have the same height at $\phi = 0$. The x-axis is ϕ/m_{Pl} and the y-axis is $\left(\frac{V(\phi)}{m_{Pl}^4}\right)$

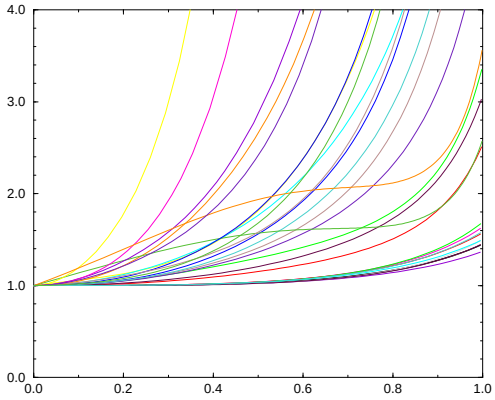

Figure 5.7: The potentials, scaled to have the same height, and all have $\frac{\phi_{\max}}{m_{Pl}} = 1$. The x-axis is ϕ/m_{Pl} and the y-axis is $\left(\frac{V(\phi)}{m_{Pl}^4}\right)$

interesting in that respect). Also a very large proportion ($\sim$ 75 %) out of all non-trivial points stem from a late-time fix point. This is not necessarily a drawback, but could instead be considered as an indication of a possible need to fine-tune the initial SR-parameters. We have not investigated this much further, but it would be interesting to see how the initial SR-parameters correlate to the observables. One could trace the evolution of the slow-roll

parameters in time, as has been done in e.g. [73, 75]. This could however be difficult and time consuming to do for a large number of non-trivial points.

The other possible drawback we will discuss here is the number of possible potentials. In figure (5.7) we see there are many different shapes and values for the reconstructed potentials, and the same can be seen in [75, 73, 30]. It is clear from figures (5.5, 5.6, 5.7) that most of the reconstructed potentials do possess a common shape, but the reconstruction method is not able to constrain the energy scale of the inflaton and its potential.

Furthermore we note that we have observed an indication of a dependence on the starting point N_{initial}. Ref. [30, 73, 74] suggest that N_{initial} be set equal to a large number, e.g. 1000, and then one evolves the flow equations forward in time until either inflation ends or a late-time fixed point is reached (or $|{}^{\ell}\lambda_H| > 100$). This typically means for $\Delta N \sim 40 - 80$. On our first attempts to implement the Monte Carlo reconstruction method we misunderstood [30], and used a starting N randomly drawn in the interval $N_{\text{initial}} \in [40, 80]$ and otherwise followed the same procedure as outlined in section (5.4). It was then noted that the ratio of late-time fixed points to $\epsilon > 1$ points was more or less the opposite of what is found when using $N_{\text{initial}} = 1000$. This could be a problem with the ODE solver we have used, and unfortunately we have not had the possibility to cross-check using another ODE solver (e.g. one from Numerical Recipies [77]). Alternatively it could be caused by the flow equations and the solutions to them, although it is not clear to us what should cause such a behaviour. There should be no dependence on the starting point N_{initial}.

There are several possible sources of error and we comment on some in the following. Obviously there is a human side, which could misinterpret the Monte Carlo reconstruction procedure altogether, but after discussions with W. Kinney [74], we are confident that our understanding of the method is correct. Furthermore, there could be errors in the software used. As can be seen in sections (5.3) and (5.4) the flow equations involve many terms, especially the ${}^{\ell}\lambda_H$ equatins. Errors could thus arise from both the derivation of these, implementation in software, and numerically when the solutions are found.

However, comparing with [30, 75, 73] we see that our results are qualitatively in agreement with the results obtained in previous works. This strengthens our confidence in that our use of the Monte Carlo reconstruction method and the results obtained are correct.

As our work in this chapter is based heavily on the article [30], we must include in our discussion some issues brought up by Liddle in [78] concerning the inflationary flow equations (5.16-5.18). We have used the flow equations to generate slow-roll inflation potentials with corresponding observables (n_s,

r, $\frac{dn_s}{dlnk}$). According to Liddle it is fundamentally wrong to use the inflationary flow equations as they are derived by Kinney and relate them to inflationary dynamics. There is actually no connection between the two according to Liddle, due to the fact that the flow equations have been derived without mentioning what Liddle considers "the main dynamical equation of inflation", the Hamilton-Jacobi equation (2.13). This equation relates the expansion rate to the potential $V(\phi)$, and should be used to determine the actual trajectories of the slow-roll parameters in parameter space. The way the flow equations are defined, through the use of the e-foldings N they are instead just measures of distance along the trajectory and the inflationary dynamics do not determine the actual shape of the trajectory. Liddle summarizes the above by saying that solving the flow equations has nothing to do with solving the inflationary equations of motion. Despite of this, the flow equations appear to correspond to inflationary models [79, 75, 30]. As we have seen the flow equations, when solved, produce a function $\epsilon(\phi)$ (or rather $\epsilon(N)$, but that can be transformed to $\epsilon(\phi)$), which is less than one as long as inflation takes place (i.e. inflation ends for $\epsilon(\phi) > 1$). Normally an inflation model is specified by $V(\phi)$ or alternatively $H(\phi)$. From the definition of $\epsilon(\phi)$ (2.14) we can obtain:

$$H(\phi) = H_i \exp\left(\int_{\phi_i}^{\phi} \sqrt{4\pi\epsilon(\phi)}\frac{d\phi}{m_{Pl}}\right) \tag{5.25}$$

and we also have (2.16):

$$V(\phi) = \frac{3m_{Pl}^2}{8\pi}H^2(\phi)[1 - \frac{1}{3}\epsilon(\phi)] \tag{5.26}$$

From this it is easy to realize that for any function $\epsilon(\phi)$ between zero and unity, it is possible to obtain a slow-roll inflation model with potential $V(\phi)$ which gives that $\epsilon(\phi)$. So what we have done, according to Liddle, is to use "a rather complicated algorithm for generating functions $\epsilon(\phi)$", and due to the constraints put on the flow equations (or the solutions of the flow equations), these "have the correct general form to be interpretted as inflationary models". But the main point remains, that the functions $\epsilon(\phi)$ do not incorporate the inflationary dynamics in themselves. In fact, if the inflationary dynamical equations changed, it would not change the trajectories in parameterspace as found by solving the flow equations. It would change the equation relating N and ϕ (5.15), but that only introduces a change of the length of the trajectories, i.e. the point corresponding to a given number of e-foldings would change. This makes it clear that the flow equations are far less responsive to changes in dynamical assumption than one would wish, one can not say

anything about the inflationary dynamics based on the flow equations alone. One should also note that due to the flow equations being "so loosely related to the inflationary dynamics" (Liddle [78]) the results obtained, specifically the way inflation models sample different regions of observable parameter space (figures 5.2, 5.4, 5.4) are not necessarily correct and there is a need for a more thorough investigation into this.

Is the Monte Carlo reconstruction of the inflaton potential a successfull and applicable method? As the current situation is concerning cosmological parameter constraints, the method suffers from its great ability to produce vast numbers of different potentials base on fairly tight parameter constraints. There are just too many possible realisations of the inflaton potential that can be found using the MonteCarlo reconstruction. It is therefore impossible to claim that *the* inflaton potential has been found. However, future data could possibly put such tight constraints on r, n_s and $\frac{dn_s}{d\ln k}$ that the number of possible potentials get reduced dramatically, and perhaps a dependence on initial slow-roll parameters can be found. If that is the case, the Monte Carlo reconstruction method might be able to tell us something about the real inflaton potential given that some of the issues brought up in [78] and discussed above can be resolved.

Chapter 6

Excluding models

6.1 Introduction

Thrilled by the success of the WMAP-satellite [49], one can imagine that some time in the future we will have instruments providing new data, with higher accuracy. One can even imagine datasets with no errors, that is perfect instruments, measuring perfectly at all scales, and one is able to subtract all foregrounds and non-CMB sources contributing to the observed data. This situation will unfortunatley always be restricted to our imagination, but we can simulate such perfect datasets. Perfect datasets are easier to work with, as there are many factors one does not have to consider, and in our analysis we use such simulated datasets.

A cosmological model has a number of parameters determining its evolution. The complexity of the model determines, in most cases, the number of parameters needed to describe it. The standard model used to satisfactorily describe current observations, have 7 base parameters [80]. As observations improve in the future it might be necessary to add more parameters to find a model which satisfactorily describes the observed data.

Naively one may then think that it is a simple matter of fitting parameters in our models until you find a set of parameters that give you exactly the observed, perfect power spectrum. However, the fact is that no matter how well we measure, the end result will always have an associated error. Errors which are impossible to overcome.

These errors in the data are called cosmic variance, and arise from the fact that we only observe one realisation of the whole universe. That is, if we believe the observable universe to be a part of a stochastic process, and we do, then what we see is of course just the outcome of one of these possible random processes. We get a random value for the observables, and can't say

for certain how "true" that value is. An analogy could be to throw dice. From just one result you can't say anything about the statistical outcome of many throws. This cosmic variance is most significant at large scales, i.e. when we measure temperature correlation between points separated by large distances. The cosmic variance is (see the appendix 8.1):

$$\sigma^2_{C_\ell} = C_\ell^2 \frac{2}{2\ell+1} \tag{6.1}$$

and we clearly see that for the low multipoles, e.g. $\ell \leq 10$, the variance is of the same order of magnitude as the measured C_ℓ. It is therefore more difficult to say whether a measured C_ℓ for low ℓ is contradicting the model, or if it is just due to the cosmic variance. On the other hand, for C_ℓ's measured at high ℓ the variance is much smaller, and a measured value does not have to deviate much from a model value before we can conclude that something is wrong with the model.

6.2 Simulation of data

We wish to examine the possibility of discriminating between different classes of classes of inflationary models (see chapter 3) based on CMB data. Currently this is not possible, as the errorbars on the cosmological parameters of interest, n_s and r, are too large [41]. Therefore we will use simulated datasets since they allow us to effectively control the level of noise in the power spectra. Concequently we choose to have noise-free data, not very realistic, but easier to both generate, and work with. We use the software package `CAMB` [81] to generate the power spectra for the models we wish to investigate. `CAMB` enables us to produce power spectra for a given cosmological model within a minute using a reasonable fast workstation. The input to `CAMB` is values for the parameters used in the cosmological model, and in table (6.1) we list the input parameters used in our simulations.

From the input data `CAMB` produces the power spectra (C_ℓ^{TT}, C_ℓ^{TE}, C_ℓ^{EE} and, if desired, C_ℓ^{BB}), using a parameterization of the curvature perturbation spectrum (equation 2.68) and gravitational wave spectrum (equation 2.90):

$$\mathcal{P}_\mathcal{R}(k) = \mathcal{P}_{\text{amp}} \left(\frac{k}{k_*}\right)^{(n_s - 1 + \frac{\alpha_s}{2}\ln\left(\frac{k}{k_*}\right))} \tag{6.2}$$

$$\mathcal{P}_g(k) = \mathcal{R}\mathcal{P}_{\mathcal{R}_{\text{amp}}} \left(\frac{k}{k_*}\right)^{n_T} \tag{6.3}$$

$$\tag{6.4}$$

Parameter	Value	Min (MCMC analysis)	Max (MCMC analysis)
$\Omega_b h^2$	0.022	0.005	0.1
$\Omega_{cdm} h^2$	0.12	0.01	0.99
Ω_Λ	0.7102		
Ω_m	0.2898		
τ	0.092	0.01	0.8
$z_{\rm re}$	12		
Age (Gyr)	13.59		
H_0	70		
$\log[10^{10}\, A_s]$		2.7	4.0
n_s	0.96	0.5	1.5
n_T	-0.04	-0.1	0.1
r	0.248	0	2
$\frac{dn_s}{d\ln k}$	0	-0.1	0.1

Table 6.1: Input parameters used in `CAMB` when simulating CMB power spectra. The power spectra are calculated to $\ell = 2500$.

where $\mathcal{R} = \frac{\mathcal{P}_\mathcal{R}(k)}{\mathcal{P}_g(k)}$ and $\mathcal{P}_{\rm amp}$ is the amplitude of the scalar power spectrum. The other symbols are k_* which is a pivot scale taken to be $k_* = 0.05\,\mathrm{Mpc}^{-1}$. Furthermore, n_s is the scalar spectral index (equation 2.96), α_s is the running of n_s (equation 2.100), and n_T is the tensor spectral index (equation 2.97).

As a special case we consider power-law inflation, and therefore substitute the above expressions, (6.2) and (6.3), with the exact expressions found in section (2.5.3):

$$\mathcal{P}_\mathcal{R}^{\frac{1}{2}}(k) = \left[2^{\frac{1}{p-1}} \frac{\Gamma(\frac{3}{2} + \frac{1}{p-1})}{\Gamma(\frac{3}{2})} \left(1 - \frac{1}{p}\right)^{\frac{p}{p-1}}\right] \sqrt{\frac{p}{2}} \frac{p^{\frac{p}{p-1}}}{2\pi} \left(\frac{1}{k}\right)^{\frac{1}{p-1}} \tag{6.5}$$

for the curvature perturbation spectrum and

$$\mathcal{P}_g^{\frac{1}{2}}(k) = \sqrt{\frac{2}{p}} P_R^{\frac{1}{2}}(k) \tag{6.6}$$

giving the gravitational wave spectrum. In equation (6.5) we have used that $H = \frac{p}{t}$, $a = t^p$ and $k_* = a_* H_*$. The power-law model can, given the right choice of p, produce power spectra similar to those observed with the WMAP satellite. This does not mean that the power-law model is a good model for our Universe, other observations and properties can rule it out; most importantly the fact that power-law inflation never ends.

The power spectra produced by CAMB does not take into account cosmic variance, and we therefore use a seperate program to introduce a χ^2-distribution to the computed C_ℓ's (see Appendix 8.1). In figure (6.1) one can see a set of power spectra (total C_ℓ) from different cosmological models, created using CAMB, whereas in figure (6.2) we see one of the model's power spectrum both with and without cosmic variance included. As already mentioned in section (6.1), the cosmic variance is clearly largest at low values of ℓ.

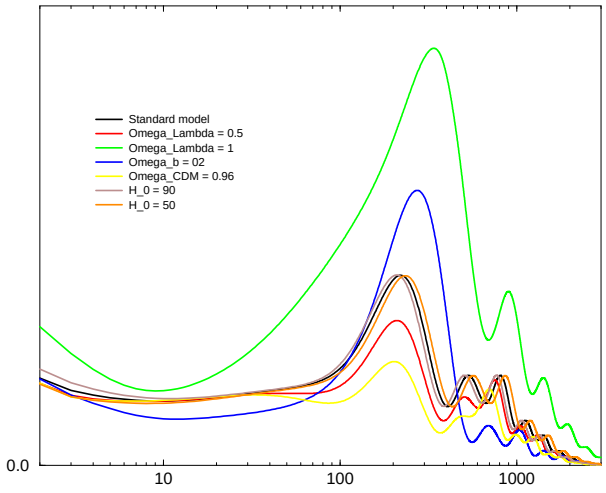

Figure 6.1: A log-linear plot of various power spectra created using CAMB. The x-axis is ℓ, and the y-axis shows the temperature fluctuations δT in μK. See table (6.2) for input parameters.

COSMOMC [82], the software program we for analysis of the simulated data, has built in support for a full-sky power spectrum format, all_l_exact [83], and we utilize this function in our work. In CAMB we therefore set the parameters scalar_amp(1) $= 2.3e-9$ and CMB_outputscale $= 7.4311e12$ as suggested by [83]. This give the value of each C_ℓ in μ K. Furthermore, the all_l_exact data format supported in COSMOMC should allow for the inclusion of C_ℓ^{BB} data as well, but it has proved impossible to get this to work despite much correspondance with Antony Lewis, one of the creators of COSMOC [84, 83]. In this respect, it should be noted that A. Lewis has not tried to use data containing B-mode polarisation himself [84], and our findings should be taken

Parameter	Standard model	$\Omega_\Lambda = 0.5$ model	$\Omega_\Lambda = 1$ model	$\Omega_b = 0.2$ model
$\Omega_b h^2$	0.022	0.023	$9.8e-3$	0.098
$\Omega_{CDM} h^2$	0.12	0.22	0	0.049
Ω_Λ	0.71	0.5	0.98	0.7
H_0	70	70	70	70
Parameter	$\Omega_{CDM} = 0.96$ model	$H_0 = 90$ model	$H_0 = 50$ model	
$\Omega_b h^2$	0.023	0.022	0.022	
$\Omega_{CDM} h^2$	0.467	0.12	0.12	
Ω_Λ	0	0.71	0.71	
H_0	70	90	50	

Table 6.2: Parameters used when calculating the power spectra in figure 6.1. Only parameters which are different among the models are listed, the remaining input parameters are the same as in table 6.1

as an indication to check the software for any possible bugs[1].

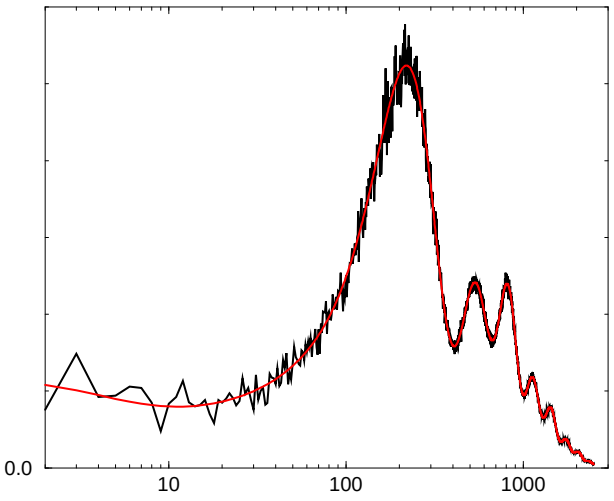

Figure 6.2: A cosmological model calculated using `CAMB`, shown with and without cosmic variance included. log-linear plot, ℓ along the x-axis, the temperature fluctuations δT in μK along the y-axis.

[1]We have already discovered one bug other than the possible bug mentioned here, but the former has been corrected [84].

In figure (6.3) we see some of the present observations of the power spectrum and readily see that the error bars for these experiments far exceed the cosmic variance. Future observations will probably have noise-error bars smaller than the cosmic variance limit, at least for $\ell < 400$.

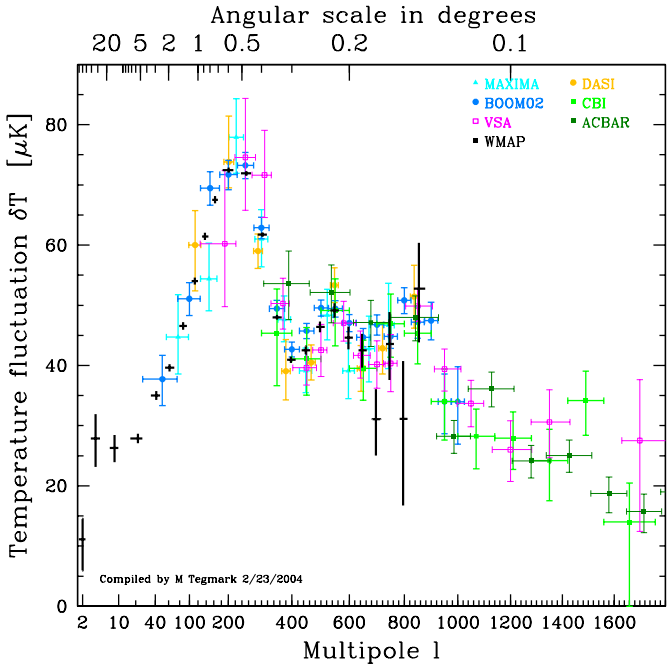

Figure 6.3: The measured temperature power spectrum from various CMB experiments. Figure taken from [56].

In the following analysis we will explore the possibility of model exclusion, meaning, given good enough data, can we say that the observed data must be from a specific model or model class?

6.3 A Markov Chain Monte-Carlo exploration of cosmological parameter space

The MonteCarloMarkovChain (MCMC) method is used as a way to simulate posterior distributions [85]. In our work we use the computer package `COSMOMC` [86, 82], which apply MCMC to simulate observations from the posterior distribution $\mathcal{P}(\theta|\tilde{C}_\ell)$. Here θ is a set of cosmological parameters, and

the event $\tilde{C}_\ell$ is the observed power spectrum (chapter 4.1.2). The simulated observations are obtained from Bayes theorem:

$$\mathcal{P}(\theta|\tilde{C}_\ell) = \frac{\mathcal{P}(\tilde{C}_\ell|\theta)\mathcal{P}(\theta)}{\int \mathcal{P}(\tilde{C}_\ell|\theta)\mathcal{P}(\theta)d\theta} \tag{6.7}$$

In the expression above, the quantity $\mathcal{P}(\tilde{C}_\ell|\theta)$ represents the likelihood of event $\tilde{C}_\ell$, given the parameters θ. Furthermore, $\mathcal{P}(\theta)$ is the prior probability distribution.

In `COSMOC`, the Metropolis-Hastings[2] (MH) algorithm [86] is used to generate samples from the posterior distribution. The generated samples will represent a "fair" sample of the likelihood surface [85], and from this sample it is possible to estimate all quantities of interest about the posterior distribution (mean, variance, confidence levels).

The MarkovChain (MC) will move from one position θ_1, i.e. one specific set of parameters, to a new point θ_2, with a transition probability $T(\theta_1, \theta_2)$ [86]. The transition probability, also called the transition kernel, is designed so that the MC after some time will approach a stationary asymptotic distribution $\mathcal{P}(\theta)$[3], where $\mathcal{P}(\theta)$ is the distribution we want to sample from. In loose terms one can say that $\mathcal{P}(\theta)$ is the parameter distribution which give sensible parameters, or a parameter distribution that fits the observed data well.

There is a fundamental problem with the MCMC method in that not all areas of the target distribution will be covered by a finite chain, i.e. not all parameter combinations will be tested. It is therefore crucial to have good mixing (see section 6.5.1). One will not get correct results if one try to use a chain which has not fully explored the likelihood surface [85].

The way to ensure that the chain will approach $\mathcal{P}(\theta)$, is to use a proposal density distribution $q(\theta_n, \theta_{n+1})$ such that the proposed new point θ_{n+1}, given the current position θ_n, is accepted with probability:

$$\alpha(\theta_n, \theta_{n+1}) = \min\left\{1, \frac{\mathcal{P}(\theta_{n+1})q(\theta_{n+1}, \theta_n)}{\mathcal{P}(\theta_n)q(\theta_n, \theta_{n+1})}\right\} \tag{6.8}$$

The transition kernel is then written as

$$T(\theta_n, \theta_{n+1}) = \alpha(\theta_n, \theta_{n+1})q(\theta_n, \theta_{n+1}) \tag{6.9}$$

[2]Other methods can also be used, but we do not consider them here. For more information see e.g. [87, 88]

[3]By after some time, we mean the burn-in time of a chain. After burn-in all further samples can be thought of as coming from the stationary distribution$\mathcal{P}(\theta)$ [85]

and this ensures that the detailed balance holds [86]:

$$\mathcal{P}(\theta_{n+1})T(\theta_{n+1},\theta_n) = \mathcal{P}(\theta_n)T(\theta_n,\theta_{n+1}) \tag{6.10}$$

and $\mathcal{P}(\theta)$ is the equilibrium distribution of the chain [86].

It is obvious from the above, that the choice of proposal density is important. The specific choice of proposal density affects the performance of the Metropolis Hastings algorithm [86]. Therefore it is best to have a proposal density which is of similar shape to the posterior. If this is the case, then large changes are proposed to parameters along the degeneracy directions [86]. If we furthermore only change a subset of the parameters for each step, we will have a faster piecewise movement around parameter space [86]. The parameter set θ can be divided in the so-called fast and slow parameters. The theoretical C_ℓ power spectra are computed using `CAMB` [89, 90], and parameters governing the perturbation evolution, such as Ω_b and Ω_c, are computationally intensive to change, and belong to the slow parameters. The fast parameters are those that govern the initial power spectra of the scalar and tensor perturbations, i.e. n_s, n_T, A_s etc. It is quickly done to vary these, once the transfer function for each wavenumber has been computed [86].

It is also clear that the choice of base parameters θ is important. We want to use a set of parameters where the parameters have essentially orthogonal effects on the angular power spectrum. If such a parameter set is found, it will reduce the degeneracies in the MCMC and also speed up convergence and improve mixing [85]. We choose our base parameters to be the baryon density $\Omega_b h^2$, cold dark matter density $\Omega_c h^2$, optical depth τ, scalar spectral index n_s, tensor spectral index n_T, running of the scalar spectral index $\frac{dn_s}{d\ln k}$ and the tensor/scalar ratio r. Furthermore the power spectrum amplitude parameter $\ln A_s$ is used. Because the small scale amplitude of C_ℓ is determined by $A_s e^{-2\tau}$, the power spectrum amplitude is very well constrained in linear combination with the optical depth τ [91]. We do not use the Hubble parameter H_0 as a base parameter, but instead derive it from the base parameter θ_r. The parameter θ_r is defined as the approximate ratio of the sound horizon at last scattering to the angular diameter distance at last scattering [85, 91], and θ_r is very well constrained by the position of the acoustic peaks [91].

The choice of base parameters has an effect on the prior; different choices of base parameters can lead to changes to the posterior constraints [86]. We have however not investigated how a possible change in base parameters would affect our results in this thesis.

We now sum up how the MCMC method is implemented in `COSMOMC`:

1. Assume a cosmological model to be tested. We assume a flat, adiabatic ΛCDM model where neutrinoes are massless, and general relativity holds. From the simulated data we wish to constrain the base parameters mentioned above.

2. `COSMOMC` will start a random walk in parameter space: from the base parameter set θ choose initial parameters θ_1, then compute, using `CAMB`, the power spectra $C_\ell^{1\text{theory}}$ and calculate the corresponding likelihood $\mathcal{L}_1 = \mathcal{L}(C_\ell^{1\text{theory}} \,|\, \tilde{C}_\ell)$ (see appendix (8.3)), where $\tilde{C}_\ell$ are the observed/simulated power spectra.

3. The MCMC method takes a random step and find a new set of parameters, θ_2.

4. From θ_2, the power spectra $C_\ell^{2\text{theory}}$ and likelihood $\mathcal{L}_2$ is computed.

5. According to expression (6.8), the new point is either accepted or rejected.

6. If point is accepted, it is added to the chain and step 2 is started over with $\theta_1 \to \theta_2$. If the new point is rejected, step 2 is repeated, but the parameter set θ_1 is saved as part of the chain.

Step 3-6 is repeated as long as necessary, i.e. until the chain has enough samples to provide reasonable samples from the posterior distributions [85].

6.3.1 Analysis pipeline

In this section we describe the analysis pipeline we ideally would use for analyses of the simulated CMB data. The pipeline has some similarities with a pipeline suggested in [92], though the latter is aimed at testing slow-roll inflation in particular.

The first step in our pipeline is to analyse the CMB data with respect to a scale-invariant power spectrum, i.e. $n_s = 1$, $n_T = r = \alpha_s = 0$, and only the background cosmological parameters are allowed to vary. The next step is to check the data using a scale-variant model, but no tensors or running of the scalar spectral index. After the second step, one should compare the results from the two steps to see if the parameter estimates have changed, and what the likelihood values for the two analyses are. Based on a information criterion (see section 6.5.3), one must decide whether the data requires the introduction of a new parameter or not. If no, the data is consistent with the simplest model, and there is not much more to do. If the data supports the introduction of the new parameter, one goes to step 3 and let n_T and

r also be free parameters. If the data also supports these parameters, that is the information criterion says the new model is a better fit to the data than the old, one can go one step further and include a running of the scalar spectral index, then a running of the tensor spectral index, and so on. At some point, the information criterion used will say that no more parameters are needed to accurately describe the data, and a set of best fit parameters has been found. The required number of steps in this pipeline depends on the quality of the CMB data.

To accuratley describe the WMAP data, no more than 7 base parameters are needed [80], i.e. only two steps in our pipeline are needed to determine the best-fit parameters for the WMAP data. However, as the CMB measurements improve, it is *expected* that this rather simple model will be insufficient, and more steps in the pipeline are needed. This will of course increase the amount of time and CPU capacity needed.

6.4 Results

Following the procedure outlined in section (6.2), we have generated power spectra for a power-law model with power index $p = 50$, and for a model using the standard CAMB equations. For the latter we set $n_s = 0.96$, $n_T = -0.04$ and $r = 0.248$, which should correspond to the power-law model with $p = 50$. The two models are then run through the MCMC analysis software as described in section 6.3. For comparison with current observations, we have also included an analysis using the first year WMAP data, and an analysis using the first year WMAP data combined with observational data from ACBAR, CBI and VSA. The last two analyses have been performed with no tensors or running of the scalar spectral index in mine, i.e. we set $n_T = r = \frac{dn_s}{d\ln k} = 0$.

Initially we wanted to include B-mode polarisation data in our MCMC analysis, and a lot of time and effort went into making that work. After numerous attempts, we had to resign, and conclude that this is currently not possible (see section 6.5). This was a great disappointment and setback, as measurements of B-mode polarisation is the best way to constrain tensor related parameters, such as n_T and r. The inability to use B-mode polarisation can possibly make it impossible to constrain r enough to exclude inflationary parameters based on the $n_s - r$ plane, which is one of the objects of this thesis.

In each MCMC analysis we have let the cosmological parameters vary according to table (6.1), but for the analyses where we have not considered tensors an option, we have fixed $n_T = r = \frac{dn_s}{d\ln k} = 0$. The simulated model

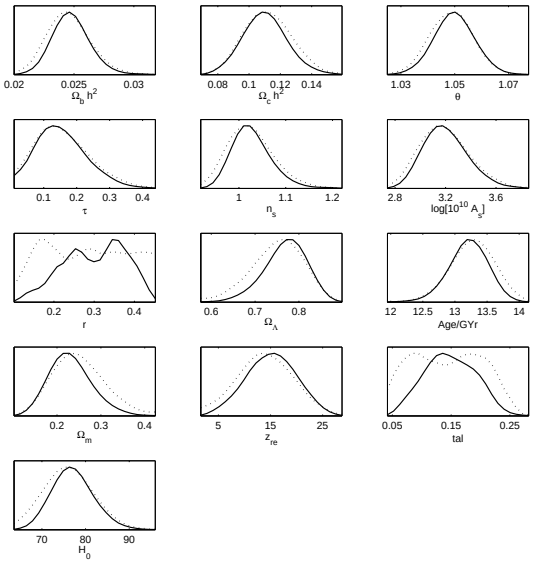

Figure 6.4: Parameter estimates and constraints obtained from the analysis of the first year WMAP data. Tensors and running are not considered, i.e. $n_T = 0$, $\frac{dn_s}{d\ln k} = 0$ and $r = 0$

computed using standard CAMB expressions for the power spectra has only been analysed with respect to n_s. We had hoped to analyse this model with respect to n_T and r also, but due to time and computational power being limited, this has not been done. Parameter constraints from the analysis of this model are presented in table (6.5) and figures (6.12, 6.8, 6.9). For the WMAP data analysis, and the combined WMAP, ACBAR, CBI and VSA analysis, the results are summarized in table (6.3) (WMAP only data) and table (6.4) (combined analysis), and also in figure (6.4, 6.5) and figure (6.6, 6.7).

We have also conducted an limited analysis where we have used TT, TE and EE data from a simulated power-law model ($p = 50$), to constrain n_T, r and $\frac{dn_s}{d\ln k}$ in addition to the other cosmological parameters. By limited, we here mean that the MCMC has only generated a short chain (18361 steps), which is not ideal (see chapter 4 and ref. [85]).

The results obtained from this last analysis are presented in table (6.6) and figures (6.10, 6.11, 6.13, 6.14,6.15, 6.16).

Due to the problems with COSMOMC, and limited amount of CPU power and time available, we have not been able to complete the full data analysis we had planned (see section 6.3.1 and 6.5). However, it is still useful to compare the parameter constraints obtained from an ideal experiment to

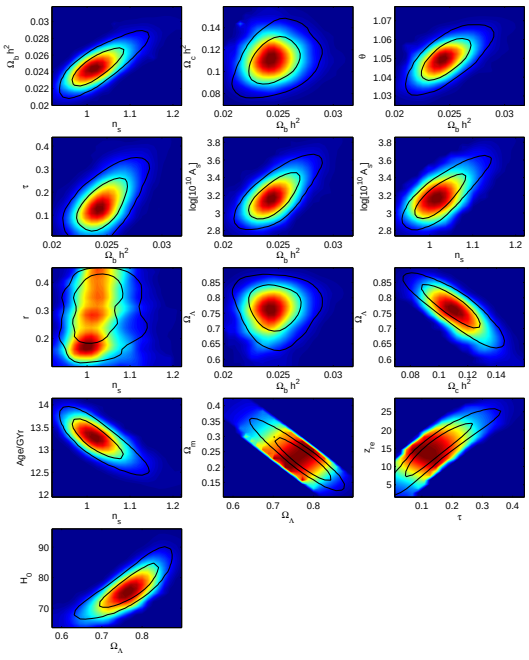

Figure 6.5: Two dimensional plot of parameter constraints from the analysis of the first year WMAP data. Tensors and running are not considered, i.e. $n_T = 0$, $\frac{dn_s}{d\ln k} = 0$ and $r = 0$

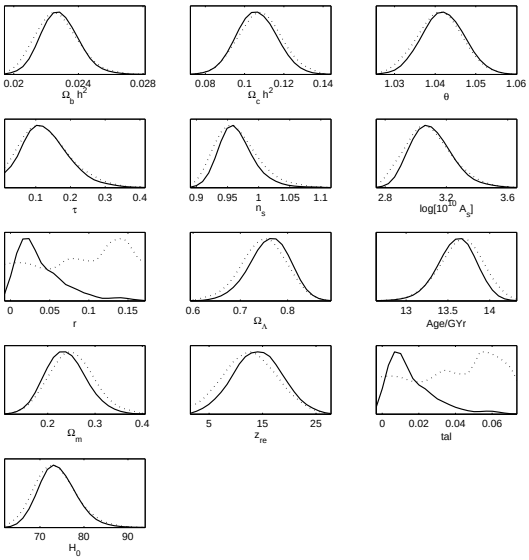

Figure 6.6: Parameter estimates and constraints obtained from the combined analysis of WMAP, ACBAR, CIB and VSA data. Tensors and running are not considered, i.e. $n_T = 0$, $\frac{dn_s}{d\ln k} = 0$ and $r = 0$

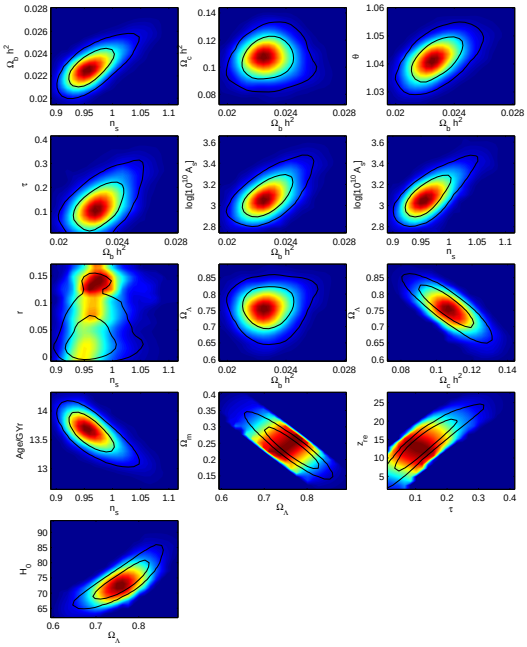

Figure 6.7: Two dimensional parameter constraints from the combined analysis of WMAP, ACBAR, CIB and VSA data. Tensors and running are not considered, i.e. $n_T = 0$, $\frac{dn_s}{d\ln k} = 0$ and $r = 0$

WMAP data only			
parameter	best-fit point	68 % CL	95 % CL
$\Omega_b h^2$	0.0240	$0.02043 < \Omega_b h^2 < 0.0293$	$0.0203 < \Omega_b h^2 < 0.0312$
$\Omega_{cdm} h^2$	0.1114	$0.0824 < \Omega_{cdm} h^2 < 0.1560$	$0.0724 < \Omega_{cdm} h^2 < 0.1600$
Ω_Λ	0.7575	$0.5530 < \Omega_\Lambda < 0.8567$	$0.5548 < \Omega_\Lambda < 0.8818$
Ω_m	0.2425	$0.1433 < \Omega_m < 0.4472$	$0.1182 < \Omega_m < 0.4452$
τ	0.1212	$0.0103 < \tau < 0.3890$	$0.0100 < \tau < 0.4308$
$z_{\rm re}$	13.477	$2.515 < z_{\rm re} < 27.513$	$2.388 < z_{\rm re} < 27.852$
Age (Gyr)	13.368	$12.421 <$ Age < 14.102	$12.09 <$ Age < 14.147
H_0	74.726	$62.194 < H_0 < 89.200$	$62.4176 < H_0 < 94.906$
$\log[10^{10} A_s]$	3.130	$2.845 < \log[10^{10} A_s] < 3.771$	$2.772 < \log[10^{10} A_s] < 3.823$
n_s	1.0005	$0.9146 < n_s < 1.1542$	$0.9230 < n_s < 1.2056$
$-\ln \mathcal{L}$	714.078		

Table 6.3: WMAP data analysis - parameter constraints

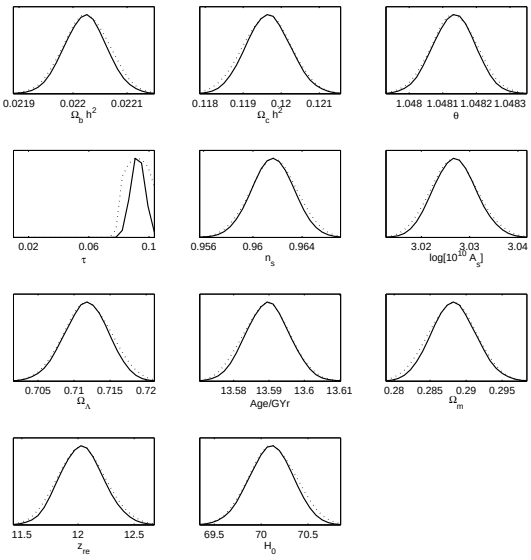

Figure 6.8: Parameter constraints from an analysis of simulated, noise-free data. Only temperature, E-mode polarisation and the TE-cross-correlation data are used. Tensors and running are not considered, i.e. $n_T = 0$, $\frac{dn_s}{d\ln k} = 0$ and $r = 0$

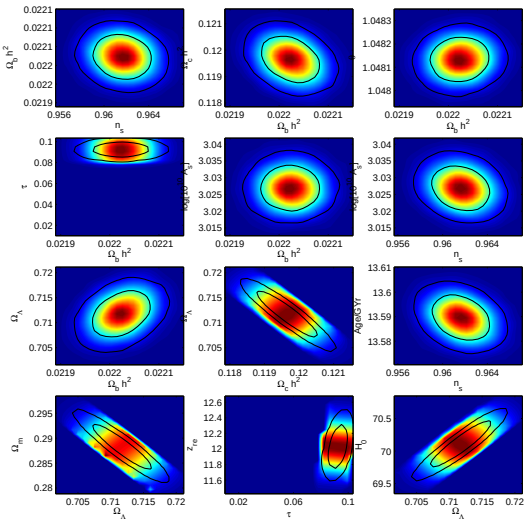

Figure 6.9: Two dimensional parameter constraints from an analysis of simulated, noise-free data. Only temperature, E-mode polarisation and the TE-cross-correlation data are used. Tensors and running are not considered, i.e. $n_T = 0$, $\frac{dn_s}{d\ln k} = 0$ and $r = 0$

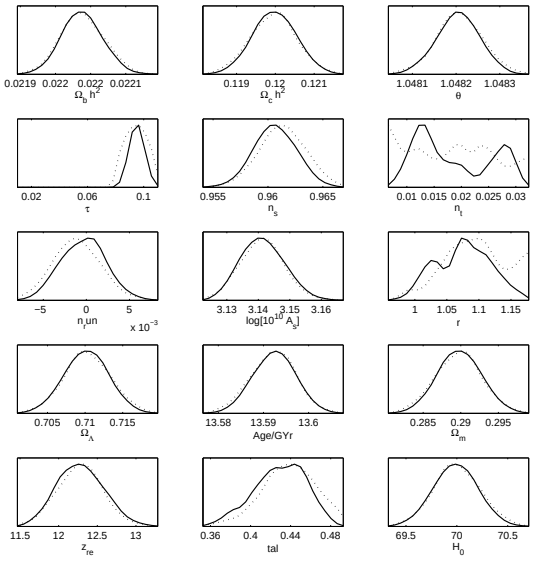

Figure 6.10: Parameter constraints from the limited analysis of simulated data, allowing tensors and running of the scalar spectral index in the parameter estimation.

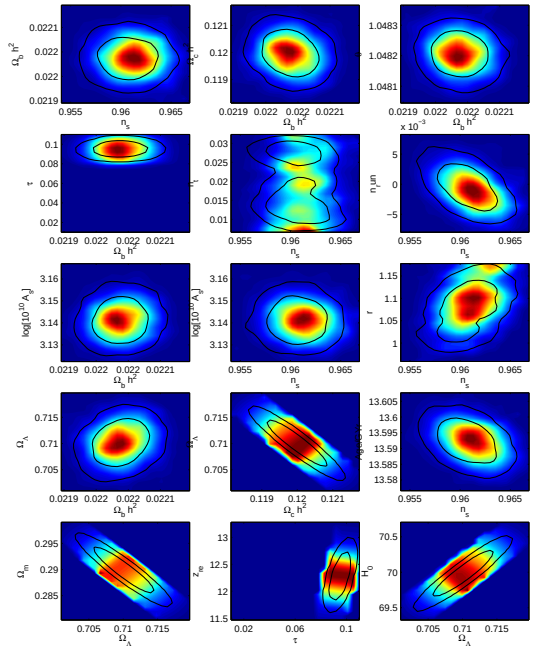

Figure 6.11: Two dimensional parameter constraints from the limited analysis of simulated data, allowing tensors and running of the scalar spectral index in the parameter estimation.

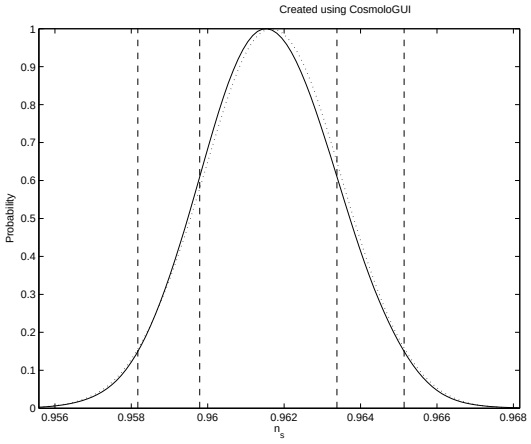

Figure 6.12: The scalar spectral index, estimated from simulated, noise-free data. Tensors and running are not considered, i.e. $n_T = 0$, $\frac{dn_s}{d\ln k} = 0$ and $r = 0$

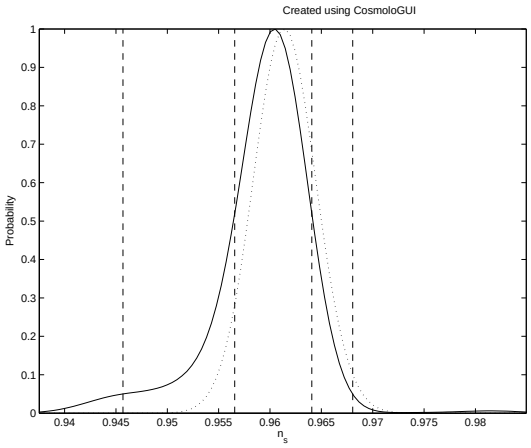

Figure 6.13: The scalar spectral index, estimated from a limited analysis of simulated, noise-free data. Tensor inflationary parameters, i.e. n_T and r, and running of the spectral index, are free parameters.

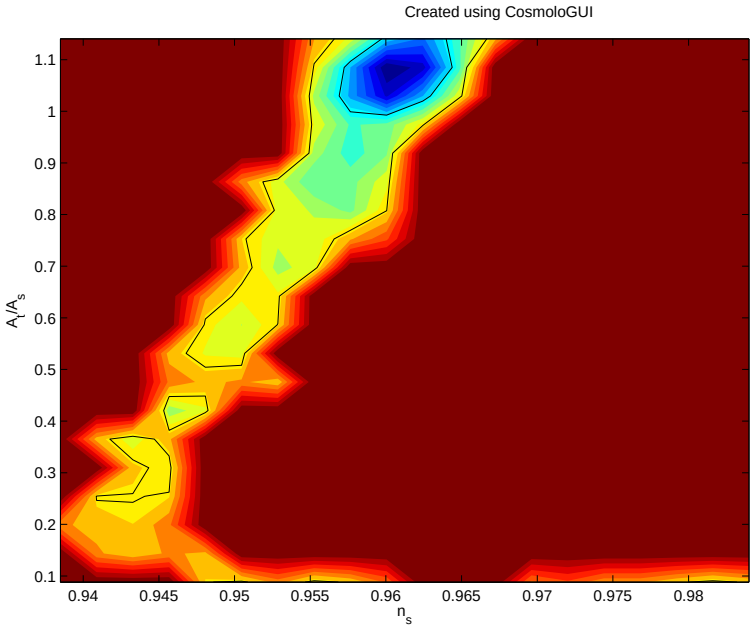

Figure 6.14: The $n_s - r$ plane from the limited analysis of the simulated data.

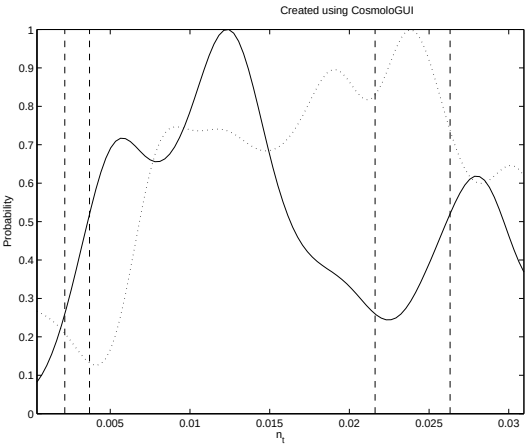

Figure 6.15: The tensor spectral index n_T estimated in the limited analysis of simulated, noise-free data.

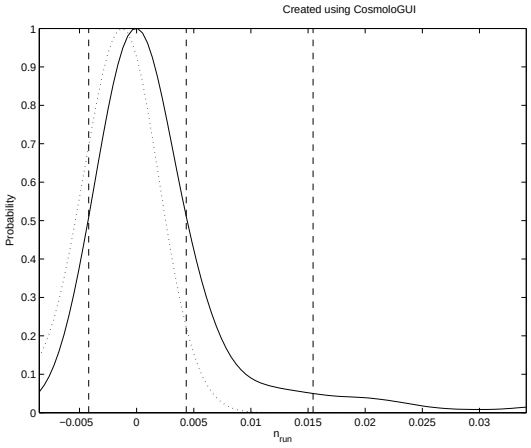

Figure 6.16: Estimate of $\frac{dn_s}{d\ln k}$, the running of the spectral index, found in the limited analysis of the simulated data.

WMAP, ACBAR, CBI and VSA combined analysis			
parameter	best-fit point	68 % CL	95 % CL
$\Omega_b h^2$	0.02261	$0.02005 < \Omega_b h^2 < 0.02654$	$0.01942 < \Omega_b h^2 < 0.02814$
$\Omega_{cdm} h^2$	0.1041	$0.0811 < \Omega_{cdm} h^2 < 0.134$	$0.0772 < \Omega_{cdm} h^2 < 0.1425$
Ω_Λ	0.77099	$0.62868 < \Omega_\Lambda < 0.85225$	$0.5728 < \Omega_\Lambda < 0.87719$
Ω_m	0.2290	$0.147747 < \Omega_m < 0.37132$	$0.12281 < \Omega_m < 0.4272$
τ	0.0865	$0.010067 < \tau < 0.3243$	$0.01003 < \tau < 0.4195$
$z_{\rm re}$	10.883	$2.4770 < z_{\rm re} < 24.535$	$2.461 < z_{\rm re} < 27.257$
Age (Gyr)	13.6395	$12.9233 < \text{Age} < 14.1785$	$12.628 < \text{Age} < 14.3193$
H_0	74.3744	$64.494 < H_0 < 86.388$	$62.081 < H_0 < 93.243$
$\log[10^{10} A_s]$	3.00	$2.80 < \log[10^{10} A_s] < 3.50$	$2.77 < \log[10^{10} A_s] < 3.70$
n_s	0.95872	$0.90602 < n_s < 1.0654$	$0.896 < n_s < 1.1258$
$-\ln \mathcal{L}$	725.9968		

Table 6.4: WMAP, ACBAR, CBI and VSA data combined analysis - parameter constraints

Simulated data, tensors are not considered			
parameter	best-fit point	68 % CL	95 % CL
$\Omega_b h^2$	0.0220	$0.02193 < \Omega_b h^2 < 0.02212$	$0.0219 < \Omega_b h^2 < 0.0221$
$\Omega_{cdm} h^2$	0.1196	$0.11819 < \Omega_{cdm} h^2 < 0.12101$	$0.11779 < \Omega_{cdm} h^2 < 0.12149$
Ω_Λ	0.7119	$0.70460 < \Omega_\Lambda < 0.71942$	$0.70199 < \Omega_\Lambda < 0.7216$
Ω_m	0.2881	$0.28058 < \Omega_m < 0.29540$	$0.2784 < \Omega_m < 0.2980$
τ	0.0923	$0.08752 < \tau < 0.098004$	$0.085897 < \tau < 0.0997$
$z_{\rm re}$	12.0135	$11.577 < z_{\rm re} < 12.521$	$11.4245 < z_{\rm re} < 12.6570$
Age (Gyr)	13.589	$13.574 < \text{Age} < 13.604$	$13.5705 < \text{Age} < 13.6085$
H_0	70.119	$69.562 < H_0 < 70.701$	$69.379 < H_0 < 70.877$
$\log[10^{10} A_s]$	3.0265	$3.017 < \log[10^{10} A_s] < 3.038$	$3.013 < \log[10^{10} A_s] < 3.041$
n_s	0.9617	$0.95750 < n_s < 0.96577$	$0.9562 < n_s < 0.96697$
$-\ln \mathcal{L}$	1029.68		

Table 6.5: CMB data analysis, no tensors - parameter constraints

the constraints from current experiments, to learn what improvements one can expect in the future. It is natural to compare the results obtained for the background evolution parameters, as these are free parameters in all the analyses. From table (6.3), (6.4), (6.5) and (6.6) we see that the ideal, noise-free data represents a much better way of constraining the cosmological parameters. For all parameters the reduction in error bars, compared to the current estimates, are dramatic, and we see that some parameters can be expected to be determined within 1 % of the real values. But still, there are some that cannot be as well defined, specifically n_T, r and $\frac{dn_s}{d\ln k}$ have still rather large error bars.

We see that including ACBAR, CBI and VSA data in addition to the WMAP data, does not improve the parameter constraints much, but some parameter estimates are shifted. Perhaps the most noticable is n_s, with a best fit value of 1.00047 in the WMAP only analysis, and best fit value of 0.95872 in the combined analysis. Also the redshift at reionization, $z_{\rm re}$, and the reionization optical depth τ, are different in the two analyses. The official WMAP parameter estimates give $\tau = 0.17$ [41], and such a high value is by many considered to be a problem. We see that the combined analysis brings the estimate on τ down, but still the error bars are large for this parameter.

As we can see from table (6.5) and table (6.6), there is no real improvement in the parameter estimates when including n_T, r and $\frac{dn_s}{d\ln k}$ as free parameters in the analysis. This could of course be due to the limited analysis of the simulated data when we included the above parameters. The short chain has not have time to explore the full parameter space, and thus the

Simulated data, inflationary tensor parameters included in analysis			
parameter	best-fit point	68 % CL	95 % CL
$\Omega_b h^2$	0.0220	$0.0219 < \Omega_b h^2 < 0.0221$	$0.02189 < \Omega_b h^2 < 0.0221$
$\Omega_{cdm} h^2$	0.1200	$0.1185 < \Omega_{cdm} h^2 < 0.1215$	$0.1182 < \Omega_{cdm} h^2 < 0.1217$
Ω_Λ	0.7102	$0.7023 < \Omega_\Lambda < 0.7177$	$0.7013 < \Omega_\Lambda < 0.7192$
Ω_m	0.2898	$0.2823 < \Omega_m < 0.2977$	$0.2808 < \Omega_m < 0.2987$
τ	0.0944	$0.08711 < \tau < 0.1040$	$0.0857 < \tau < 0.1057$
$z_{\rm re}$	12.2155	$11.5545 < z_{\rm re} < 13.057$	$11.433 < z_{\rm re} < 13.2095$
Age (Gyr)	13.5915	$13.581 < \text{Age} < 13.604$	$13.5775 < \text{Age} < 13.6078$
H_0	69.9945	$69.423 < H_0 < 70.562$	$69.3207 < H_0 < 70.6683$
$\log[10^{10} A_s]$	3.140	$3.125 < \log[10^{10} A_s] < 3.160$	$3.124 < \log[10^{10} A_s] < 3.164$
n_s	0.96105	$0.95604 < n_s < 0.96606$	$0.95457 < n_s < 0.96657$
n_T	0.01234	$0.00612 < n_T < 0.03184$	$0.00612 < n_T < 0.03184$
r	1.0676	$0.9787 < r < 1.1700$	$0.96691 < r < 1.1717$
$\frac{dn_s}{d\ln k}$	-0.0019	$-0.0072 < \frac{dn_s}{d\ln k} < 0.0060$	$-0.0088 < \frac{dn_s}{d\ln k} < 0.0077$
$-\ln \mathcal{L}$	1262.146		

Table 6.6: CMB data analysis, inflationary tensor parameters and running of the scalar spectral index are free parameters - parameter constraints

statistics are not as good as they should be.

6.5 Discussion

In our work we have shown that for a noise-free CMB experiment, the cosmological parameter set ($\Omega_b h^2$, $\Omega_{cdm} h^2$, Ω_Λ, H_0, age of the Universe, n_s and $\log[10^{10} A_s]$) can be estimated to within 2 % of the real values. The harder to constrain parameters τ and $z_{\rm re}$, should be possible to constrain within 10 %. Although we have been able to costrain and estimate the inflationary parameters n_T, r and α_s, the estimates are wrong for n_T and r, compared to the input values. Thus we must conclude that if we are only able to use temperature, E-mode polarisation, and the cross-correlation between the two, it is at the moment impossible to exclude any class of inflaton potentials, based on the estimates of n_s and r. Of course, this is only true if our analysis have been conducted correctly. We have had numerous problems with the MCMC method, and a thorough second analysis should have been conducted, but this has not been possible due to time limitations.

6.5.1 The MCMC method and problems faced

When the MCMC method works, it is a great tool or analysing the CMB data, but as the complexity of the cosmological models we wish to test increase and the precision of the observational data improves, the MCMC method requires a large amount of computational power. In the near future it will also be a need to test cosmological models with B-mode polarisation, but as of right now, `COSMOC` does not work with this type of data. This is of course a great hinderance when it comes to future observational data. We discuss these issues below.

We apply a Markov Chain Monte-Carlo method because we wish to determine the cosmological parameters behind a given spectrum. It is therefore essential that the method itself is effective in exploring the whole parameter space we wish to examine. As explained in greater detail in section (6.3) the parameter space is explored by first starting at a random point in this space, computing the spectrum (the C_ℓ's) and the corresponding likelihood $\mathcal{L}^1$. We then take a random step in parameter space and calculate the new likelihood value, $\mathcal{L}^2$. Based on certain criteria we decide if the new parameter set should be accepted or rejected. If accepted, we save the new parameter set as part of the chain and take a new random step. It is clear that for this method to be effective it must not get stuck at one point in parameter space, i.e. taking the step means a fair chance of finding a "better" point in parameter space (that is a higher likelihood than for the point we are comparing with). For WMAP like data the errors in observations are relatively large and finding a step size that yields a good exploration of parameter space and high acceptance factor (see section 6.3) is quite easy. For our simulated data however we are faced with a quite paradoxical problem; the low errors (only cosmic variance) actually make it very hard to get an effective MCMC exploration of parameter space. To understand this we examine the asymptotic distribution $\mathcal{P}_\theta$, which is the region in parameter space we wish to sample from, and for data with cosmic variance as the only error, this is a very small region in parameter space. This means that if the chosen step size is too large, there is very little chance at actually ending up in $\mathcal{P}_\theta$, or alternatively, if you are at a 2σ point in parameter space it is hard to get to a better point (say within the 1σ bound), if your step size is much larger than 1σ, as any step you take will bring you far away from $\mathcal{P}_\theta$. You get stuck at the relatively poor fit 2σ point. To remedy this, we have to first guesstimate the expected 1σ level/error and set the step size to be at least as low as this, preferably somewhat lower. However this raises another problem. Since we do not know the true parameter set (of course we do since we are using simulated data, so we pretend not to know), we can only guess at where in parameter space to

start. If we are unlucky, and since $\mathcal{P}_\theta$ is so small, in most cases we will be, we would start at a point "far" from $\mathcal{P}_\theta$, and with the small step size it would take a very long time, i.e. many steps, to find/approach good parameter values.

We see from the above that data with such a high degree of precision require enormous amounts of computing power and time. With the WMAP data you could get good results in a couple of hours on a multi-processor machine [82], but it will take a minimum of days on the same machine to get acceptable results for the high precision simulated data.

The above discussion relates to a problem of a practical nature. Time and computational effort are needed to get an effective MCMC exploration of parameter space and thus good parameter estimates, when using high accuracy data. However, in the following we will discuss two issues concerning `COSMOMC` directly, and not the MCMC method in itself. First is that every attempt to include B-mode polarisation in our data has failed. We get likelihood values of 10^{30}, and `COSMOMC` will quit after a short time. The high likelihood values could indicate that there is something wrong with our data, and that it is the additional calculation of the C_ℓ^{BB} likelihood which is causing the problem. However, we have checked, and the problem arises before the C_ℓ^{BB} likelihood is even calculated. Using our own likelihood routine, and removing the calculation of C_ℓ^{BB} does not help either. There seems as though something is wrong in the way the `COSMOMC` code handles the calculation and subsequent inclusion of B-mode polarisation in the MCMC analysis.

The second issue we would like to mention, is that the option in `COSMOMC` to calculate the covariance matrix, is not working satisfactoryly with low-noise data. We have not tested this option exhaustively, and further tests should be conducted, but we have noticed that there seems to be some connection between how successful this option is, and the type of machine it is ran on. The covariance matrix is related to the C_ℓ's [64], and the problems with the C_ℓ^{BB} data and the covariance matrix could therefore be connected.

6.5.2 What can be improved?

It is natural to ask what could be improved and changed, compared to our work. An approach could be to investigate the different MCMC routines available in `COSMOMC`, to see if that could help on some of the issues discussed above. Another approach, which should be performed (we would have done it if there had been time), is to run through the analysis pipeline without using B-mode polarisation data, but still noise-free data, and making sure the MCMC method is effective at each step in the pipeline. Analyses of simulated data without B-mode polarisation have been conducted, see e.g.

[91], but in most cases the simulated data also include some simulated noise in addition to the cosmic variance. Of course, if one knows the expected error bars from future experiments, such analyses would give a more realistic picture of what can be expected from future observations. That has not been our aim in this thesis. We have aimed at seeing if it is at all possible to exclude whole classes of inflaton potentials from perfect CMB data alone. Unfortunately, it has not been possible to reach a firm conclusion on this.

We have seen that the WMAP satellite gives good estimates of the cosmological parameters, but it is nonetheless clear that the Planck satellite will provide another leap forward in terms of precision cosmology. And of special interest will be accurate measurements of the polarisation spectra, which are needed of the methods discussed in this thesis are to be successful.

6.5.3 The Bayesian information criterion

The following discussion is not directly connected to the results we have obtained, but if we had been able to follow the analysis pipeline described in section (6.3.1), the issues we discuss would have had relevance. As seen in section (6.4), we are able to put quite tight constraints on the cosmological parameters, especially the background evolution parameters and n_s. If the analysis pipeline had been completed, we would have ended up with a set of models. For each model, or parameter set, the likelihood value is a measurement of how good the parameter fit is.

To illustrate the use of the information criterion, we now assume we had been able to complete four steps of the analysis pipeline for a power spectrum with data up to $\ell = 2500$, and have ended up with four parameter sets, each having a likelihood value $\mathcal{L}$. The first step gave a parameter set with likelihood $-2\ln\mathcal{L}_1 = 1205$, the second step yielded likelihood $-2\ln\mathcal{L}_2 = 1182$, the third and fourth step both gave likelihood $-2\ln\mathcal{L}_{3,4} = 1179$. Based on the likelihood values alone, one would conclude that the third and fourth step gave an equally good, and the best, fit to the observed data, since these sets have the highest likelihood $\mathcal{L}$ (lowest $-2\ln\mathcal{L}$). However, in this case, this conclusion is wrong. One cannot only compare likelihood values among different models, since the number of free parameters are different. In most any case, more free parameters would provide a better fit to the data. Therefore we should take into account some sort of information criterion when we assess the results obtained. We apply the Bayesian information criterion (BIC) [80]:

$$\mathrm{BIC} = -2\ln\mathcal{L} + k\ln N$$

where N is the nimber of datapoints used in the fit (in our case $N = 2500$).

The number of parameters used in the fit is represented by k. The best model, or more precisely, the model which gives the most information from the input data, with the least amount of free parameters, has the lowest BIC [80]. Adding more parameters will normally give a lower likelihood, but the BIC will punish the extra parameters. With a large number of datapoints, more parameters are penalized quite a lot, i.e. we need a real improvement in likelihood to justify the introduction of extra parameters. For our toy model results above, we need an improvement in likelihood of approximately $\ln 2500 \simeq 7.8$ to justify one additional parameter in a fit. Furthermore a difference of 6 or more in BIC is considered to be strong evidence against the model with the larger value [80]. Looking then at our toy example, we see that the parameter set from the first step in the pipeline has $\mathrm{BIC}_1 = 1205 + 7 * 7.8 \simeq 1259.6$, the second had $\mathrm{BIC}_2 = 1244.4$, the third has $\mathrm{BIC}_3 = 1250.2$, while the fourth and last parameter step has $\mathrm{BIC}_4 = 1257.5$. Thus we see that the second step in the pipeline in this example gave the best model for the observed data, and that the introduction of new parameters could not reveal any new information. We point out that the BIC cannot be used to tell about how models from different datasets compare to each other.

Chapter 7

Summary and final discussions

In this thesis we have looked at the possibility of reconstructing the inflaton potential from observations of the cosmic microwave background. The Monte Carlo reconstruction method has been considered in detail, and is found to be effective in its ability to construct inflaton potentials, but since the method produces so many possible potentials, it is hard to conclude anything about the real inflaton potential, if it exists. There is a need for future high accuracy measurements of the CMB, and we can hope that the Planck satellite will yield such tight parameter constraints that the Monte Carlo reconstruction method can be an effective tool in the search for the inflaton potential.

Awaiting the launch of the Planck satellite, we have simulated noise-free CMB data to see what parameter constraints one can expect in the future, and if these constraints are tight enough to either allow exclusion of whole classes of inflaton potentials, or a successful reconstructiong of the inflaton potential, or possibly a combination of both. We find that the software commonly used in CMB analysis, `COSMOC`, is unable to tackle high precision B-mode polarisation data. This inability to use B-mode polarisation data is not of concequence for current observational data, but must be addressed since the launch of Planck should provide measurements of B-mode polarisation, if such exists [54]. Therefore there is a need to closer investigate the software, and possibly devise other methods of parameter estimation. Our experience with the MCMC method also indicates that, although it is possible to get fairly tight constraints on the inflationary parameters n_T and r from measurements of temperature anisotropies and E-mode polarisation alone, the parameter estimates are in many cases wrong. This makes us certain that future experiments must be sensitive to possible B-mode polarisation, and the tools we use must be refined, if we are to come closer to the true origin of the inflaton potential.

The Monte Carlo reconstruction of the inflaton potential depends on

thight constrains of the parameters n_s and r to be successful, and this also requires measurements of B-mode polarisation. If such measurements can be achieved, estimates for the amplitude A_T of the tensor perturbations are also found, and thus the perturbative reconstruction framework could be a good alternative to the Monte Carlo reconstruction. The two methods could also serve as cross-checks of each other.

We are the first to admit that the results from our MCMC analysis in chapter 6 are imperfect and insufficient. Therefore we would like to point out that those analyses are not the only ones done, but they are the only ones leading to somewhat sensible results. All other attempts have produced what we consider useless chains, i.e. the chains are to short to provide good statistics since the full parameter space has not been explored. As we have stated earlier, a lot of time and effort has gone into making the analysis of B-mode polarisation data work. At first we simulated data and scaled that data to be compatible with the WMAP data [50], and based on our simulations, we wrote our own likelihood code. However, we could not get the B-mode polarisation data to work, and assumed that there was something wrong with either our data or the likelihood code, or possibly both. We now see that our problems were caused by the way `COSMOC` handles B-mode polarisation data. If this had been realized at an earlier time, more work could have been directed at finding the bug(s) in `COSMOMC`, or more thorough analyses of data not containing B-mode polarisation.

In retrospect it is easy to see that there are numerous aspects of this thesis which could have been done differently. We should have realized sooner that our many attempts to make the B-mode polarisation data work with `COSMOC` failed due to bugs in `COSMOMC`, and not because of faults in our data. We could also hae realized earlier the amount of computing power and time needed to analyse noise-free, all-sky data. But still, in themself, these are interesting findings, and should be considered in future work.

As a conclusion we would like to say that these are truly exciting times for cosmologists, and much research is done to understand the Universe we live in. Several papers investigate the nature of the inflaton potential [75, 24, 69, 73, 93], and several approaches are considered. However, they all conclude that tighter constraints on the inflationary parameters n_s, n_T, r, A_s and A_T are needed. In that respect, there is also much research going into parameter estimation from the cosmic microwave background [92, 94, 64, 95]. As the observations of the CMB radiation improves, there is a wealth of subtle non-linear physical effects one must take into account, e.g. lensing of the CMB. Lensing will induce non-Gaussianities in the lensed CMB sky, and also change the power spectra of the perturbations [91]. We once again point out that the future high precision measurements of the cosmic microwave background

require a continous research into parameter estimation methodology and a better understanding of the physical background of the inflation epoch, if we are to take advantage of this new information.

Chapter 8

Appendix

8.1 Cosmic variance and the χ^2-distribution

When simulating data the key ingredient is the dataset's probability distribution. As we observe the CMB radiation and the power spectrum C_ℓ, we only see a single realization of the power spectrum. From statistics it is known that a finite sampling of events generated from a random process, will lead to a uncertainty in variance, called sample variance. For the power spectrum, this sample variance is called cosmic variance.

We simulate data by drawing random values from the probability distributions. This means we must find the probability distribution for C_ℓ given a value of ℓ. Remembering the definition of the power spectrum in chapter 2 we have the observed temperature fluctuations as a sum of spherical functions $Y_{\ell m}$ (chapter 4):

$$\frac{\delta T}{T}(\theta,\phi) = \sum_{\ell=0}^{\infty} \sum_{m=-\ell}^{\ell} a_{\ell m} Y_{\ell m}(\theta,\phi) \tag{8.1}$$

The fluctuations are thus completely characterized by the complex coefficients $a_{\ell m}$. Since $\delta T = T - T_0$, with T_0 being the mean temperature, we see that the coefficients have mean (value) 0. The simplest models of inflation predict the $a_{\ell m}$s to be gaussian. Given a ℓ value the variance $<\mid a_{\ell m} \mid^2>= C_\ell$, independent of m. For each ℓ there are $2\ell + 1$ independent m-values, and this allows us to define the power spectrum as

$$C_\ell = \frac{1}{2\ell+1} \sum_{m=-\ell}^{\ell} \mid a_{\ell m} \mid^2 \tag{8.2}$$

It is possible to show that the real(R) and imaginary(I) parts of $a_{\ell m}$ also are gaussian with mean 0 and variance $\frac{C_\ell}{2}$. To find the probability distribution

of C_ℓ we are required to find the distribution of a sum of the squared of two gaussian distributed quantities. The so-called χ^2-distribution is what we need and for a continous stochastic variable z $(0 \leq z < \infty)$ is defined as:

$$f(z;n) = \frac{1}{2^{\frac{n}{2}}\Gamma(\frac{n}{2})} z^{\frac{n}{2}-1} e^{-\frac{z}{2}} \tag{8.3}$$

where n is an integer and is called the degree of freedom for z. Γ is the gamma function defined as:

$$\Gamma(x) = \int_0^\infty e^{-t} t^{x-1} \mathrm{dt} \tag{8.4}$$

The most important properties the gamma function has are $\Gamma(n) = (n-1)$ for integer n, $\Gamma(x+1) = x\Gamma(x)$ and $\Gamma(\frac{1}{2}) = \sqrt{\pi}$. The expected value of z:

$$\overline{z} = \int_0^\infty z f(z;n) \mathrm{dz} = n \tag{8.5}$$

and furthermore the variance is given as:

$$\sigma_z^2 = \int_0^\infty (z-n)^2 f(z;n) \mathrm{dz} = 2n \tag{8.6}$$

It can be shown that given N independent gaussian stochastic variables x_i having mean value μ_i and variance σ_i then:

$$z = \sum_{i=1}^{N} \frac{(x_i - \mu_i)^2}{\sigma_i^2} \tag{8.7}$$

is χ^2-distributed with N degrees of freedom. This can be applied tp the background radiation. Forming the quantity:

$$z = \sum_{m=-\ell}^{\ell} \frac{R^2 + I^2}{\frac{1}{2} C_\ell} \tag{8.8}$$

we see that this is a sum of $2(2\ell+1)$ independent and Gaussian distributed stochastic variables of the form given above (8.7). Therefore z is χ^2-distributed with $2(2\ell+1)$ degrees of freedom, and since z is proportional to C_ℓ, then C_ℓ will have the same distribution. The expected value is then given as $2(2\ell+1)$ which leads to $< C_\ell > \frac{C_\ell}{2} \frac{1}{2\ell+1} < z >= C_\ell$ as it should be. Furthermore the variance (square of the standard deviation) of z is $2 * 2(2\ell+1) = 4(2\ell+1)$, and this yields the variance of C_ℓ:

$$\delta C_\ell = \frac{1}{2} \left(\frac{C_\ell}{2\ell+1} \right)^2 4(2\ell+1) = \frac{2C_\ell^2}{2\ell+1} \tag{8.9}$$

Thus for a given value of ℓ there is a relative error in C_ℓ:

$$\frac{\delta C_\ell}{C_\ell} = \sqrt{\frac{2}{2\ell+1}} \tag{8.10}$$

We see that the cosmic variance is proportional to $\ell^{-\frac{1}{2}}$, which means it is less significant on smaller angular scales.

8.2 χ^2-test for goodness of fit

The chi-square test for goodness of fit tests the hypothesis that the distribution of the population from which nominal data are drawn agrees with a posited distribution. The test compares observed and expected frequencies, in our case the observed(simulated) $C_\ell^{\rm data}$ with the $C_\ell^{\rm theory}$ which `COSMOMC` is suggesting. Mathematically it is:

$$\chi^2 = \sum_{\ell=2}^{\ell=\ell_{max}} \frac{\left(C_\ell^{\rm data}(\ell) - C_\ell^{\rm theory}(\ell)\right)^2}{\sigma^2_{C_\ell}(\ell)} \tag{8.11}$$

where $\sigma^2_{C_\ell}(\ell)$ is the variance of $C_\ell^{\rm data}(\ell)$. The chi-square test will tell us whether a proposed model is a good fit to the observed data or not. A theoretical model proposal that gives a chi-square value of approximately $\chi^2 \simeq \ell_{max}$ is considered to be a good fit to the observed data. If χ^2 is larger than this, not even by a factor two the theoretical model is considered a poor fit and one should come up with a new and improved model.

The χ^2-test was used in our initial work with `COSMOMC` and the WMAP data format.

8.3 Likelihood function

The full-sky Gaussian likelihood function $\mathcal{L}$ used in `COSMOMC`, is obtained from the assumed Gaussianity of the temperature ansisotropies T, and E and B polarisation (see section 4.1.2). We have

$$\mathcal{L}(C_\ell) \equiv \mathcal{P}(\tilde{C}_\ell|C_\ell) = \frac{1}{\sqrt{2\pi|\mathbf{C}|}} e^{-\frac{1}{2}d^\dagger \mathbf{C}_\ell^{-1} d} \tag{8.12}$$

where

$$\mathbf{C}_\ell = \begin{pmatrix} C_\ell^{TT} & C_\ell^{TE} & 0 \\ C_\ell^{TE} & C_\ell^{EE} & 0 \\ 0 & 0 & C_\ell^{BB} \end{pmatrix} \tag{8.13}$$

and $d = [a_{\ell m}]$ with components consisting of all combinations of ℓ and m. This yield

$$-2\ln\mathcal{L} = d^{\dagger}\mathbf{C}^{-1}d + \ln|\mathbf{C}| \tag{8.14}$$

$$= \sum_{\ell}\frac{1}{C_\ell}\sum_{m=-\ell}^{\ell} a^{*}_{\ell m}a_{\ell m} + \ln\prod_{\ell=0}^{\infty} C_\ell^{(2\ell+1)} \tag{8.15}$$

where

$$\sum_{m=-\ell}^{\ell} a^{*}_{\ell m}a_{\ell m} = (2\ell+1)\tilde{C}_\ell$$

Thus we find that

$$-2\ln\mathcal{L} = \sum_{\ell}(2\ell+1)\left[\frac{\tilde{C}_\ell}{C_\ell} + \ln\frac{C_\ell}{\tilde{C}_\ell} - 1\right] \tag{8.16}$$

where $\tilde{C}_\ell$ is the observed (or simulated) power spectrum, while C_ℓ represents the theoretical calculated power spectrum one wish to test [85, 96].

The above equation (8.16) is for temperature only data. If we also include polarisation, the total likelihood function will be modified, and expressed as [82]:

$$\begin{aligned}-2\ln\mathcal{L} = \sum_{\ell}(2\ell+1)\Bigg[&C_\ell^{TT}\tilde{C}_\ell^{EE} + C_\ell^{EE}\tilde{C}_\ell^{TT} - \frac{2C_\ell^{TE}\tilde{C}_\ell^{TE}}{C_\ell^{TT}C_\ell^{EE} - \tilde{C}_\ell^{TE^2}} \\ &+ \ln\left(\frac{C_\ell^{TT}C_\ell^{EE} - \tilde{C}_\ell^{TE^2}}{\tilde{C}_\ell^{TT^2}\tilde{C}_\ell^{EE^2} - \tilde{C}_\ell^{TE^2}}\right) - 2\Bigg] \\ &+ \sum_{\ell}(2\ell+1)\left[\frac{\tilde{C}_\ell^{BB}}{C_\ell^{BB}} + \ln\left(\frac{C_\ell^{BB}}{\tilde{C}_\ell^{BB}}\right)\right]\end{aligned} \tag{8.17}$$

where the last summation term is only included if we look at B mode polarisation.

8.4 Derivation of the flow equations

It is possible to derive an expression for $\frac{d}{dN}$. From equation (2.30) we have

$$\begin{aligned} N &= \int_t^{t_e} H dt = \int_\phi^{\phi_e} \frac{H}{\dot{\phi}} d\phi \\ &= \frac{4\pi}{m_{\rm Pl}} \int_{\phi_e}^{\phi} \frac{H}{H'} d\phi \\ \rightarrow dN &= \frac{2\sqrt{\pi}}{m_{\rm Pl}} \frac{d\phi}{\sqrt{\epsilon}} \\ \rightarrow \frac{d}{dN} &= \frac{m_{\rm Pl}}{2\sqrt{\pi}} \sqrt{\epsilon} \frac{d}{d\phi} \end{aligned} \tag{8.18}$$

where we have used equations (2.15, 2.12). In the following we let m denote $m_{\rm Pl}$.
We use equation (8.18) when we in the following derive the derivative of ϵ, η, σ and ${}^{\ell}\lambda_H$. For $\frac{d\epsilon}{dN}$ we find:

$$\begin{aligned} \frac{d\epsilon}{dN} &= \frac{m}{2\sqrt{\pi}} \sqrt{\epsilon} \frac{d\epsilon}{d\phi} \\ &= 2 \left(\frac{m^2}{4\pi} \right)^2 \frac{H'^2}{H^2} \left[\frac{H''}{H} - \frac{H'^2}{H^2} \right] \\ &= 2\epsilon[\eta - \epsilon] \end{aligned} \tag{8.19}$$

Which it is trivial to show is equal to $\epsilon[\sigma + 2\epsilon]$. For $\frac{d\eta}{dN}$ we have:

$$\begin{aligned} \frac{d\eta}{dN} &= \frac{m}{2\sqrt{\pi}} \sqrt{\epsilon} \frac{d\eta}{d\phi} \\ &= \left(\frac{m^2}{4\pi} \right)^2 \frac{H'}{H} \left[\frac{H'''}{H} - \frac{H''H'}{H^2} \right] \\ &= {}^2\lambda_H - \epsilon\eta \end{aligned} \tag{8.20}$$

and it is trivial to then show $\frac{d\sigma}{dN}$:

$$\begin{aligned} \frac{d\sigma}{dN} &= \frac{d}{dN}(2\eta - 4\epsilon) \\ &= 2^2\lambda_H - 5\sigma\epsilon - 12\epsilon^2 \end{aligned} \tag{8.21}$$

Finally we derive $\frac{d^\ell \lambda_H}{dN}$:

$$\begin{aligned}
\frac{d^\ell \lambda_H}{dN} &= \frac{m}{2\sqrt{\pi}}\sqrt{\epsilon}\left(\frac{m^2}{4\pi}\right)^\ell \left[\frac{(\ell-1)(H')^\ell H'' H^{ell}}{H^{2\ell}}\right. \\
&\quad \left. -\frac{(H')^\ell \ell H^{\ell-1}}{H^{2\ell}}\right] \frac{d^{(\ell+1)}H}{d\phi^{(\ell+1)}} \\
&\quad + \frac{m}{2\sqrt{\pi}}\sqrt{\epsilon}\left(\frac{m^2}{4\pi}\right)^\ell \frac{(H')^{(\ell-1)}}{H^\ell}\left(\frac{d^{(\ell+2)}}{d\phi^{(\ell+2)}}\right) \\
&\vdots \\
\frac{d^\ell \lambda_H}{dN} &= \left[\frac{\ell-1}{2}\sigma + (\ell-2)\epsilon\right]{}^\ell\lambda_H + {}^{\ell+1}\lambda_H \qquad (8.22)
\end{aligned}$$

Bibliography

[1] P. Coles and F. Lucchin. *Cosmology: the origin and evolution of cosmic structure*. John Wiley & Sons, 2002.

[2] A. R. Liddle and D. H. Lyth, editors. *Cosmological inflation and large-scale structure*, 2000.

[3] A. G. Riess, A. V. Filippenko, P. Challis, A. Clocchiattia, A. Diercks, P. M. Garnavich, R. L. Gilliland, C. J. Hogan, S. Jha, R. P. Kirshner, B. Leibundgut, M. M. Phillips, D. Reiss, B. P. Schmidt, R. A. Schommer, R. C. Smith, J. Spyromilio, C. Stubbs, N. B. Suntzeff, and J. Tonry. Observational Evidence from Supernovae for an Accelerating Universe and a Cosmological Constant. *ArXiv Astrophysics e-prints*, May 1998.

[4] A. V. Filippenko and A. G. Riess. Evidence from Type Ia Supernovae for an Accelerating Universe. *ArXiv Astrophysics e-prints*, August 2000.

[5] G. A. Baker and Jr. Supernovae evidence for an accelerating expansion of the universe. *ArXiv Astrophysics e-prints*, June 2000.

[6] R. A. Knop and Supernova Cosmology Project Team. Latest Cosmological Results from Type Ia Supernovae. *Bulletin of the American Astronomical Society*, 32:1569–+, December 2000.

[7] K. A. Olive. Big Bang Baryogenesis. *ArXiv High Energy Physics - Phenomenology e-prints*, April 1994.

[8] B. Gumjudpai. Introductory Overview of Modern Cosmology. *ArXiv Astrophysics e-prints*, May 2003.

[9] J. Frieman. The Standard Cosmology. *ArXiv Astrophysics e-prints*, April 1994.

[10] Everyone. Timeline of the big bang. *Wikipedia*, 2005. http://www.wikipedia.org/wiki/Timeline_of_the_Big_Bang.

[11] Ø. Grøn. Lecture notes on general relativity. http://www.uio.no/studier/emner/matnat/fys/FYS4160/v04/undervisningsmateriale/kor 2005.

[12] L. M. Ord. From COBE to WMAP: A Decade of Data Under Scrutiny. *ArXiv Astrophysics e-prints*, December 2004.

[13] A. A. Starobinskii. Spectrum of relict gravitational radiation and the early state of the universe. *ZhETF Pis ma Redaktsiiu*, 30:719–723, December 1979.

[14] A. H. Guth. Inflationary universe: A possible solution to the horizon and flatness problems. Phys. Rev. D, 23:347–356, January 1981.

[15] Ø. Elgarøy. Lecture notes in cosmology, 2003.

[16] D. S. Salopek and J. R. Bond. Nonlinear evolution of long-wavelength metric fluctuations in inflationary models. Phys. Rev. D, 42:3936–3962, December 1990.

[17] A. R. Liddle, P. Parsons, and J. D. Barrow. Formalizing the slow-roll approximation in inflation. Phys. Rev. D, 50:7222–7232, December 1994.

[18] J. H. Traschen and R. H. Brandenberger. Particle production during out-of-equilibrium phase transitions. Phys. Rev. D, 42:2491–2504, October 1990.

[19] L. Kofman, A. Linde, and A. A. Starobinsky. Reheating after inflation. *Physical Review Letters*, 73:3195–3198, December 1994.

[20] L. Kofman, A. Linde, and A. A. Starobinsky. Towards the theory of reheating after inflation. Phys. Rev. D, 56:3258–3295, September 1997.

[21] L. F. Abbott, E. Farhi, and M. B. Wise. Particle production in the new inflationary cosmology. *Phys. Lett. B*, 117:29, 1982.

[22] A. D. Dolgov and A. D. Linde. Baryon asymmetry in the inflationary universe. *Physics Letters B*, 116:329–334, October 1982.

[23] E. D. Stewart and D. H. Lyth. A more accurate analytic calculation of the spectrum of cosmological perturbations produced during inflation. *Physics Letters B*, 302:171–175, March 1993.

[24] J. E. Lidsey, A. R. Liddle, E. W. Kolb, E. J. Copeland, T. Barreiro, and M. Abney. Reconstructing the inflaton potential-an overview. *Reviews of Modern Physics*, 69:373–410, April 1997.

[25] E. R. Harrison. Fluctuations at the Threshold of Classical Cosmology. Phys. Rev. D, 1:2726–2730, May 1970.

[26] Y. B. Zel'Dovich. Gravitational instability: an approximate theory for large density perturbations. A&A, 5:84–89, March 1970.

[27] F. Mandl and G. Shaw. *Quantum Field Theory*. Wiley, revised edition, 1993.

[28] D. H. Lyth and E. D. Stewart. The curvature perturbation in power law (e.g. extended) inflation. *Physics Letters B*, 274:168–172, January 1992.

[29] W. H. Kinney. Inflation: Flow, fixed points, and observables to arbitrary order in slow roll. Phys. Rev. D, 66(8):083508–+, October 2002.

[30] W. H. Kinney, E. W. Kolb, A. Melchiorri, and A. Riotto. Inflationary physics from the Wilkinson Microwave Anisotropy Probe. Phys. Rev. D, 69(10):103516–+, May 2004.

[31] Edmund J. Copeland, Andrew R. Liddle, David H. Lyth, Ewan D. Stewart, and David Wands. False vacuum inflation with einstein gravity. *Phys. Rev.*, D49:6410–6433, 1994.

[32] Andrei D. Linde. Axions in inflationary cosmology. *Phys. Lett.*, B259:38–47, 1991.

[33] Andrei D. Linde. Hybrid inflation. *Phys. Rev.*, D49:748–754, 1994.

[34] Andrei D. Linde. A new inflationary universe scenario: A possible solution of the horizon, flatness, homogeneity, isotropy and primordial monopole problems. *Phys. Lett.*, B108:389–393, 1982.

[35] Andreas Albrecht and Paul J. Steinhardt. Cosmology for grand unified theories with radiatively induced symmetry breaking. *Phys. Rev. Lett.*, 48:1220–1223, 1982.

[36] Katherine Freese, Joshua A. Frieman, and Angela V. Olinto. Natural inflation with pseudo - nambu-goldstone bosons. *Phys. Rev. Lett.*, 65:3233–3236, 1990.

[37] Andrei D. Linde. Chaotic inflation. *Phys. Lett.*, B129:177–181, 1983.

[38] A. A. Penzias and R. W. Wilson. A Measurement of Excess Antenna Temperature at 4080 Mc/s. ApJ, 142:419–421, July 1965.

[39] R. A. Alpher and R. Herman. Evolution of the Universe. *Nature*, 162:774–775, 1948.

[40] R. A. Alpher and R. C. Herman. On the Relative Abundance of the Elements. *Physical Review*, 74:1737–1742, December 1948.

[41] WMAP team. Wmap best-fit cosmological parameters, 2005. http://lambda.gsfc.nasa.gov/product/map/wmap_parameters.cfm.

[42] COBE. Cosmic background explorer, 2005. http://lambda.gsfc.nasa.gov/product/cobe/.

[43] Maxima. Millimeter anisotropy experiment imaging array, 2005. http://cosmology.berkeley.edu/group/cmb/index.html.

[44] Boomerang. Balloon observations of millimetric extragalactic radiation and geophysics, 2005. http://cmb.phys.cwru.edu/boomerang/.

[45] VSA. The very small array, 2005. http://www.mrao.cam.ac.uk/telescopes/vsa/index.html.

[46] CBI. The cosmic background imager, 2005. http://www.astro.caltech.edu/~tjp/CBI/.

[47] DASI. Degree angular scale interferometer, 2005. http://astro.uchicago.edu/dasi/.

[48] NASA. National aeronautics and space administration, 2005. http://www.nasa.gov.

[49] WMAP team. Wilkinson microwave anisotropy probe, 2005. http://lambda.gsfc.nasa.gov/product/map/.

[50] WMAP team. Wmap first year data, May 2005. http://lambda.gsfc.nasa.gov/product/map/m_products.cfm.

[51] D. N. Spergel, L. Verde, H. V. Peiris, E. Komatsu, M. R. Nolta, C. L. Bennett, M. Halpern, G. Hinshaw, N. Jarosik, A. Kogut, M. Limon, S. S. Meyer, L. Page, G. S. Tucker, J. L. Weiland, E. Wollack, and E. L. Wright. First-Year Wilkinson Microwave Anisotropy Probe

(WMAP) Observations: Determination of Cosmological Parameters. ApJS, 148:175–194, September 2003.

[52] ESA. European space agency, 2005. http://www.esa.int.

[53] ESA. Planck, 2005. http://sci.esa.int/science-e/www/area/index.cfm?fareaid=17.

[54] J. Delabrouille. Measuring CMB polarisation with the Planck mission. Ap&SS, 290:87–103, 2004.

[55] ARCHEOPS. The acheops experiment, 2005. http://www.archeops.org/index_english.html.

[56] M. Tegmark. Max tegmark's cosmic microwave background data analysis center: experiments, 2005. http://space.mit.edu/home/tegmark/cmb/experiments.html.

[57] Wayne Hu. Cmb temperature and polarization anisotropy fundamentals. *Ann. Phys.*, 303:203–225, 2003.

[58] M. Tegmark. Doppler Peaks and all that: CMB Anisotropies and What They Can Tell Us. In *Dark Matter in the Universe, Italian Physical Society, Proceedings of the International School of Physics Course CXXXII, Varenna on Lake Como, Villa Monastero, 25 July - 4 August 1995, Edited by S. Bonometto, J.R. Primack, and A. Provenzale Oxford, GB: IOS Press, 1996, p.379*, pages 379–+, 1996.

[59] R. K. Sachs and A. M. Wolfe. Perturbations of a Cosmological Model and Angular Variations of the Microwave Background. ApJ, 147:73–+, January 1967.

[60] R. A. Sunyaev and Y. B. Zeldovich. The Observations of Relic Radiation as a Test of the Nature of X-Ray Radiation from the Clusters of Galaxies. *Comments on Astrophysics and Space Physics*, 4:173–+, November 1972.

[61] R. A. Sunyaev and I. B. Zeldovich. Microwave background radiation as a probe of the contemporary structure and history of the universe. ARA&A, 18:537–560, 1980.

[62] M. J. Rees and D. W. Sciama. Larger scale Density Inhomogeneities in the Universe. Nature, 217:511–+, 1968.

[63] J. Trulsen. Radiation i, 2003.

[64] M. Zaldarriaga and U. Seljak. All-sky analysis of polarization in the microwave background. Phys. Rev. D, 55:1830–1840, February 1997.

[65] M. S. Turner. Production of scalar and tensor perturbations in inflationary models. Phys. Rev. D, 48:3502–3512, October 1993.

[66] M. S. Turner. Recovering the inflationary potential. Phys. Rev. D, 48:5539–5545, December 1993.

[67] E. J. Copeland, E. W. Kolb, A. R. Liddle, and J. E. Lidsey. Reconstructing the inflaton potential: Perturbative reconstruction to second order. Phys. Rev. D, 49:1840–1844, February 1994.

[68] E. J. Copeland, E. W. Kolb, A. R. Liddle, and J. E. Lidsey. Observing the inflation potential. *Physical Review Letters*, 71:219–222, July 1993.

[69] E. J. Copeland, E. W. Kolb, A. R. Liddle, and J. E. Lidsey. Reconstructing the inflaton potential: In principle and in practice. Phys. Rev. D, 48:2529–2547, September 1993.

[70] A. R. Liddle and M. S. Turner. Second-order reconstruction of the inflationary potential. Phys. Rev. D, 50:758–768, July 1994.

[71] J. D. Barrow and A. R. Liddle. Perturbation spectra from intermediate inflation. Phys. Rev. D, 47:5219–+, June 1993.

[72] L. Knox. Determination of inflationary observables by cosmic microwave background anisotropy experiments. Phys. Rev. D, 52:4307–4318, October 1995.

[73] C. Chen, B. Feng, X. Wang, and Z. Yang. Reconstructing large running index inflaton potentials. *Classical and Quantum Gravity*, 21:3223–3235, July 2004.

[74] W. H. Kinney. Personal communication, 2005.

[75] R. Easther and W. H. Kinney. Monte Carlo reconstruction of the inflationary potential. Phys. Rev. D, 67(4):043511–+, February 2003.

[76] Numerical Algorithms Group. Nag homepage, 2005. http://www.nag.co.uk.

[77] Numerical Recipes. Numerical recipes home page, 2005. http://www.nr.com.

[78] A. R. Liddle. Inflationary flow equations. Phys. Rev. D, 68(10):103504–+, November 2003.

[79] H. Peiris. First year Wilkinson Microwave Anisotropy Probe results: implications for cosmology and inflation. *Contemporary Physics*, 46:77–91, February 2005.

[80] A. R. Liddle. How many cosmological parameters? MNRAS, 351:L49–L53, July 2004.

[81] Lewis, A. and Challinor, A. Camb - august 2004 version. http://camb.info, 2004.

[82] Lewis, A. and Bridle, S. Cosmomc - october 13 2004 version. http://cosmologist.info/cosmomc/, 2004.

[83] Lewis, A. Cosmomc: all_l_exact data format, 2005. http://cosmocoffee.info/viewtopic.php?t=231.

[84] A. Lewis. Personal communication, 2005.

[85] L. Verde, H. V. Peiris, D. N. Spergel, M. R. Nolta, C. L. Bennett, M. Halpern, G. Hinshaw, N. Jarosik, A. Kogut, M. Limon, S. S. Meyer, L. Page, G. S. Tucker, E. Wollack, and E. L. Wright. First-Year Wilkinson Microwave Anisotropy Probe (WMAP) Observations: Parameter Estimation Methodology. ApJS, 148:195–211, September 2003.

[86] Antony Lewis and Sarah Bridle. Cosmological parameters from CMB and other data: a Monte- Carlo approach. *Phys. Rev.*, D66:103511, 2002.

[87] Antony Lewis and Sarah Bridle. CosmoMC Notes. http://cosmologist.info/notes/cosmomc.ps.gz.

[88] A. Lewis and S. Bridle. Cosmomc++, 2005. http://cosmologist.info/notes/cosmomc.ps.gz.

[89] Lewis, A. and Challinor, A. Code for anisotropies in the microwave background. http://camb.info, 2005.

[90] Antony Lewis, Anthony Challinor, and Anthony Lasenby. Efficient computation of CMB anisotropies in closed FRW models. *Astrophys. J.*, 538:473–476, 2000.

[91] A. Lewis. Lensed CMB simulation and parameter estimation. Phys. Rev. D, 71(8):083008–+, April 2005.

[92] S. M. Leach, A. R. Liddle, J. Martin, and D. J. Schwarz. Cosmological parameter estimation and the inflationary cosmology. Phys. Rev. D, 66(2):023515–+, July 2002.

[93] D. Boyanovsky, H. J. de Vega, and N. G. Sanchez. The Classical and Quantum Inflaton: the Precise Inflationary Potential and Quantum Inflaton Decay after WMAP. *ArXiv Astrophysics e-prints*, March 2005.

[94] S. Habib, A. Heinen, K. Heitmann, and G. Jungman. Inflationary perturbations and precision cosmology. Phys. Rev. D, 71(4):043518–+, February 2005.

[95] J. R. Bond, C. R. Contaldi, A. M. Lewis, and D. Pogosyan. The Cosmic Microwave Background and Inflation Parameters. *ArXiv Astrophysics e-prints*, June 2004.

[96] H. K. Eriksen. Personal communication, 2005.

[97] Uros Seljak and Matias Zaldarriaga. A line of sight approach to cosmic microwave background anisotropies. *Astrophys. J.*, 469:437–444, 1996.

[98] A. Kogut et al. Wilkinson Microwave Anisotropy Probe (WMAP) first year observations: TE polarization. *Astrophys. J. Suppl.*, 148:161, 2003.

[99] G. Hinshaw et al. First year Wilkinson Microwave Anisotropy Probe (WMAP) observations: Angular power spectrum. *Astrophys. J. Suppl.*, 148:135, 2003.

[100] CBI. Cbi supplementary data. http://www.astro.caltech.edu/ tjp/CBI/data2004/index.htr 2004.

[101] A. C. S. Readhead et al. Extended mosaic observations with the cosmic background imager. *astro-ph/0402359*, 2004.

[102] Chao-lin Kuo et al. High resolution observations of the cmb power spectrum with acbar. *Astrophys. J.*, 600:32–51, 2004.

[103] Clive Dickinson et al. High sensitivity measurements of the cmb power spectrum with the extended very small array. *astro-ph/0402498*, 2004.

[104] Will J. Percival et al. The 2dF Galaxy Redshift Survey: The power spectrum and the matter content of the universe. *MNRAS*, 327:1297, 2001.

[105] Max Tegmark et al. The 3d power spectrum of galaxies from the sdss. *astro-ph/0310725*, 2003.

[106] S. Perlmutter et al. Measurements of Omega and Lambda from 42 High-Redshift Supernovae. *Astrophys. J.*, 517:565–586, 1999.

[107] W. L. Freedman et al. Final Results from the Hubble Space Telescope Key Project to Measure the Hubble Constant. *Astrophys. J.*, 553:47–72, 2001.